CHAPTER 3: SENSORS

SECTION 3.5: STRAIN, FORCE, PRESSURE AND FLOW MEASUREMENTS (CONT)

CHAPTER 3: SENSORS

SECTION 3.1: POSITIONAL SENSORS

Linear Variable Differential Transformers (LVDTs)

The linear variable differential transformer (LVDT) is an accurate and reliable method for measuring linear distance. LVDTs find uses in modern machine-tool, robotics, avionics, and computerized manufacturing.

The LVDT (see Figure 3.1) is a position-to-electrical sensor whose output is proportional to the position of a movable magnetic core. The core moves linearly inside a transformer consisting of a center primary coil and two outer secondary coils wound on a cylindrical form. The primary winding is excited with an AC voltage source (typically several kHz), inducing secondary voltages which vary with the position of the magnetic core within the assembly. The core is usually threaded in order to facilitate attachment to a nonferromagnetic rod which in turn in attached to the object whose movement or displacement is being measured.

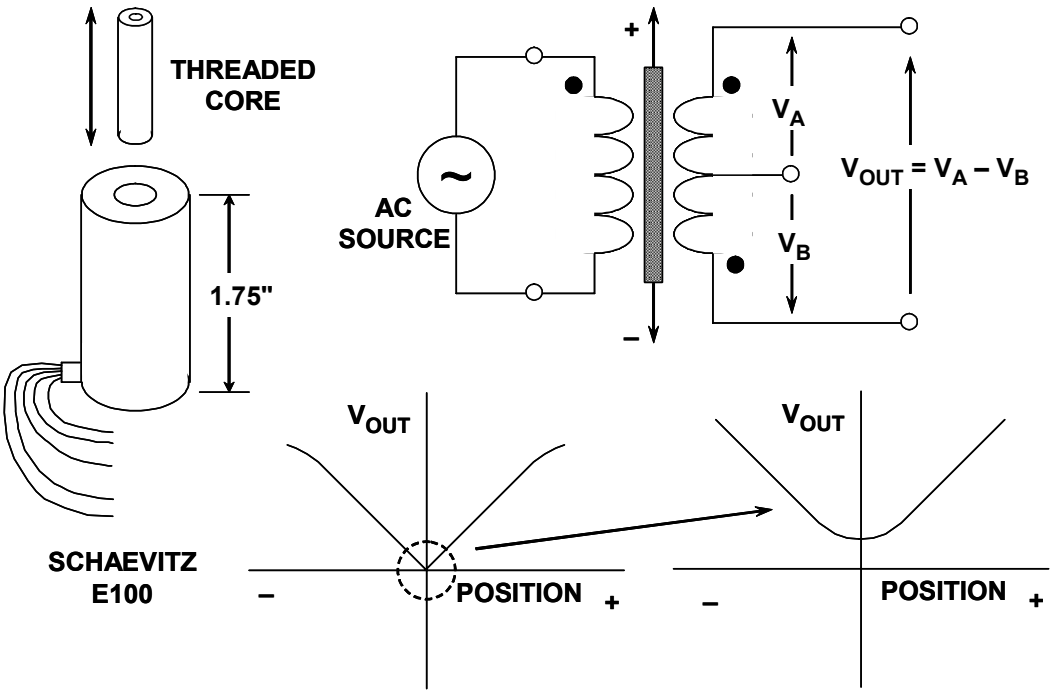

Figure 3.1: *Linear Variable Differential Transformer (LVDT)*

The secondary windings are wound out of phase with each other, and when the core is centered the voltages in the two secondary windings oppose each other, and the net

output voltage is zero. When the core is moved off center, the voltage in the secondary toward which the core is moved increases, while the opposite voltage decreases. The result is a differential voltage output which varies linearly with the core's position. Linearity is excellent over the design range of movement, typically 0.5% or better. The LVDT offers good accuracy, linearity, sensitivity, infinite resolution, as well as frictionless operation and ruggedness.

A wide variety of measurement ranges are available in different LVDTs, typically from ±100 μm to ±25 cm. Typical excitation voltages range from 1 V to 24 V_{RMS}, with frequencies from 50 Hz to 20 kHz.

Note that a true null does not occur when the core is in center position because of mismatches between the two secondary windings and leakage inductance. Also, simply measuring the output voltage V_{OUT} will not tell on which side of the null position the core resides.

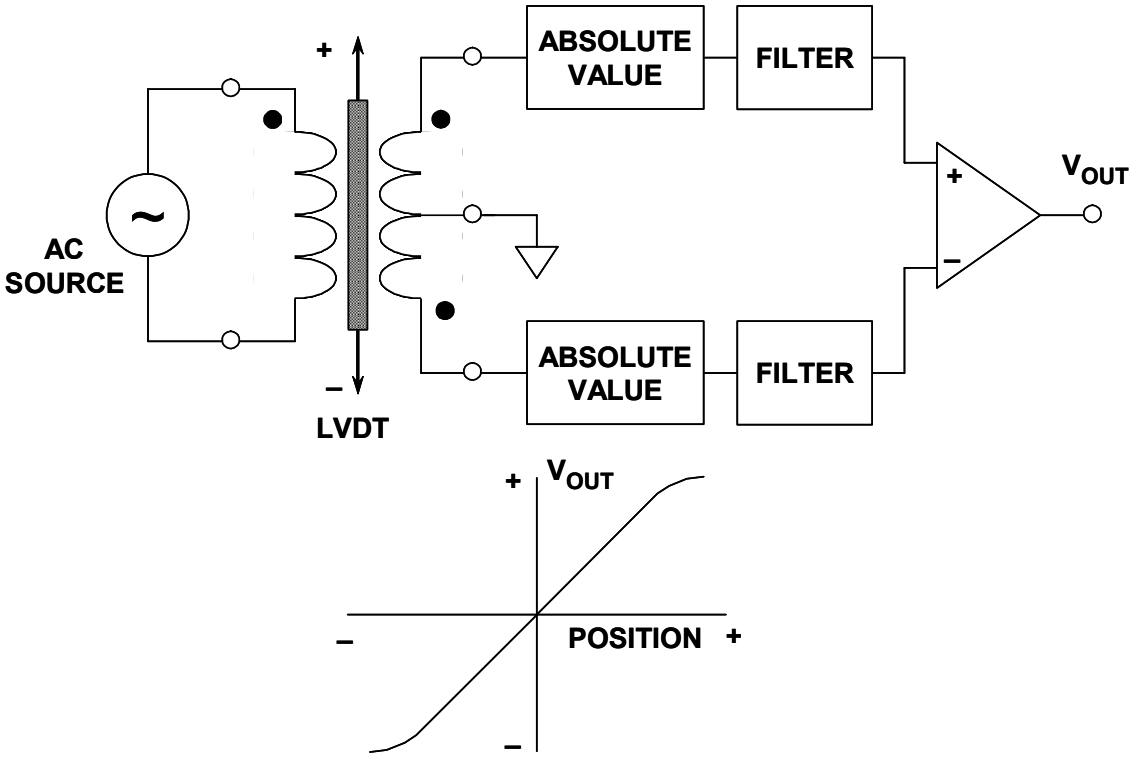

Figure 3.2: *Improved LVDT Output Signal Processing*

A signal conditioning circuit which removes these difficulties is shown in Figure 3.2 where the absolute values of the two output voltages are subtracted. Using this technique, both positive and negative variations about the center position can be measured. While a diode/capacitor-type rectifier could be used as the absolute value circuit, the precision rectifier shown in Figure 3.3 is more accurate and linear. The input is applied to a V/I converter which in turn drives an analog multiplier. The sign of the differential input is

detected by the comparator whose output switches the sign of the V/I output via the analog multiplier. The final output is a precision replica of the absolute value of the input. These circuits are well understood by IC designers and are easy to implement on modern bipolar processes.

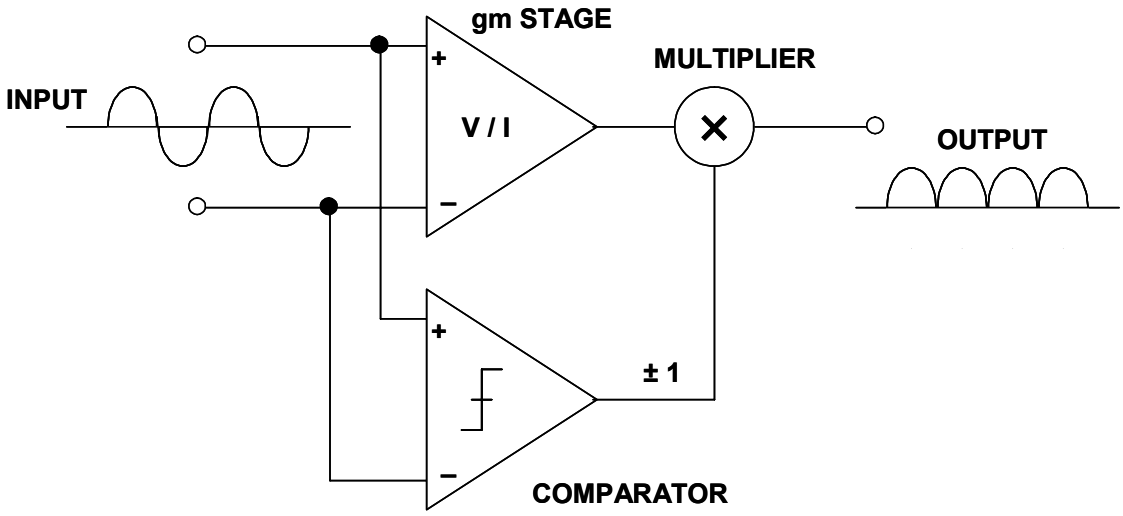

Figure 3.3: *Precision Absolute Value Circuit (Full Wave Rectifier)*

The industry-standard AD598 LVDT signal conditioner shown in Figure 3.4 (simplified form) performs all required LVDT signal processing. The on-chip excitation frequency oscillator can be set from 20 Hz to 20 kHz with a single external capacitor. Two absolute value circuits followed by two filters are used to detect the amplitude of the A and B channel inputs. Analog circuits are then used to generate the ratiometric function [A – B]/[A + B]. Note that this function is independent of the amplitude of the primary winding excitation voltage, assuming the sum of the LVDT output voltage amplitudes remains constant over the operating range. This is usually the case for most LVDTs, but the user should always check with the manufacturer if it is not specified on the LVDT data sheet. Note also that this approach requires the use of a 5-wire LVDT.

A single external resistor sets the AD598 excitation voltage from approximately 1 V_{RMS} to 24 V_{RMS}. Drive capability is 30 mA_{RMS}. The AD598 can drive an LVDT at the end of 300 feet of cable, since the circuit is not affected by phase shifts or absolute signal magnitudes. The position output range of V_{OUT} is ±11 V for a 6 mA load and it can drive up to 1000 feet of cable. The V_A and V_B inputs can be as low as 100 mV RMS.

The AD698 LVDT signal conditioner (see Figure 3.5) has similar specifications as the AD598 but processes the signals slightly differently and uses synchronous demodulation. The A and B signal processors each consist of an absolute value function and a filter. The A output is then divided by the B output to produce a final output which is ratiometric and independent of the excitation voltage amplitude. Note that the sum of the LVDT secondary voltages does not have to remain constant in the AD698.

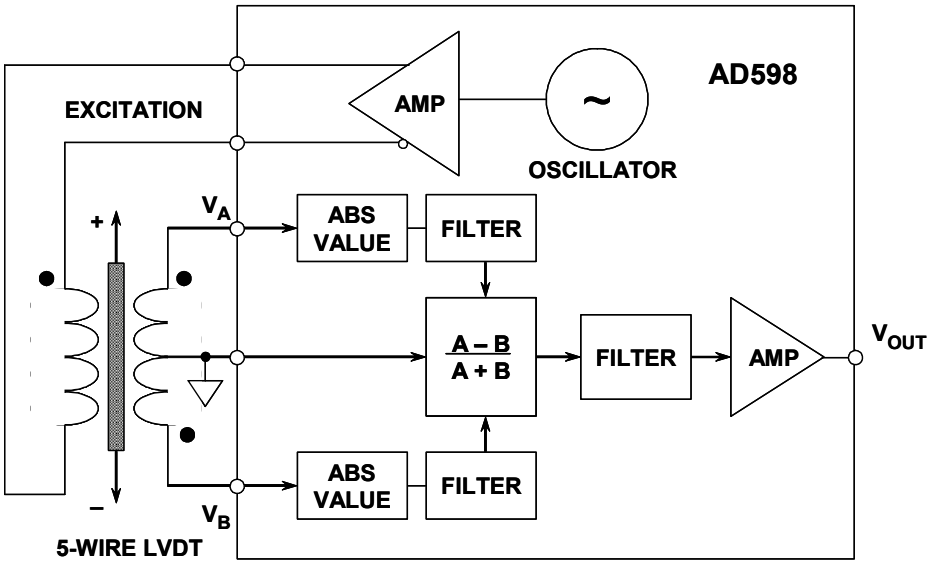

Figure 3.4: *AD598 LVDT Signal Conditioner (Simplified)*

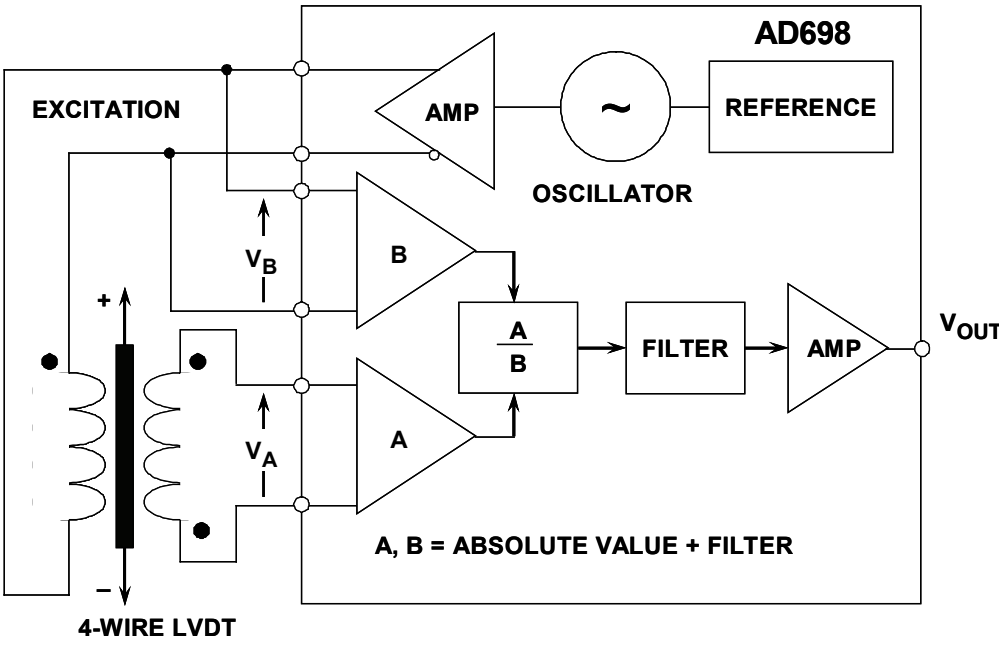

Figure 3.5: *AD698 LVDT Signal Conditioner (Simplified)*

The AD698 can also be used with a half-bridge (similar to an auto-transformer) LVDT as shown in Figure 3.6. In this arrangement, the entire secondary voltage is applied to the B processor, while the center-tap voltage is applied to the A processor. The half-bridge LVDT does not produce a null voltage, and the A/B ratio represents the range-of-travel of the core.

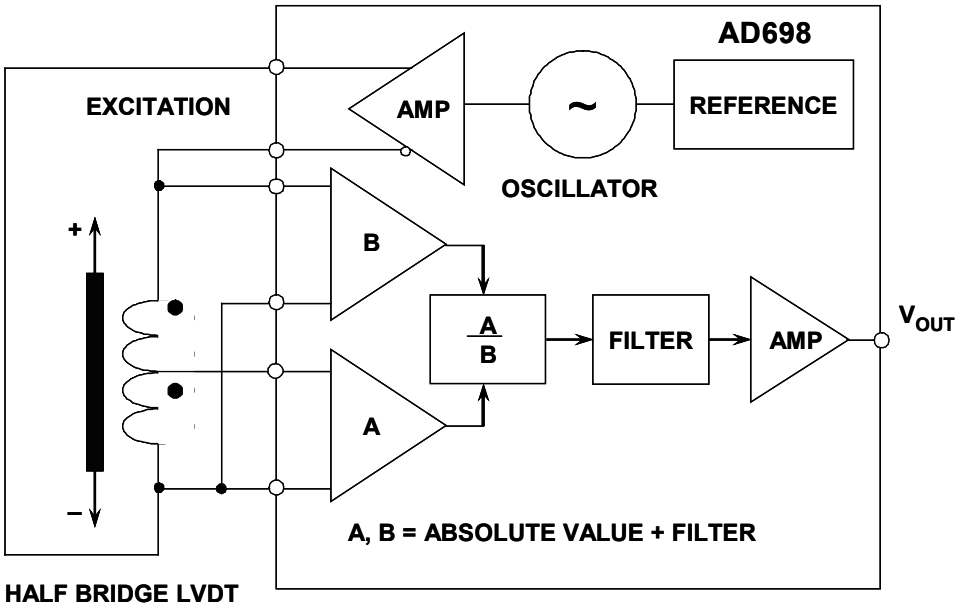

Figure 3.6: *Half-Bridge LVDT Configuration*

It should be noted that the LVDT concept can be implemented in rotary form, in which case the device is called a *rotary variable differential transformer* (RVDT). The shaft is equivalent to the core in an LVDT, and the transformer windings are wound on the stationary part of the assembly. However, the RVDT is linear over a relatively narrow range of rotation and is not capable of measuring a full 360º rotation. Although capable of continuous rotation, typical RVDTs are linear over a range of about ±40º about the null position (0º). Typical sensitivity is 2 to 3mV per volt per degree of rotation, with input voltages in the range of $3V_{RMS}$ at frequencies between 400 Hz and 20 kHz. The 0º position is marked on the shaft and the body.

Hall Effect Magnetic Sensors

If a current flows in a conductor (or semiconductor) and there is a magnetic field present which is perpendicular to the current flow, then the combination of current and magnetic field will generate a voltage perpendicular to both (see Figure 3.7). This phenomenon is called the *Hall Effect*, was discovered by E. H. Hall in 1879. The voltage, V_H, is known as the *Hall Voltage*. V_H is a function of the current density, the magnetic field, and the charge density and carrier mobility of the conductor.

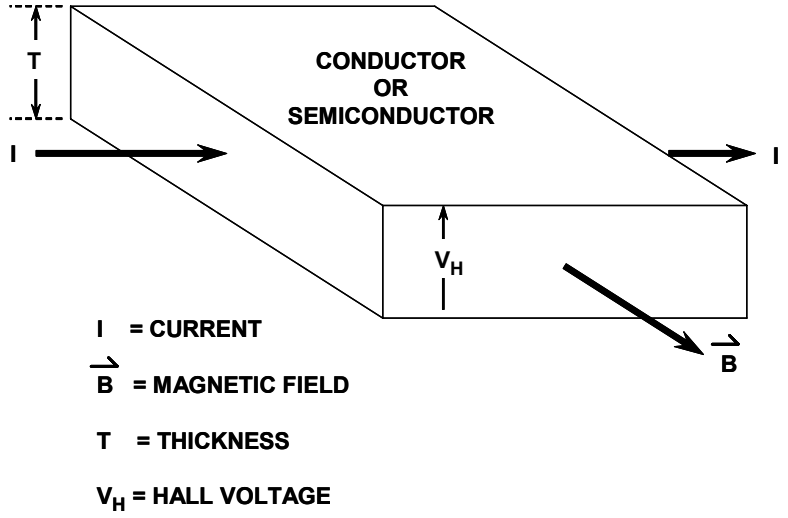

Figure 3.7: *Hall Effect Sensor*

The Hall effect may be used to measure magnetic fields (and hence in contact-free current measurement), but its commonest application is in motion sensors where a fixed Hall sensor and a small magnet attached to a moving part can replace a cam and contacts with a great improvement in reliability. (Cams wear and contacts arc or become fouled, but magnets and Hall sensors are contact free and do neither.) Since V_H is proportional to magnetic field and not to rate of change of magnetic field like an inductive sensor, the Hall Effect provides a more reliable low speed sensor than an inductive pickup.

Although several materials can be used for Hall effect sensors, silicon has the advantage that signal conditioning circuits can be integrated on the same chip as the sensor. CMOS processes are common for this application. A simple rotational speed detector can be made with a Hall sensor, a gain stage, and a comparator as shown in Figure 3.8. The circuit is designed to detect rotation speed as in automotive applications. It responds to small changes in field, and the comparator has built-in hysteresis to prevent oscillation. Several companies manufacture such Hall switches, and their usage is widespread.

There are many other applications, particularly in automotive throttle, pedal, suspension, and valve position sensing, where a linear representation of the magnetic field is desired. The AD22151 is a linear magnetic field sensor whose output voltage is proportional to a magnetic field applied perpendicularly to the package top surface (see Figure 3.9). The AD22151 combines integrated bulk Hall cell technology and conditioning circuitry to minimize temperature related drifts associated with silicon Hall cell characteristics.

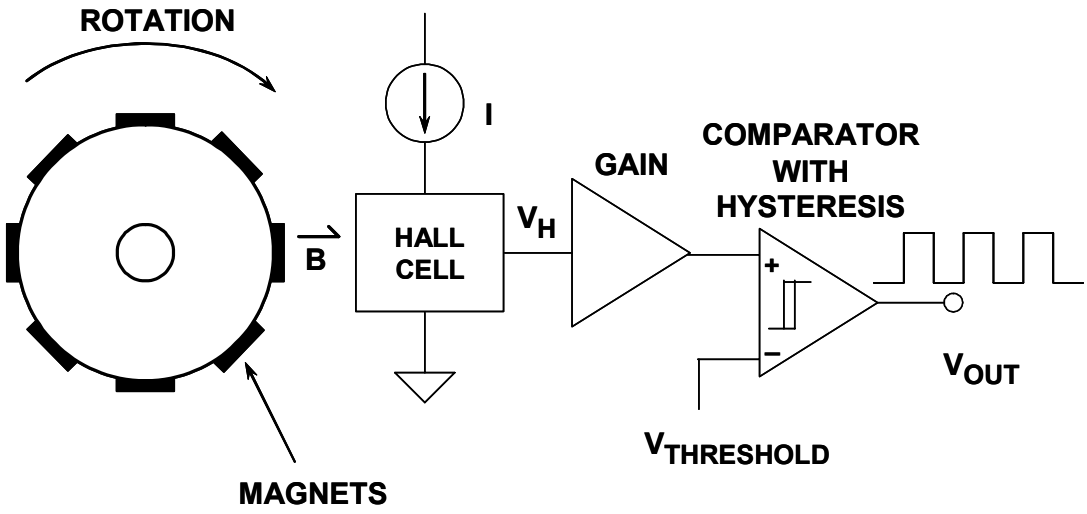

Figure 3.8: *Hall Effect Sensor Used as a Rotational Sensor*

The architecture maximizes the advantages of a monolithic implementation while allowing sufficient versatility to meet varied application requirements with a minimum number of external components. Principal features include dynamic offset drift cancellation using a chopper-type op amp and a built-in temperature sensor. Designed for single +5 V supply operation, low offset and gain drift allows operation over a –40ºC to +150ºC range. Temperature compensation (set externally with a resistor R1) can accommodate a number of magnetic materials commonly utilized in position sensors. Output voltage range and gain can be easily set with external resistors. Typical gain range is usually set from 2 mV/Gauss to 6 mV/Gauss. Output voltage can be adjusted from fully bipolar (reversible) field operation to fully unipolar field sensing. The voltage output achieves near rail-to-rail dynamic range (+0.5 V to +4.5 V), capable of supplying 1 mA into large capacitive loads. The output signal is ratiometric to the positive supply rail in all configurations.

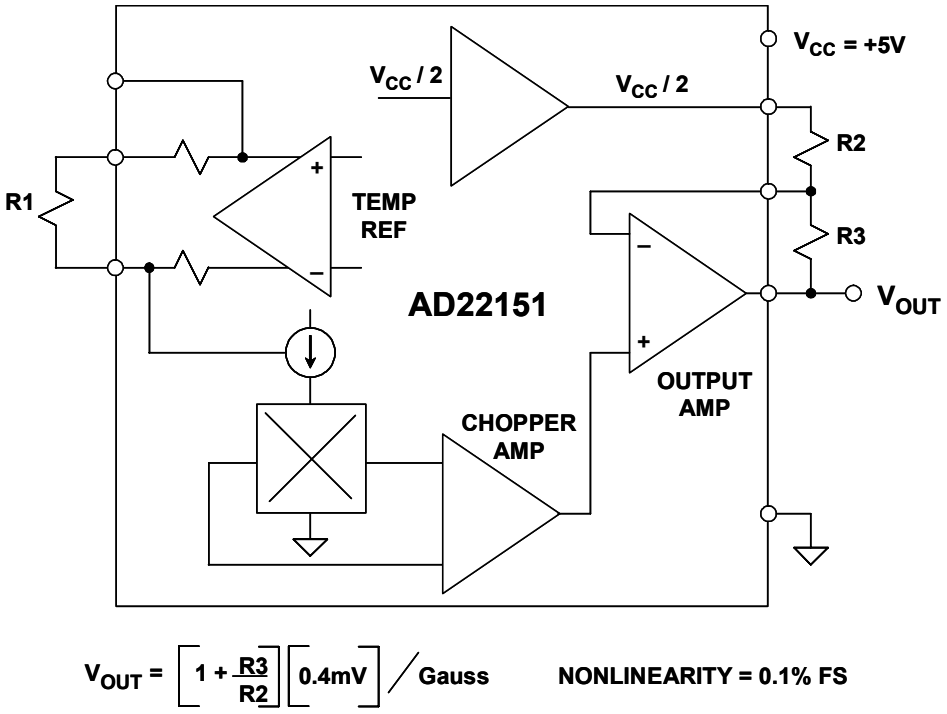

Figure 3.9: *AD22151 Linear Output Magnetic Field Sensor*

Resolvers and Synchros

Machine-tool and robotics manufacturers have increasingly turned to resolvers and synchros to provide accurate angular and rotational information. These devices excel in demanding factory applications requiring small size, long-term reliability, absolute position measurement, high accuracy, and low-noise operation.

A diagram of a typical synchro and resolver is shown in Figure 3.10. Both synchros and resolvers employ single-winding rotors that revolve inside fixed stators. In the case of a simple synchro, the stator has three windings oriented 120º apart and electrically connected in a Y-connection. Resolvers differ from synchros in that their stators have only two windings oriented at 90º.

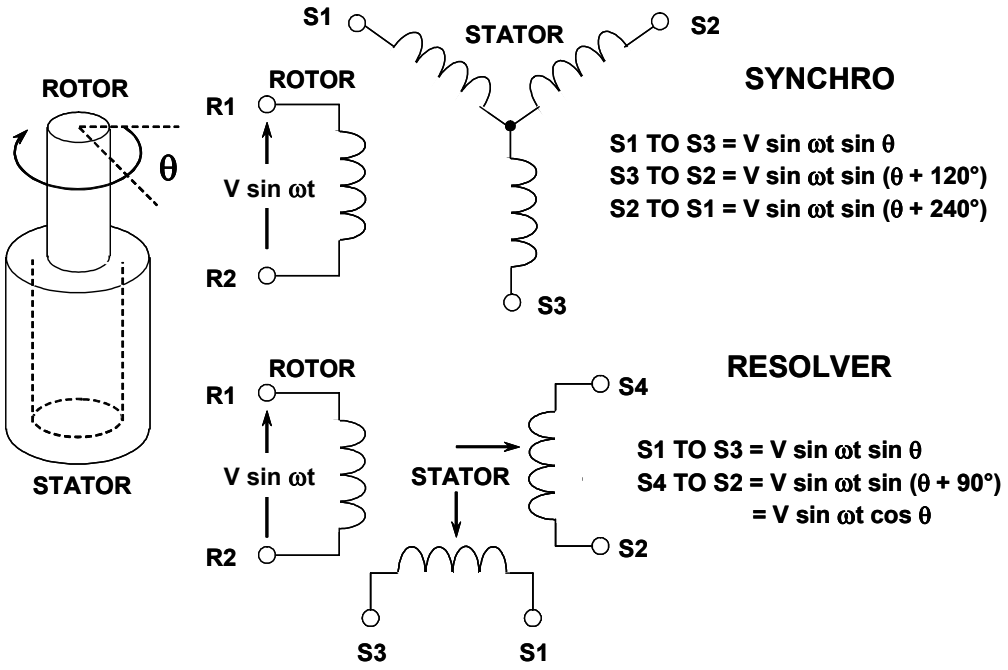

Figure 3.10: *Synchros and Resolvers*

Because synchros have three stator coils in a 120º orientation, they are more difficult than resolvers to manufacture and are therefore more costly. Today, synchros find decreasing use, except in certain military and avionic retrofit applications.

Modern resolvers, in contrast, are available in a brushless form that employ a transformer to couple the rotor signals from the stator to the rotor. The primary winding of this transformer resides on the stator, and the secondary on the rotor. Other resolvers use more traditional brushes or slip rings to couple the signal into the rotor winding. Brushless resolvers are more rugged than synchros because there are no brushes to break or dislodge, and the life of a brushless resolver is limited only by its bearings. Most resolvers are specified to work over 2 V to 40 V_{RMS} and at frequencies from 400 Hz to

10 kHz. Angular accuracies range from 5 arc-minutes to 0.5 arc-minutes. (There are 60 arc-minutes in one degree, and 60 arc-seconds in one arc-minute. Hence, one arc-minute is equal to 0.0167 degrees).

In operation, synchros and resolvers resemble rotating transformers. The rotor winding is excited by an AC reference voltage, at frequencies up to a few kHz. The magnitude of the voltage induced in any stator winding is proportional to the sine of the angle, θ, between the rotor coil axis and the stator coil axis. In the case of a synchro, the voltage induced across any pair of stator terminals will be the vector sum of the voltages across the two connected coils.

For example, if the rotor of a synchro is excited with a reference voltage, $V\sin\omega t$, across its terminals R1 and R2, then the stator's terminal will see voltages in the form:

$$S1 \text{ to } S3 = V \sin\omega t \sin\theta \qquad \text{Eq. 3-1}$$

$$S3 \text{ to } S2 = V \sin\omega t \sin(\theta + 120^\circ) \qquad \text{Eq. 3-2}$$

$$S2 \text{ to } S1 = V \sin\omega t \sin(\theta + 240^\circ), \qquad \text{Eq. 3-3}$$

where θ is the shaft angle.

In the case of a resolver, with a rotor AC reference voltage of $V\sin\omega t$, the stator's terminal voltages will be:

$$S1 \text{ to } S3 = V \sin\omega t \sin\theta \qquad \text{Eq. 3-4}$$

$$S4 \text{ to } S2 = V \sin\omega t \sin(\theta + 90^\circ) = V \sin\omega t \cos\theta. \qquad \text{Eq. 3-5}$$

It should be noted that the 3-wire synchro output can be easily converted into the resolver-equivalent format using a Scott-T transformer. Therefore, the following signal processing example describes only the resolver configuration.

A typical resolver-to-digital converter (RDC) is shown functionally in Figure 3.11. The two outputs of the resolver are applied to cosine and sine multipliers. These multipliers incorporate sine and cosine lookup tables and function as multiplying digital-to-analog converters. Begin by assuming that the current state of the up/down counter is a digital number representing a trial angle, φ. The converter seeks to adjust the digital angle, φ, continuously to become equal to, and to track θ, the analog angle being measured. The resolver's stator output voltages are written as:

$$V_1 = V \sin\omega t \sin\theta \qquad \text{Eq. 3-6}$$

$$V_2 = V \sin\omega t \cos\theta \qquad \text{Eq. 3-7}$$

where θ is the angle of the resolver's rotor. The digital angle φ is applied to the cosine multiplier, and its cosine is multiplied by V_1 to produce the term:

$$V \sin\omega t \sin\theta \cos\varphi. \qquad \text{Eq. 3-8}$$

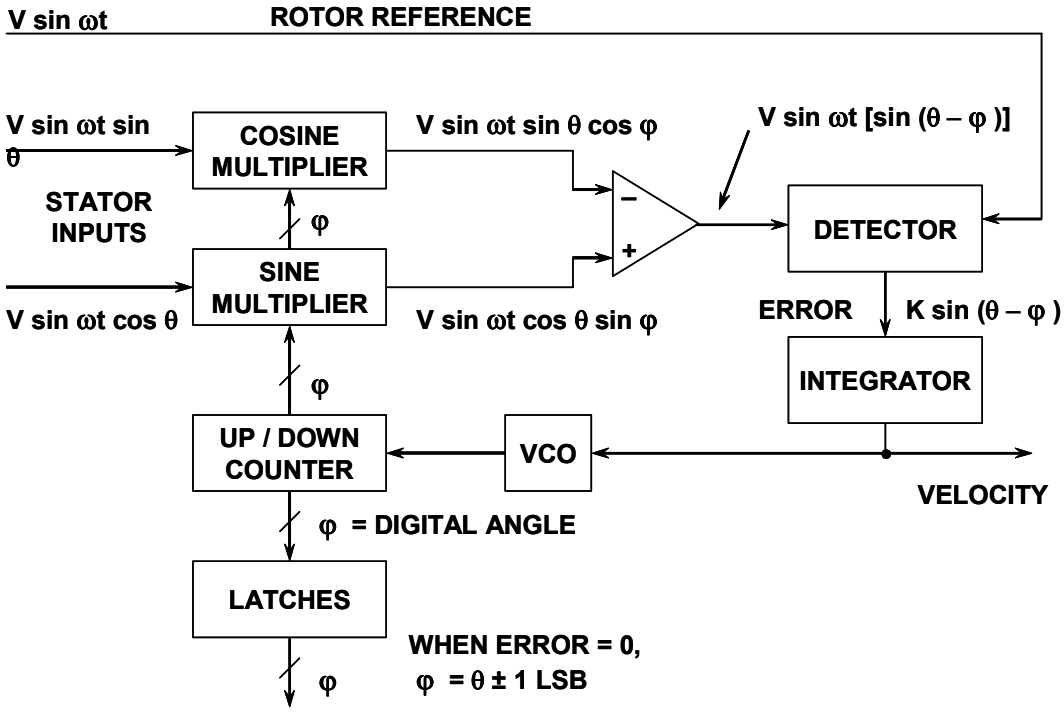

Figure 3.11: *Resolver to Digital Converter (RDC)*

The digital angle φ is also applied to the sine multiplier and multiplied by V_2 to product the term:

$$V \sin\omega t \cos\theta \sin\varphi. \qquad \text{Eq. 3-9}$$

These two signals are subtracted from each other by the error amplifier to yield an AC error signal of the form:

$$V \sin\omega t [\sin\theta \cos\varphi - \cos\theta \sin\varphi]. \qquad \text{Eq. 3-10}$$

Using a simple trigonometric identity, this reduces to:

$$V \sin\omega t [\sin (\theta - \varphi)]. \qquad \text{Eq. 3-11}$$

The detector synchronously demodulates this AC error signal, using the resolver's rotor voltage as a reference. This results in a DC error signal proportional to sin(θ–φ).

The DC error signal feeds an integrator, the output of which drives a voltage-controlled-oscillator (VCO). The VCO, in turn, causes the up/down counter to count in the proper direction to cause:

$$\sin(\theta - \varphi) \rightarrow 0. \qquad \text{Eq. 3-12}$$

When this is achieved,

$$\theta - \varphi \rightarrow 0, \qquad \text{Eq. 3-13}$$

and therefore

$$\varphi = \theta \qquad \text{Eq. 3-14}$$

to within one count. Hence, the counter's digital output, φ, represents the angle θ. The latches enable this data to be transferred externally without interrupting the loop's tracking.

Inductosyns

Synchros and resolvers inherently measure rotary position, but they can make linear position measurements when used with lead screws. An alternative, the Inductosyn™ (registered trademark of Farrand Controls, Inc.) measures linear position directly. In addition, Inductosyns are accurate and rugged, well-suited to severe industrial environments, and do not require ohmic contact.

The linear Inductosyn consists of two magnetically coupled parts; it resembles a multipole resolver in its operation (see Figure 3.12). One part, the scale, is fixed (e.g. with epoxy) to one axis, such as a machine tool bed. The other part, the slider, moves along the scale in conjunction with the device to be positioned (for example, the machine tool carrier).

The scale is constructed of a base material such as steel, stainless steel, aluminum, or a tape of spring steel, covered by an insulating layer. Bonded to this is a printed-circuit trace, in the form of a continuous rectangular waveform pattern. The pattern typically has a cyclic pitch of 0.1 inch, 0.2 inch, or 2 millimeters. The slider, about 4 inches long, has two separate but identical printed circuit traces bonded to the surface that faces the scale. These two traces have a waveform pattern with exactly the same cyclic pitch as the waveform on the scale, but one trace is shifted one-quarter of a cycle relative to the other. The slider and the scale remain separated by a small air gap of about 0.007 inch.

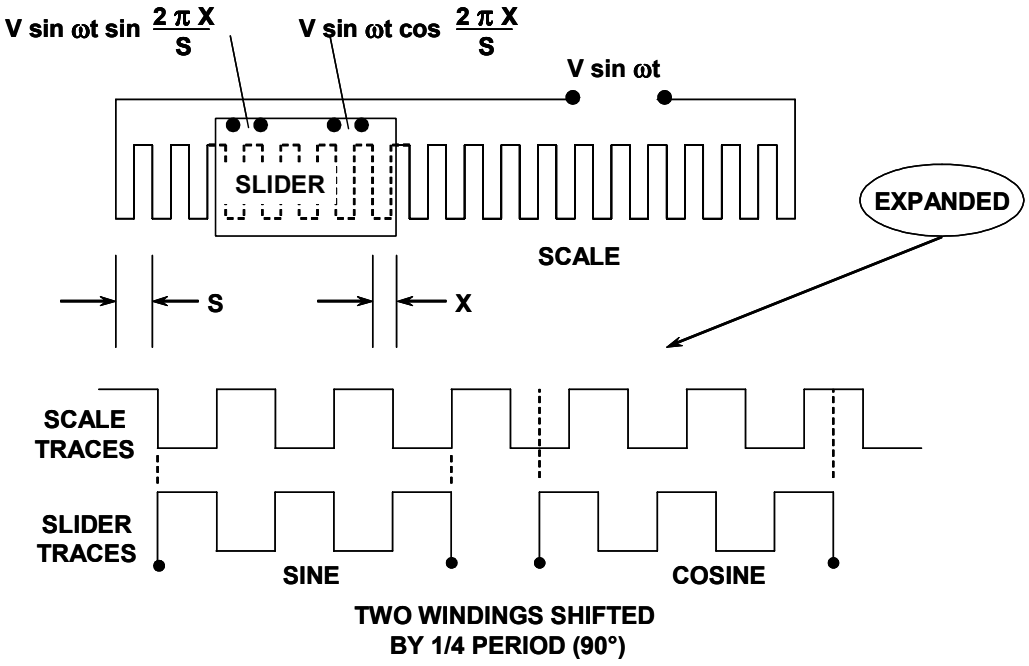

Figure 3.12: Linear Inductosyn

◘ BASIC LINEAR DESIGN

Inductosyn operation resembles that of a resolver. When the scale is energized with a sine wave, this voltage couples to the two slider windings, inducing voltages proportional to the sine and cosine of the slider's spacing within the cyclic pitch of the scale. If S is the distance between pitches, and X is the slider displacement within a pitch, and the scale is energized with a voltage V sinωt, then the slider windings will see terminal voltages of:

$$V \text{ (sine output)} = V \sin\omega t \sin[2\pi X/S] \quad \text{Eq. 3-15}$$

$$V \text{ (cosine output)} = V \sin\omega t \cos[2\pi X/S]. \quad \text{Eq. 3-16}$$

As the slider moves the distance of the scale pitch, the voltages produced by the two slider windings are similar to those produced by a resolver rotating through 360º. The absolute orientation of the Inductosyn is determined by counting successive pitches in either direction from an established starting point. Because the Inductosyn consists of a large number of cycles, some form of coarse control is necessary in order to avoid ambiguity. The usual method of providing this is to use a resolver or synchro operated through a rack and pinion or a lead screw.

In contrast to a resolver's highly efficient transformation of 1:1 or 2:1, typical Inductosyns operate with transformation ratios of 100:1. This results in a pair of sinusoidal output signals in the millivolt range which generally require amplification.

Since the slider output signals are derived from an average of several spatial cycles, small errors in conductor spacing have minimal effects. This is an important reason for the Inductosyn's very high accuracy. In combination with 12-bit RDCs, linear Inductosyns readily achieve 25 microinch resolutions.

Rotary inductosyns can be created by printing the scale on a circular rotor and the slider's track pattern on a circular stator. Such rotary devices can achieve very high resolutions. For instance, a typical rotary Inductosyn may have 360 cyclic pitches per rotation, and might use a 12-bit RDC. The converter effectively divides each pitch into 4096 sectors. Multiplying by 360 pitches, the rotary Inductosyn divides the circle into a total of 1,474,560 sectors. This corresponds to an angular resolution of less than 0.9 arc seconds. As in the case of the linear Inductosyn, a means must be provided for counting the individual pitches as the shaft rotates. This may be done with an additional resolver acting as the coarse measurement.

Accelerometers

Accelerometers are widely used to measure tilt, inertial forces, shock, and vibration. They find wide usage in automotive, medical, industrial control, and other applications. Modern micromachining techniques allow these accelerometers to be manufactured on CMOS processes at low cost with high reliability. Analog Devices iMEMS® (Integrated Micro Electro Mechanical Systems) accelerometers represent a breakthrough in this technology. A significant advantage of this type of accelerometer over piezoelectric-type charge-output accelerometers is that DC acceleration can be measured (e.g. they can be used in tilt measurements where the acceleration is a constant 1g).

The basic unit cell sensor building block for these accelerometers is shown in Figure 3.13. The surface micromachined sensor element is made by depositing polysilicon on a sacrificial oxide layer that is then etched away leaving the suspended sensor element. The actual sensor has tens of unit cells for sensing acceleration, but the diagram shows only one cell for clarity. The electrical basis of the sensor is the differential capacitor (CS1 and CS2) which is formed by a center plate which is part of the moving beam and two fixed outer plates. The two capacitors are equal at rest (no applied acceleration). When acceleration is applied, the mass of the beam causes it to move closer to one of the fixed plates while moving further from the other. This change in differential capacitance forms the electrical basis for the conditioning electronics shown in Figure 3.14.

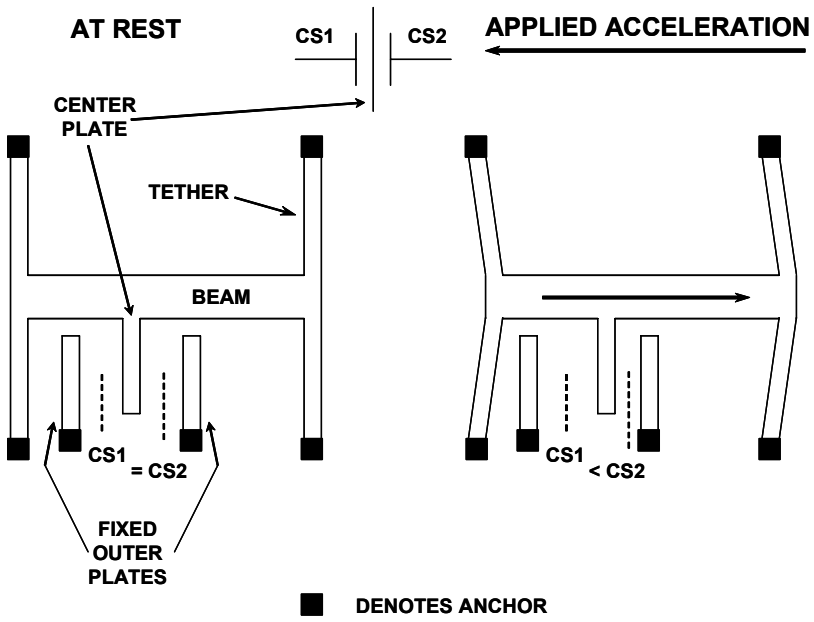

Figure 3.13: *ADXL-Family Micromachined Accelerometers (Top View of IC)*

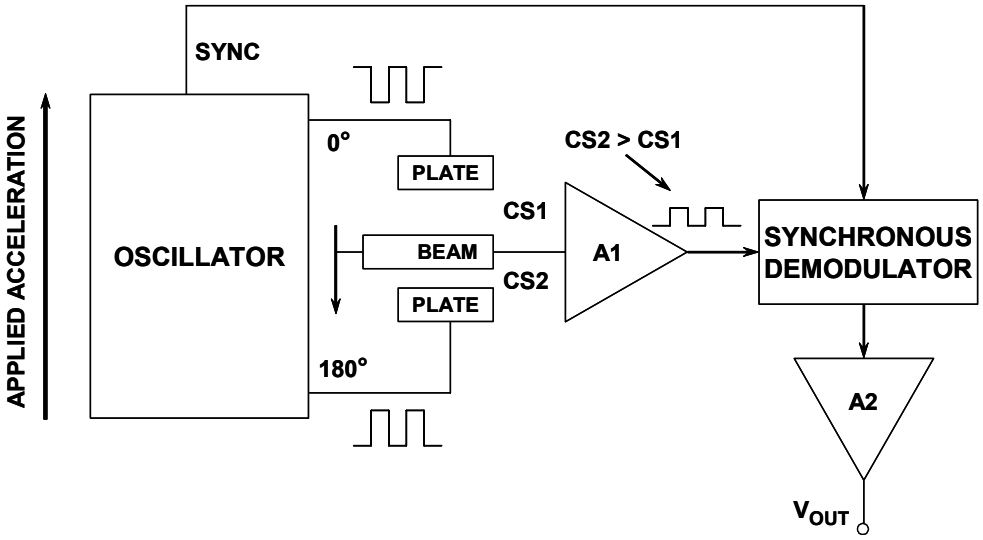

Figure 3.14: *Accelerometer Internal Signal Conditioning*

The sensor's fixed capacitor plates are driven differentially by a 1 MHz square wave: the two square wave amplitudes are equal but are 180º out of phase. When at rest, the values of the two capacitors are the same, and therefore the voltage output at their electrical center (i.e., at the center plate attached to the movable beam) is zero. When the beam begins to move, a mismatch in the capacitance produces an output signal at the center plate. The output amplitude will increase with the acceleration experienced by the sensor. The center plate is buffered by A1 and applied to a synchronous demodulator. The direction of beam motion affects the phase of the signal, and synchronous demodulation is therefore used to extract the amplitude information. The synchronous demodulator output is amplified by A2 which supplies the acceleration output voltage, V_{OUT}.

An interesting application of low-g accelerometers is measuring tilt. Figure 3.15 shows the response of an accelerometer to tilt. The accelerometer output on the diagram has been normalized to 1g fullscale. The accelerometer output is proportional to the sine of the tilt angle with respect to the horizon. Note that maximum sensitivity occurs when the accelerometer axis is perpendicular to the acceleration. This scheme allows tilt angles from –90º to +90º (180º of rotation) to be measured. However, in order to measure a full 360º rotation, a dual-axis accelerometer must be used.

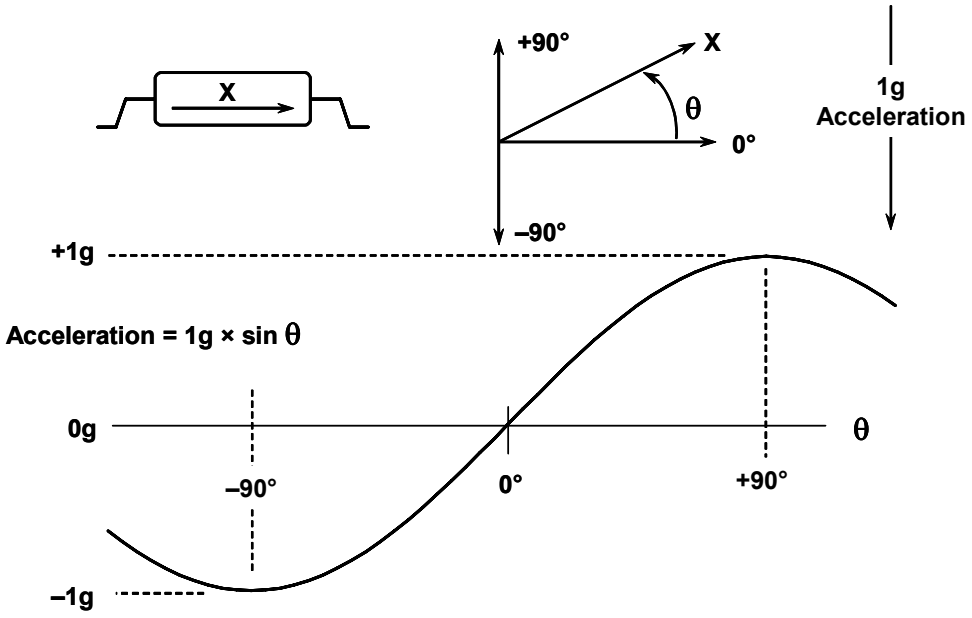

Figure 3.15: *Using an Accelerometer to Measure Tilt*

Figure 3.16 shows a simplified block diagram of the ADXL202 dual axis ±2 g accelerometer. The output is a pulse whose duty cycle contains the acceleration information. This type of output is extremely useful because of its high noise immunity, and the data is transmitted over a single wire. Standard low cost microcontrollers have timers which can be easily used to measure the T1 and T2 intervals. The acceleration in g is then calculated using the formula:

$$A(g) = 8\,[T1/T2 - 0.5]\,. \qquad \text{Eq. 3-17}$$

Note that a duty cycle of 50 % (T1 = T2) yields a 0g output. T2 does not have to be measured for every measurement cycle. It need only be updated to account for changes due to temperature. Since the T2 time period is shared by both X and Y channels, it is necessary to only measure it on one channel. The T2 period can be set from 0.5 ms to 10 ms with an external resistor.

Analog voltages representing acceleration can be obtained by buffering the signal from the X_{FILT} and Y_{FILT} outputs or by passing the duty cycle signal through an RC filter to reconstruct its DC value.

A single accelerometer cannot work in all applications. Specifically, there is a need for both low-g and high-g accelerometers. Low-g devices are useful in such applications as tilt measurements, but higher-g accelerometers are needed in applications such as airbag crash sensors.

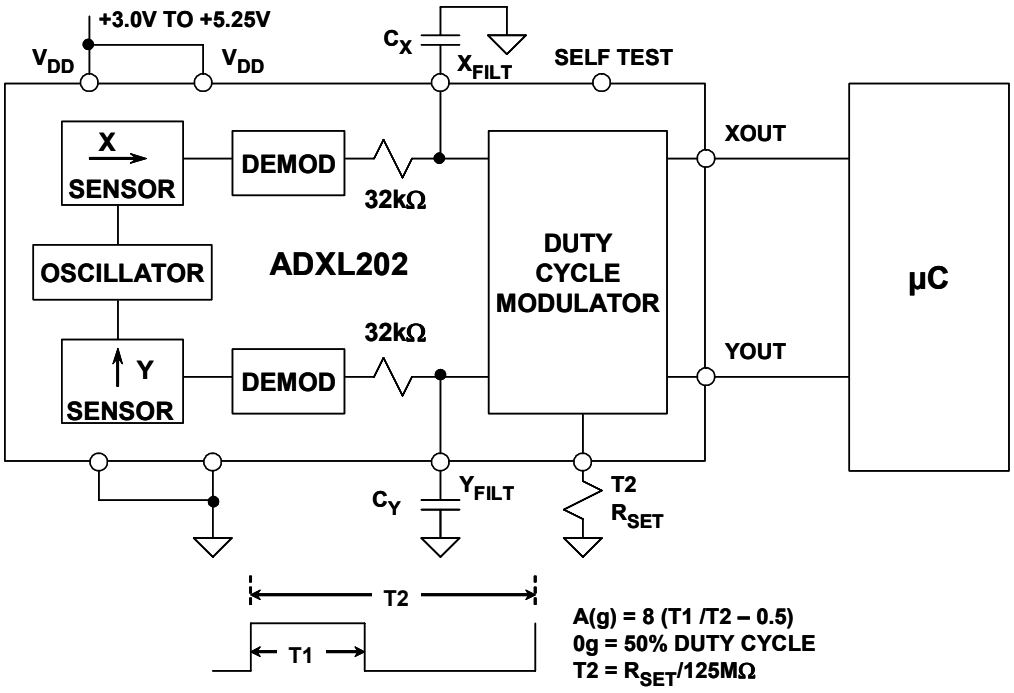

Figure 3.16: *ADXL202 ±2g Dual Axis Accelerometer*

iMEMS® Angular-Rate-Sensing Gyroscope

The new ADXRS150 and ADXRS300 gyros, with full-scale ranges of 150°/s and 300°/s, represent a quantum jump in gyro technology. The first commercially available surface-micromachined angular rate sensors with integrated electronics, they are smaller—with lower power consumption, and better immunity to shock and vibration—than any gyros having comparable functionality.

Gyroscope Description

Gyroscopes are used to measure *angular* rate—how quickly an object turns. The rotation is typically measured in reference to one of three axes: yaw, pitch, or roll. Figure 3.17 shows a diagram representing each axis of sensitivity relative to a package mounted to a flat surface. Depending on how a gyro normally sits, its primary axis of sensitivity can be one of the three axes of motion: yaw, pitch, or roll. The ADXRS150 and ADXRS300 are yaw-axis gyros, but they can measure rotation about other axes by appropriate mounting orientation. For example, at the right of Fig. 3.17 a yaw-axis device is positioned to measure roll.

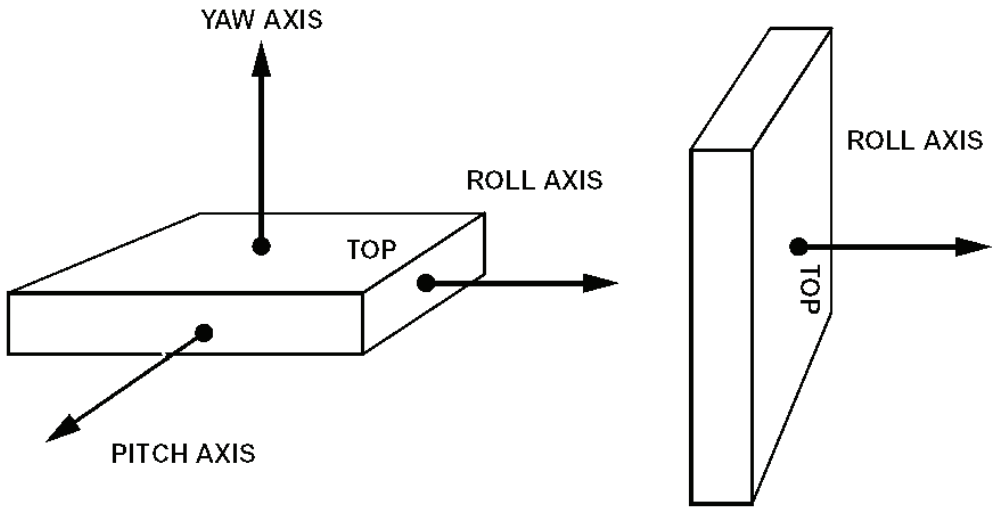

Fig. 3.17: *Gyro Axes of Rotational Sensitivity*

A gyroscope with one axis of sensitivity can also be used to measure other axes by mounting the gyro differently, as shown in the right-hand diagram. Here, a yaw-axis gyro, such as the ADXRS150 or ADXRS300, is mounted on its side so that the yaw axis becomes the roll axis.

As an example of how a gyro could be used, a yaw-axis gyro mounted on a turntable rotating at 33 1/3 rpm (revolutions per minute) would measure a constant rotation of 360°

times 33 1/3 rpm divided by 60 seconds, or 200°/s. The gyro would output a voltage proportional to the angular rate, as determined by its sensitivity, measured in millivolts per degree per second (mV/°/s). The full-scale voltage determines how much angular rate can be measured, so in the example of the turntable, a gyro would need to have a full-scale voltage corresponding to at least 200°/s. Full-scale is limited by the available voltage swing divided by the sensitivity. The ADXRS300, for example, with 1.5 V full-scale and a sensitivity of 5 mV/°/s, handles a full-scale of 300°/s. The ADXRS150, has a more limited full-scale of 150°/s but a greater sensitivity of 12.5 mV/°/s.

One practical application is to measure how quickly a car turns by mounting a gyro inside the vehicle; if the gyro senses that the car is spinning out of control, differential braking engages to bring it back into control. The angular rate can also be integrated over time to determine angular position—particularly useful for maintaining continuity of GPS-based navigation when the satellite signal is lost for short periods of time.

Coriolis Acceleration

Analog Devices' ADXRS gyros measure angular rate by means of Coriolis acceleration. The Coriolis effect can be explained as follows, starting with Figure 3.16. Consider yourself standing on a rotating platform, near the center. Your speed relative to the ground is shown as the arrow lengths in Figure 3.18. If you were to move to a point near the outer edge of the platform, your speed would increase relative to the ground, as indicated by the longer blue arrow. The rate of increase of your tangential speed, caused by your radial velocity, is the *Coriolis* acceleration (after Gaspard G. de Coriolis, 1792-1843—a French mathematician).

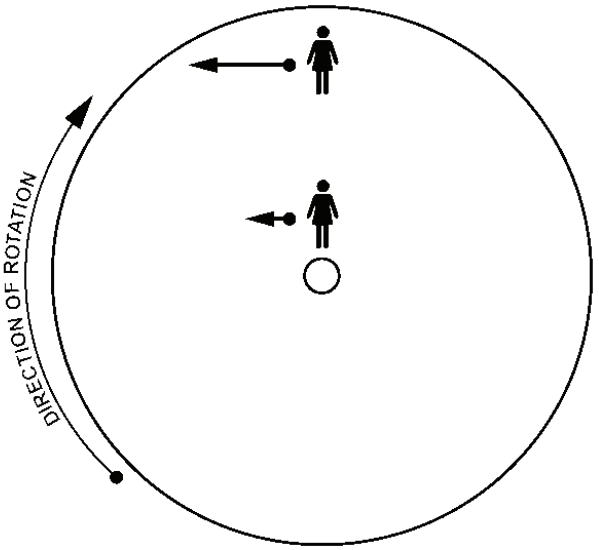

Figure 3.18: *Coriolis acceleration example.*

If Ω is the angular rate and r the radius, the tangential velocity is Ωr. So, if r changes at speed, v, there will be a tangential acceleration Ωv. This is half of the Coriolis acceleration. There is another half from changing the direction of the radial velocity giving a total of $2\Omega v$. If you have mass, M, the platform must apply a force, $2M\Omega v$, to cause that acceleration, and the mass experiences a corresponding reaction force.

Motion in 2 dimensions

Consider the position coordinate, $z = r\varepsilon^{i\theta}$, in the complex plane. Differentiating with respect to time, t, the velocity is:

$$\frac{dz}{dt} = \frac{dr}{dt}\varepsilon^{j\theta} + ir\frac{d\theta}{dt}\varepsilon^{j\theta} \qquad \text{Eq. 3-19}$$

The two terms are the respective radial and tangential components, the latter arising from the angular rate. Differentiating again, the acceleration is:

$$\frac{d^2z}{dt^2} = \left[\frac{d^2r}{dt^2}\varepsilon^{j\theta} + i\frac{dr}{dt}\frac{d\theta}{dt}\varepsilon^{j\theta}\right] + \left[i\frac{dr}{dt}\frac{d\theta}{dt}\varepsilon^{j\theta} + ir\frac{d^2\theta}{dt^2}\varepsilon^{j\theta} - r\left[\frac{d\theta}{dt}\right]^2\varepsilon^{j\theta}\right] \qquad \text{Eq. 3-20}$$

The first term is the radial linear acceleration and the fourth term is the tangential component arising from angular acceleration. The last term is the familiar centripetal acceleration needed to constrain r. The second and third terms are tangential and are the Coriolis acceleration components. They are equal, respectively arising from the changing direction of the radial velocity and from the changing magnitude of the tangential velocity. If the angular rate and radial velocities are constant,

$$\frac{d\theta}{dt} = \Omega \qquad \text{Eq.3-21}$$

and

$$\frac{dr}{dt} = v \qquad \text{Eq. 3-22}$$

then

$$\frac{d^2z}{dt^2} = I\,2\,\Omega\, v\,\varepsilon^{i\theta} - \Omega^2\, r\,\varepsilon^{i\theta} \qquad \text{Eq. 3-23}$$

where the angular component, $i\varepsilon^{i\theta}$, indicates a tangential direction in the sense of positive θ for the Coriolis acceleration, $2\Omega v$, and $-\varepsilon^{i\theta}$ indicates towards the center (i.e., *centripetal*) for the $\Omega^2 r$ component

The ADXRS gyros take advantage of this effect by using a resonating mass analogous to the person moving out and in on a rotating platform. The mass is micromachined from

polysilicon and is tethered to a polysilicon frame so that it can resonate only along one direction.

Figure 3.19 shows that when the resonating mass moves toward the outer edge of the rotation, it is accelerated to the right and exerts on the frame a reaction force to the left. When it moves toward the center of the rotation, it exerts a force to the right, as indicated by the arrows.

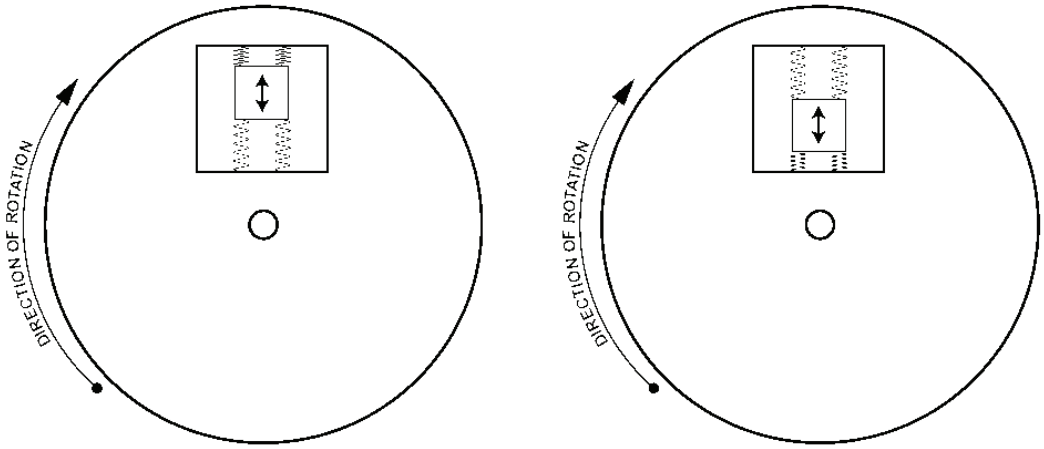

Figure 3.19: *Coriolis Effect Demo 1*

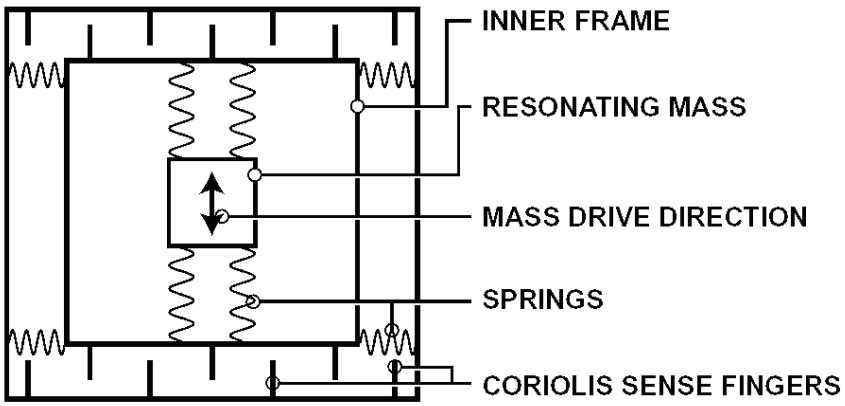

Figure 3.20: *Schematic of the gyro's mechanical structure.*

To measure the Coriolis acceleration, the frame containing the resonating mass is tethered to the substrate by springs at 90° relative to the resonating motion, as shown in Figure 3.20. This figure also shows the Coriolis sense fingers that are used to capacitively sense displacement of the frame in response to the force exerted by the mass, as described Figure 3.19, a demonstration of the Coriolis effect in response to a resonating silicon

mass suspended inside a frame. The orange arrows indicate the force applied to the structure, based on status of the resonating mass.

In figure 3.21 the frame and resonating mass are displaced laterally in response to the Coriolis effect. The displacement is determined from the change in capacitance between the Coriolis sense fingers on the frame and those attached to the substrate.

further on. If the springs have a stiffness, *K*, then the displacement resulting from the reaction force will be 2 Ω*vM/K*

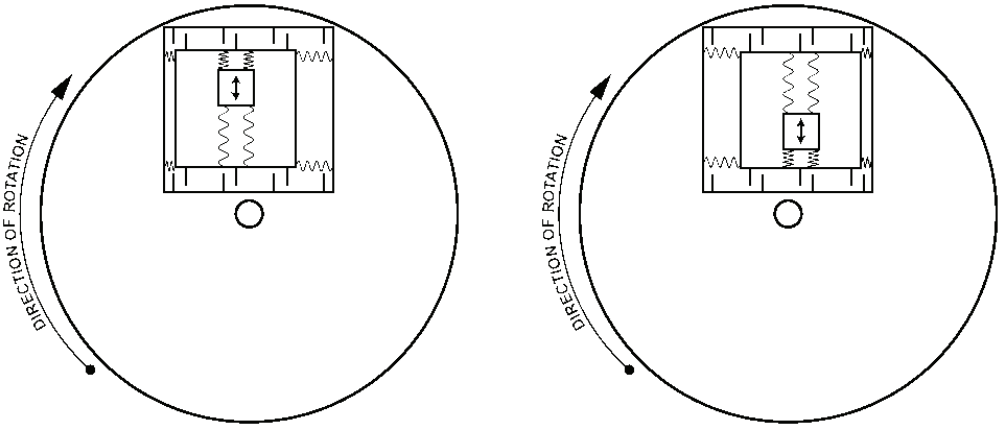

Figure 3.21: *Displacement due to the Coriolis Effect*

Figure 3.21, which shows the complete structure, demonstrates that as the resonating mass moves, and as the surface to which the gyro is mounted rotates, the mass and its frame experience the Coriolis acceleration and are translated 90° from the vibratory movement. As the rate of rotation increases, so does the displacement of the mass and the signal derived from the corresponding capacitance change.

It should be noted that the gyro may be placed anywhere on the rotating object and at any angle, so long as its sensing axis is parallel to the axis of rotation. The above explanation is intended to give an intuitive sense of the function and has been simplified by the placement of the gyro.

Capacitive Sensing

ADXRS gyros measure the displacement of the resonating mass and its frame due to the Coriolis effect through capacitive sensing elements attached to the resonator, as shown in Figures 3.19, 20, and 21. These elements are silicon beams inter-digitated with two sets of stationary silicon beams attached to the substrate, thus forming two nominally equal capacitors. Displacement due to angular rate induces a differential capacitance in this system. If the total capacitance is C and the spacing of the beams is *g*, then the differential capacitance is 2 Ω*vMC/gK*, and is directly proportional to the angular rate. The fidelity of this relationship is excellent in practice, with nonlinearity less than 0.1%.

The ADXRS gyro electronics can resolve capacitance changes as small as 12 x 10^{-21} farads (12 zeptofarads) from beam deflections as small as 0.00016 Angstroms (16 femtometers). The only way this can be utilized in a practical device is by situating the electronics, including amplifiers and filters, on the same die as the mechanical sensor. The differential signal alternates at the resonator frequency and can be extracted from the noise by correlation.

These sub atomic displacements are meaningful as the *average* positions of the surfaces of the beams, even though the individual atoms on the surface are moving randomly by much more. There are about 1012 atoms on the surfaces of the capacitors, so the statistical averaging of their individual motions reduces the uncertainty by a factor of 106. So why can't we do 100 times better? The answer is that the impact of the *air molecules* causes the structure to move—although similarly averaged, their effect is far greater! So why not remove the air? The device is not operated in a vacuum because it is a very fine, thin film weighing only 4 micrograms; its flexures, only 1.7 microns wide, are suspended over the silicon substrate. Air cushions the structure, preventing it from being destroyed by violent shocks—*even those experienced during firing of a guided shell from a howitzer* (as demonstrated recently)

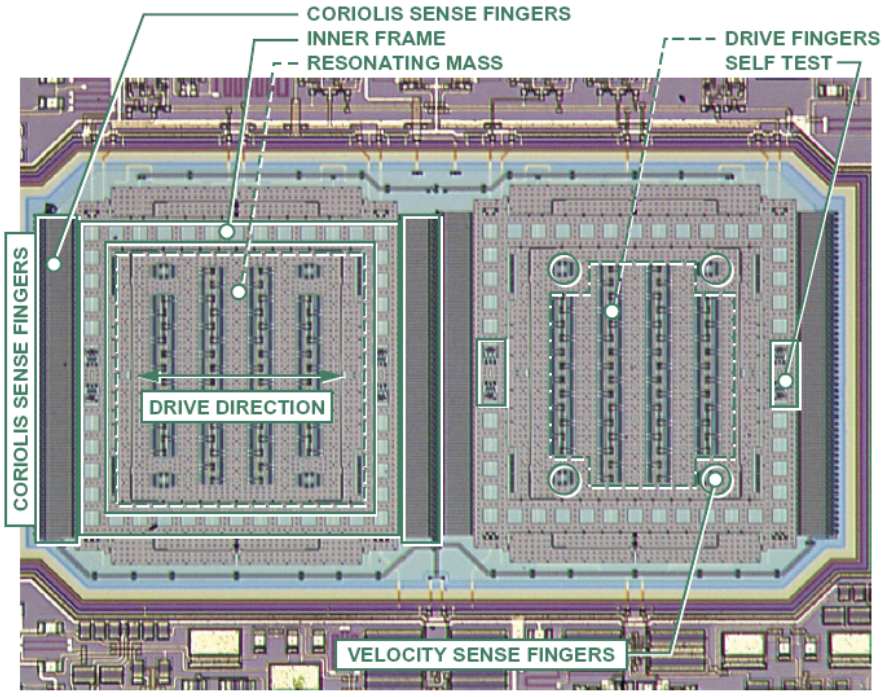

Figure 3.22: *Photograph of mechanical sensor.*

Figure 3.22 shows that the ADXRS gyros include two structures to enable differential sensing in order to reject environmental shock and vibration.

Integration of electronics and mechanical elements is a key feature of products such as the ADXRS150 and ADXRS300, because it makes possible the smallest size and cost for a given performance level. Figure 3.23 is a photograph of the ADXRS die, highlighting the integration of the mechanical rate sensor and the signal conditioning electronics.

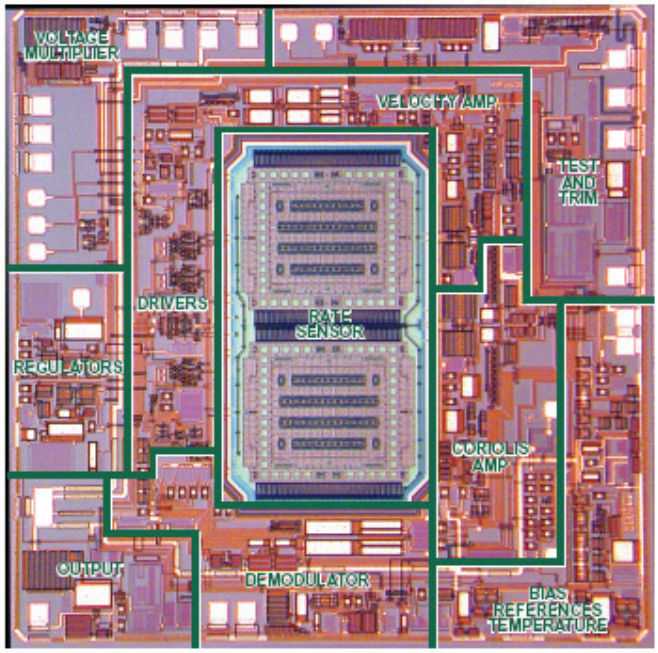

Figure 3.23: *Photograph of ADXRS gyro die*

The ADXRS150 and ADXRS300 are housed in an industry-standard package that simplifies users' product development and production. The ceramic package—a 32-pin ball grid-array, (BGA)—measures 7 mm wide by 7 mm deep by 3 mm tall. It is at least 100 times smaller than any other gyro having similar performance. Besides their small size, these gyros consume 30 mW, far less power than similar gyros. The combination of small size and low power make these products ideally suited for consumer applications such as toy robots, scooters, and navigation devices.

Immunity to Shock and Vibration

One of the most important concerns for a gyro user is the device's ability to reliably provide an accurate angular rate-output signal—even in the presence of environmental shock and vibration. One example of such an application is automotive rollover detection, in which a gyro is used to detect whether *or not* a car (or SUV) is rolling over. Some rollover events are triggered by an impact with another object, such as a curb, that results in a shock to the vehicle. If the shock saturates the gyro sensor, and the gyro cannot filter it out, then the airbags may not deploy. Similarly, if a bump in the road results in a shock or vibration that translates into a rotational signal, the airbags might deploy when not needed—a considerable safety hazard!

As can be seen, the ADXRS gyros employ a novel approach to angular rate-sensing that makes it possible to reject shocks of up to 1,000 *g* — they use two resonators to differentially sense signals and reject common-mode external accelerations that are unrelated to angular motion. This approach is, in part, the reason for the excellent immunity of the ADXRS gyros to shock and vibration. The two resonators in Figure 3.22 are mechanically independent, and they operate anti-phase. As a result, they measure the same magnitude of rotation, but give outputs in opposite directions. Therefore, the difference between the two sensor signals is used to measure angular rate. This cancels non-rotational signals that affect both sensors. The signals are combined in the internal hard-wiring ahead of the very sensitive preamplifiers. Thus, extreme acceleration overloads are largely prevented from reaching the electronics—thereby allowing the signal conditioning to preserve the angular rate output during large shocks. This scheme requires that the two sensors be well-matched, precisely fabricated copies of each other.

REFERENCES

1. Herman Schaevitz, "The Linear Variable Differential Transformer", **Proceedings of the SASE**, Volume IV, No. 2, 1946.

2. Dr. Ernest D.D. Schmidt, "Linear Displacement - Linear Variable Differential Transformers – LVDTs", Schaevitz Sensors, http://www.schaevitz.com.

3. E-Series LVDT Data Sheet, Schaevitz Sensors, http://www.schaevitz.com.
Schaevitz Sensors is now a division of Lucas Control Systems, 1000 Lucas Way, Hampton, VA 23666.

4. Ramon Pallas-Areny and John G. Webster, **Sensors and Signal Conditionin**g, John Wiley, New York, 1991.

5. Harry L. Trietley, **Transducers in Mechanical and Electronic Design**, Marcel Dekker, Inc., 1986.

6. AD598 and AD698 Data Sheet, Analog Devices, Inc., http://www.analog.com.

7. Bill Travis, "Hall-Effect Sensor ICs Sport Magnetic Personalitie*"s*, **EDN,** April 9, 1998, pp. 81-91.

8. AD22151 Data Sheet, Analog Devices, Inc., http://www.analog.com.

9. Dan Sheingold, **Analog-Digital Conversion Handbook, Third Edition**, Prentice-Hall, 1986.

10. F. P. Flett, "Vector Control Using a Single Vector Rotation Semiconductor for Induction and Permanent Magnet Motor"*s*, **PCIM Conference, Intelligent Motion, September 1992 Proceedings**, Available from Analog Devices.

11. F. P. Flett, "Silicon Control Algorithms for Brushless Permanent Magnet Synchronous Machines*"*, **PCIM Conference, Intelligent Motion, June 1991 Proceedings**, Available from Analog Devices.

12. P.J.M. Coussens, et al, "Three Phase Measurements with Vector Rotation Blocks in Mains and Motion Control", **PCIM Conference, Intelligent Motion, April 1992 Proceedings**, Available from Analog Devices.

13. Dennis Fu, "Digital to Synchro and Resolver Conversion with the AC Vector Processor AD2S100", Available from Analog Devices.

14. Dennis Fu, "Circuit Applications of the AD2S90 Resolver-to-Digital Converter, AN-230", Analog Devices.

15. Aengus Murray and P. Kettle, "Towards a Single Chip DSP Based Motor Control Solution", **Proceedings PCIM - Intelligent Motion**, May 1996, Nurnberg Germany, pp. 315-326. Also available at http://www.analog.com.

16. D. J. Lucey, P. J. Roche, M. B. Harrington, and J. R. Scannell, "Comparison of Various Space Vector Modulation Strategies", **Proceedings Irish DSP and Control Colloquium**, July 1994, Dublin, Ireland, pp. 169-175.

17. Niall Lyne, "ADCs Lend Flexibility to Vector Motor Control Application", **Electronic Design**, May 1, 1998, pp. 93-100.

18. Frank Goodenough, "Airbags Boom when IC Accelerometer Sees 50g," **Electronic Design**, August 8, 1991.

SECTION 3.2: TEMPERATURE SENSORS

Introduction

Measurement of temperature is critical in modern electronic devices, especially expensive laptop computers and other portable devices with densely packed circuits which dissipate considerable power in the form of heat. Knowledge of system temperature can also be used to control battery charging as well as prevent damage to expensive microprocessors.

Compact high power portable equipment often has fan cooling to maintain junction temperatures at proper levels. In order to conserve battery life, the fan should only operate when necessary. Accurate control of the fan requires a knowledge of critical temperatures from the appropriate temperature sensor.

Accurate temperature measurements are required in many other measurement systems such as process control and instrumentation applications. In most cases, because of low-level nonlinear outputs, the sensor output must be properly conditioned and amplified before further processing can occur.

Except for IC sensors, all temperature sensors have nonlinear transfer functions. In the past, complex analog conditioning circuits were designed to correct for the sensor nonlinearity. These circuits often required manual calibration and precision resistors to achieve the desired accuracy. Today, however, sensor outputs may be digitized directly by high resolution ADCs. Linearization and calibration is then performed digitally, thereby reducing cost and complexity.

Resistance Temperature Devices (RTDs) are accurate, but require excitation current and are generally used in bridge circuits. Thermistors have the most sensitivity but are the most non-linear. However, they are popular in portable applications such as measurement of battery temperature and other critical temperatures in a system.

Modern semiconductor temperature sensors offer high accuracy and high linearity over an operating range of about –55ºC to +150ºC. Internal amplifiers can scale the output to convenient values, such as 10 mV/ºC. They are also useful in cold-junction-compensation circuits for wide temperature range thermocouples. Semiconductor temperature sensors can be integrated into multi-function ICs which perform a number of other hardware monitoring functions.

Figure 3.24 lists the most popular types of temperature transducers and their characteristics.

THERMOCOUPLE	RTD	THERMISTOR	SEMICONDUCTOR
Widest Range: –184ºC to +2300ºC	Range: –200ºC to +850ºC	Range: 0ºC to +100ºC	Range: –55ºC to +150ºC
High Accuracy and Repeatability	Fair Linearity	Poor Linearity	Linearity: 1ºC Accuracy: 1ºC
Needs Cold Junction Compensation	Requires Excitation	Requires Excitation	Requires Excitation
Low-Voltage Output	Low Cost	High Sensitivity	10mV/K, 20mV/K, or 1µA/K Typical Output

Figure 3.24: *Types of Temperature Sensors*

Semiconductor Temperature Sensors

Modern semiconductor temperature sensors offer high accuracy and high linearity over an operating range of about –55°C to +150°C. Internal amplifiers can scale the output to convenient values, such as 10 mV/°C. They are also useful in cold-junction-compensation circuits for wide temperature range thermocouples.

All semiconductor temperature sensors make use of the relationship between a bipolar junction transistor's (BJT) base-emitter voltage to its collector current:

$$V_{BE} = \frac{kT}{q} \ln\left(\frac{I_c}{I_S}\right) \qquad \text{Eq. 3-24}$$

where k is Boltzmann's constant, T is the absolute temperature, q is the charge of an electron, and I_S is a current related to the geometry and the temperature of the transistors. (The equation assumes a voltage of at least a few hundred mV on the collector, and ignores Early effects.)

If we take N transistors identical to the first (see Figure 3.25) and allow the total current I_C to be shared equally among them, we find that the new base-emitter voltage is given by the equation

$$V_N = \frac{kT}{q} \ln\left(\frac{I_c}{N \cdot I_S}\right) \qquad \text{Eq. 3-25}$$

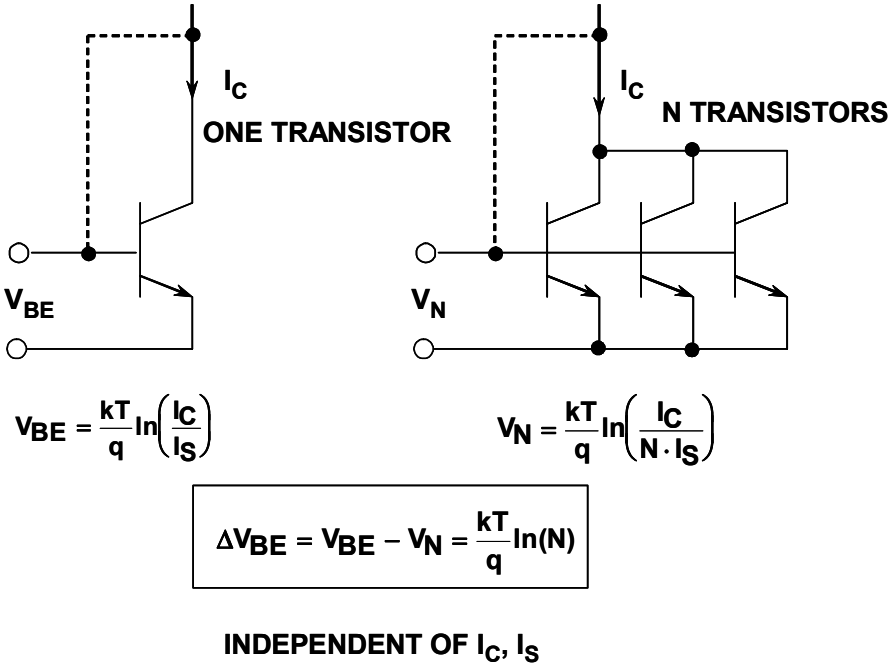

Figure 3.25: *Basic Relationships for Semiconductor Temperature Sensors*

Neither of these circuits is of much use by itself because of the strongly temperature dependent current I_S, but if we have equal currents in one BJT and N similar BJTs then the expression for the *difference* between the two base-emitter voltages is proportional to absolute temperature and does not contain I_S.

$$\Delta V_{BE} = V_{BE} - V_N = \frac{kT}{q}\ln\left(\frac{I_c}{I_S}\right) - \frac{kT}{q}\ln\left(\frac{I_c}{N \cdot I_S}\right) \qquad \text{Eq.3-26}$$

$$\Delta V_{BE} = V_{BE} - V_N = \frac{kT}{q}\left[\ln\left(\frac{I_c}{I_S}\right) - \ln\left(\frac{I_c}{N \cdot I_S}\right)\right] \qquad \text{Eq.3-27}$$

$$\Delta V_{BE} = V_{BE} - V_N = \frac{kT}{q}\ln\left[\left(\frac{I_c}{I_S}\right) \Big/ \left(\frac{I_c}{N \cdot I_S}\right)\right] = \frac{kT}{q}\ln(N) \qquad \text{Eq. 3-28}$$

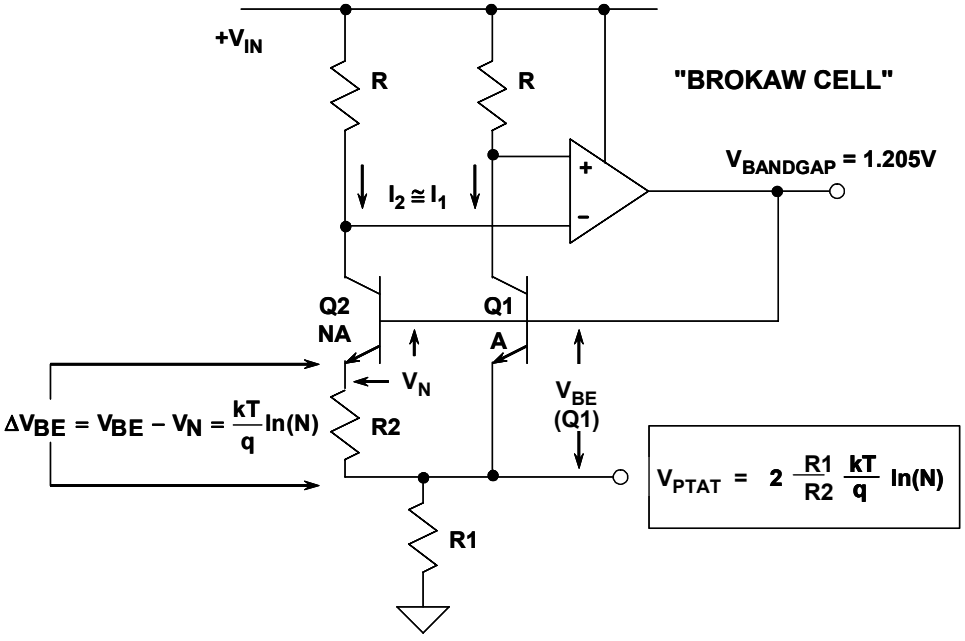

Figure 3.26: *Classic Bandgap Temperature Sensor*

The circuit shown in Figure 3.26 implements the above equation and is known as the "Brokaw Cell" (see Reference 10). The voltage $\Delta V_{BE} = V_{BE} - V_N$ appears across resistor R2. The emitter current in Q2 is therefore $\Delta V_{BE}/R2$. The op amp's servo loop and the resistors, R, force the same current to flow through Q1. The Q1 and Q2 currents

are equal and are summed and flow into resistor R1. The corresponding voltage developed across R1 is proportional to absolute temperature (PTAT) and given by:

$$V_{PTAT} = \frac{2R1(V_{BE} - V_N)}{R2} = 2\frac{R1}{R2}\frac{kT}{q}\ln(N) \qquad \text{Eq. 3-29}$$

The bandgap cell reference voltage, $V_{BANDGAP}$, appears at the base of Q1 and is the sum of $V_{BE}(Q1)$ and V_{PTAT}. $V_{BE(Q1)}$ is complementary to absolute temperature (CTAT), and summing it with V_{PTAT} causes the bandgap voltage to be constant with respect to temperature (assuming proper choice of R1/R2 ratio and N to make the bandgap voltage equal to 1.205 V). This circuit is the basic *band-gap* temperature sensor, and is widely used in semiconductor temperature sensors.

Current Out Temperature Sensors

This type of temperature sensor produces a current output proportional to absolute temperature. For supply voltages between 4 V and 30 V the device acts as a high impedance constant current regulator with an output proportional to absolute temperature with a typical transfer function of 1 µA/°K. This means that at 25°C there will be 298 µA flowing in the loop.

A current output temperature sensor such as the AD590 is particularly useful in remote sensing applications. These devices are insensitive to voltage drops over long lines due to their high impedance current outputs. The output characteristics also make this type of device easy to multiplex: the current can be switched by a simple logic gate as shown in the figure.

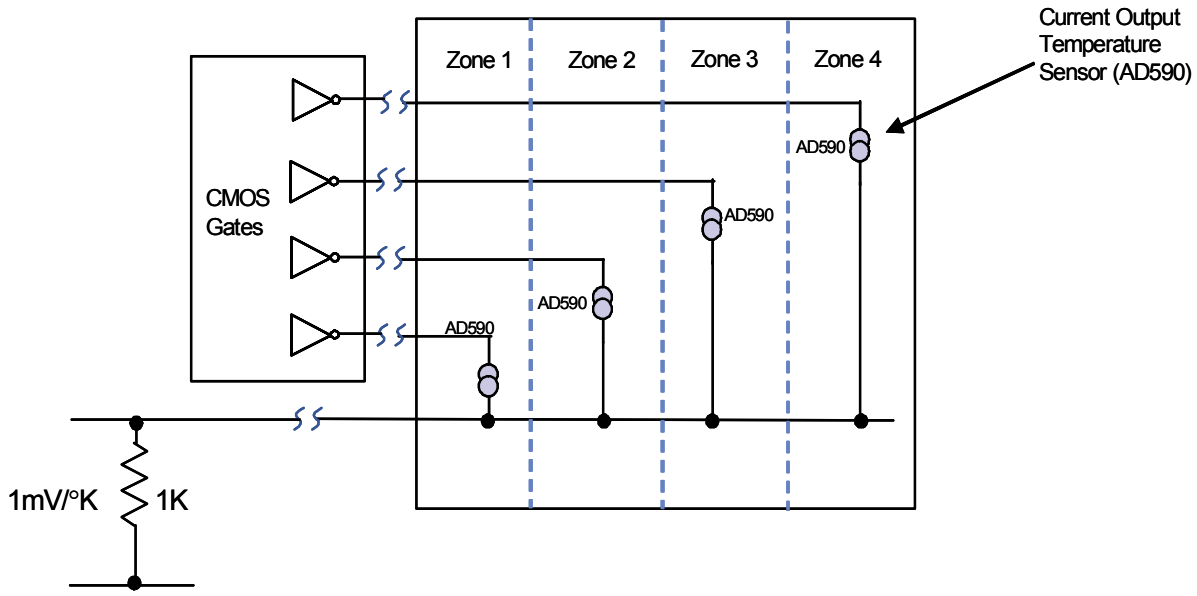

Figure 3.27: *Multiplexed AD590 Application*

Current and Voltage Output Temperature Sensors

The concepts used in the bandgap temperature sensor discussion above can be used as the basis for a variety of IC temperature sensors to generate either current or voltage outputs.

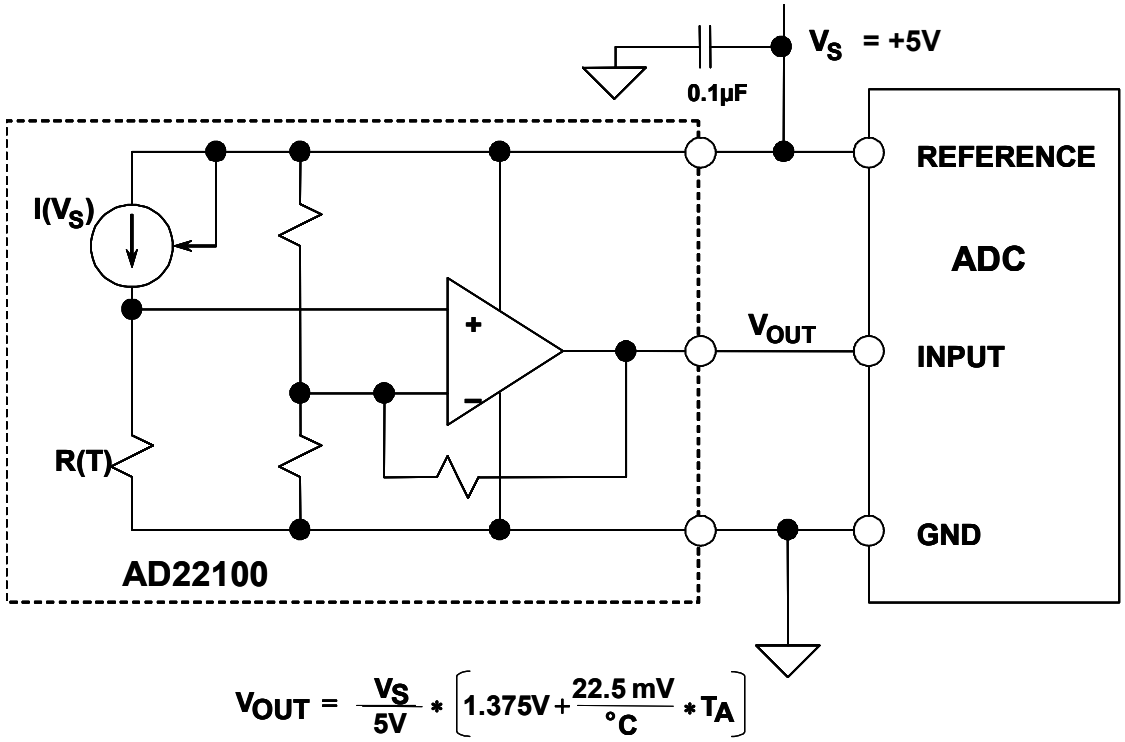

Figure 3.28: *Ratiometric Voltage Output Sensor*

In some cases, it is desirable for the output of a temperature sensor to be ratiometric with its supply voltage. The AD22100 (see Figure 3.29) has an output that is ratiometric with its supply voltage (nominally 5 V) according to the equation:

$$V_{OUT} = \frac{V_S}{5V} * \left[1.375\ V + \frac{22.5\ mV}{°C} * T_A \right] \qquad \text{Eq.3-30}$$

The circuit shown in Figure 3.28 uses the AD22100 power supply as the reference to the ADC, thereby eliminating the need for a precision voltage reference.

The thermal time constant of a temperature sensor is defined to be the time required for the sensor to reach 63.2% of the final value for a step change in the temperature. Figure 3.29 shows the thermal time constant of the ADT45/ADT50 series of sensors with the SOT-23-3 package soldered to 0.338" x 0.307" copper PC board as a function of air flow velocity. Note the rapid drop from 32 seconds to 12 seconds as the air velocity increases from 0 (still air) to 100 LFPM. As a point of reference, the thermal time constant of the ADT45/ADT50 series in a stirred oil bath is less than 1 second, which verifies that the major part of the thermal time constant is determined by the case.

The power supply pin of these sensors should be bypassed to ground with a 0.1 μF ceramic capacitor having very short leads (preferably surface mount) and located as close to the power supply pin as possible. Since these temperature sensors operate on very little supply current and could be exposed to very hostile electrical environments, it is important to minimize the effects of EMI/RFI on these devices. The effect of RFI on these temperature sensors is manifested as abnormal DC shifts in the output voltage due to rectification of the high frequency noise by the internal IC junctions. In those cases where the devices are operated in the presence of high frequency radiated or conducted noise, a large value tantalum electrolytic capacitor (>2.2 μF) placed across the 0.1 μF ceramic may offer additional noise immunity.

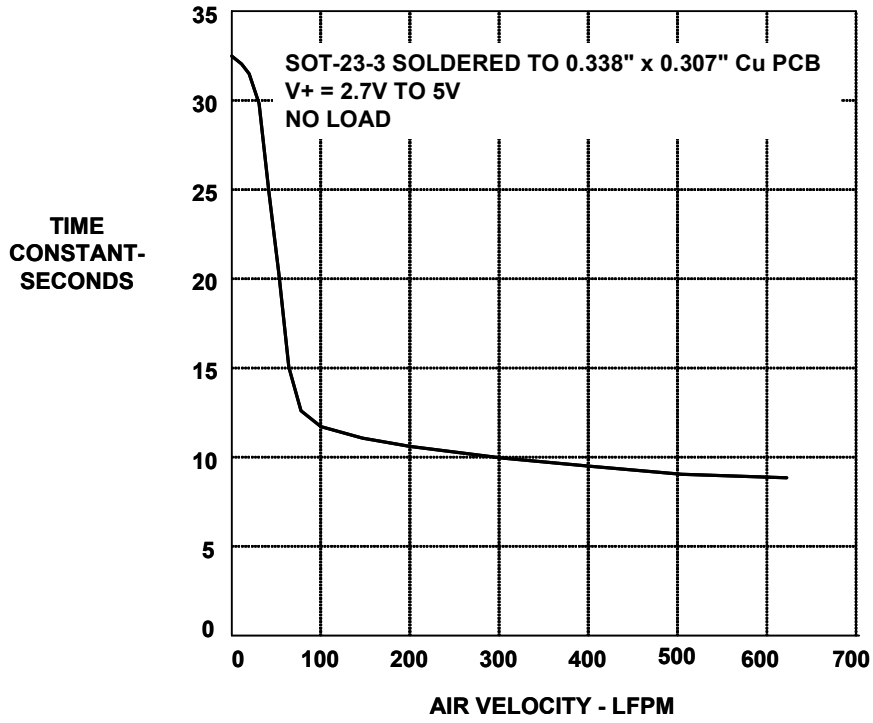

Figure 3.29: *Thermal Response in Forced Air for SOT-23-2 Package*

Thermocouple Principles and Cold-Junction Compensation

Thermocouples are small, rugged, relatively inexpensive, and operate over the widest range of all temperature sensors. They are especially useful for making measurements at extremely high temperatures (up to +2300°C) in hostile environments. They produce only millivolts of output, however, and require precision amplification for further processing. They also require cold-junction-compensation (CJC) techniques which will be discussed shortly. They are more linear than many other sensors, and their non-linearity has been well characterized. Some common thermocouples are shown in Figure 3.30. The most common metals used are Iron, Platinum, Rhodium, Rhenium, Tungsten, Copper, Alumel (composed of Nickel and Aluminum), Chromel (composed of Nickel and Chromium) and Constantan (composed of Copper and Nickel).

JUNCTION MATERIALS	TYPICAL USEFUL RANGE (ºC)	NOMINAL SENSITIVITY (µV/ºC)	ANSI DESIGNATION
Platinum (6%)/ Rhodium-Platinum (30%)/Rhodium	38 to 1800	7.7	B
Tungsten (5%)/Rhenium - Tungsten (26%)/Rhenium	0 to 2300	16	C
Chromel - Constantan	0 to 982	76	E
Iron - Constantan	0 to 760	55	J
Chromel - Alumel	–184 to 1260	39	K
Platinum (13%)/Rhodium-Platinum	0 to 1593	11.7	R
Platinum (10%)/Rhodium-Platinum	0 to 1538	10.4	S
Copper-Constantan	–184 to 400	45	T

Figure 3.30: *Common Thermocouples*

Figure 3.31 shows the voltage-temperature curves of three commonly used thermocouples, referred to a 0°C fixed-temperature reference junction. Of the thermocouples shown, Type J thermocouples are the most sensitive, producing the largest output voltage for a given temperature change. On the other hand, Type S thermocouples are the least sensitive. These characteristics are very important to consider when designing signal conditioning circuitry in that the thermocouples' relatively low output signals require low-noise, low-drift, high-gain amplifiers.

To understand thermocouple behavior, it is necessary to consider the non-linearities in their response to temperature differences. Figure 3.31 shows the relationships between sensing junction temperature and voltage output for a number of thermocouple types (in

all cases, the reference *cold* junction is maintained at 0°C). It is evident that the responses are not quite linear, but the nature of the non-linearity is not so obvious.

Figure 3.32 shows how the Seebeck coefficient (the *change* of output voltage with *change* of sensor junction temperature - i.e., the first derivative of output with respect to temperature) varies with sensor junction temperature (we are still considering the case where the reference junction is maintained at 0°C).

When selecting a thermocouple for making measurements over a particular range of temperature, we should choose a thermocouple whose Seebeck coefficient varies as little as possible over that range.

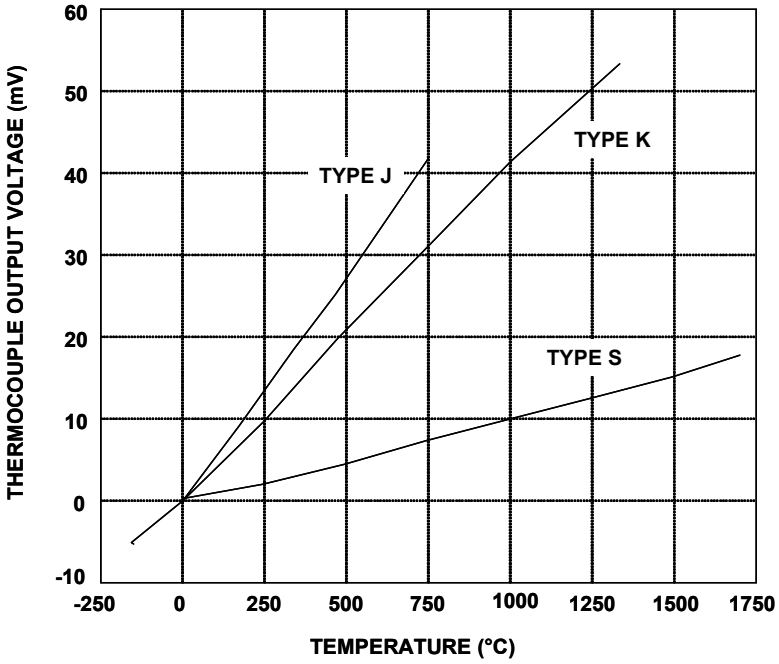

Figure 3.31: *Thermocouple Output Voltages for Type J, K and S Thermocouples*

For example, a Type J thermocouple has a Seebeck coefficient which varies by less than 1 μV/°C between 200 and 500°C, which makes it ideal for measurements in this range.

Presenting these data on thermocouples serves two purposes: First, Figure 3.30 illustrates the range and sensitivity of the three thermocouple types so that the system designer can, at a glance, determine that a Type S thermocouple has the widest useful temperature range, but a Type J thermocouple is more sensitive. Second, the Seebeck coefficients provide a quick guide to a thermocouple's linearity. Using Figure 3.31, the system designer can choose a Type K thermocouple for its linear Seebeck coefficient over the range of 400°C to 800°C or a Type S over the range of 900°C to 1700°C. The behavior of a thermocouple's Seebeck coefficient is important in applications where variations of

temperature rather than absolute magnitude are important. These data also indicate what performance is required of the associated signal conditioning circuitry.

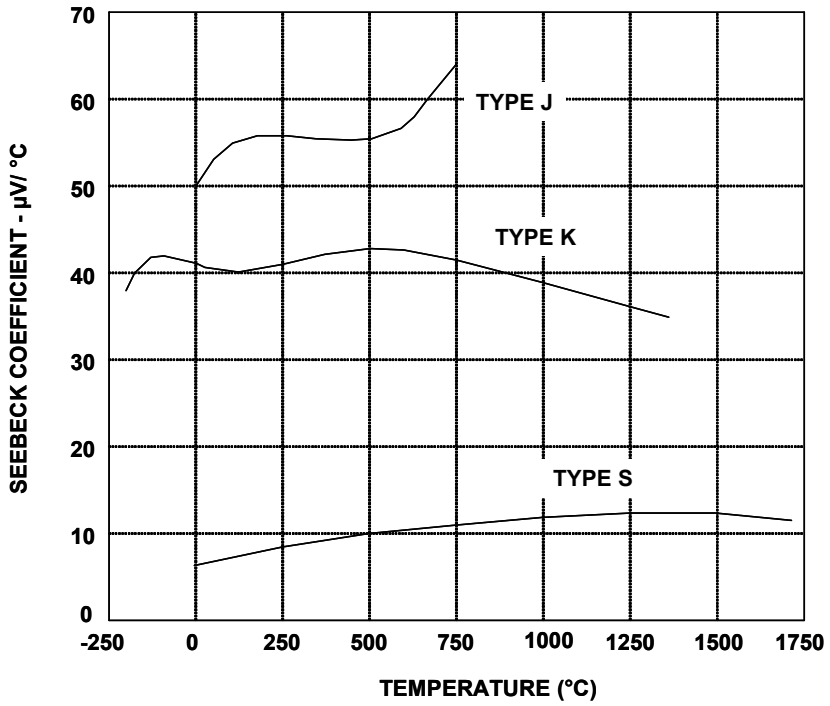

Figure 3.32: *Thermocouple Seebeck Coefficient vs. Temperature*

To use thermocouples successfully we must understand their basic principles. Consider the diagrams in Figure 3.33.

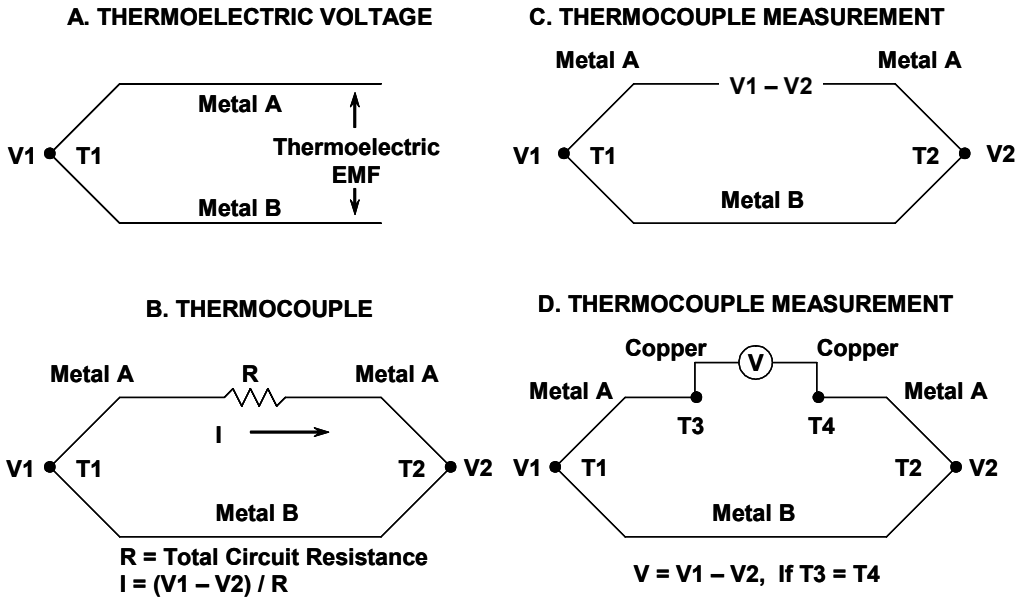

Figure 3.33: *Thermocouple Basics*

If we join two dissimilar metals at any temperature above absolute zero, there will be a potential difference between them (their "thermoelectric e.m.f." or "contact potential") which is a function of the temperature of the junction (Figure 3.33A). If we join the two wires at two places, two junctions are formed (Figure 3.33B). If the two junctions are at different temperatures, there will be a net e.m.f. in the circuit, and a current will flow determined by the e.m.f. and the total resistance in the circuit (Figure 3.33B). If we break one of the wires, the voltage across the break will be equal to the net thermoelectric e.m.f. of the circuit, and if we measure this voltage, we can use it to calculate the temperature difference between the two junctions (Figure 3.33C). *We must always remember that a thermocouple measures the temperature difference between two junctions, not the absolute temperature at one junction*. We can only measure the temperature at the measuring junction if we know the temperature of the other junction (often called the "reference" junction or the "cold" junction).

But it is not so easy to measure the voltage generated by a thermocouple. Suppose that we attach a voltmeter to the circuit in Figure 3.33C (Figure 3.33D). The wires attached to the voltmeter will form further thermojunctions where they are attached. If both these additional junctions are at the same temperature (it does not matter what temperature), then the "Law of Intermediate Metals" states that they will make no net contribution to the total e.m.f. of the system. If they are at different temperatures, they will introduce errors. Since *every pair of dissimilar metals in contact generates a thermoelectric e.m.f.* (including copper/solder, kovar/copper [kovar is the alloy used for IC leadframes] and aluminum/kovar [at the bond inside the IC]), it is obvious that in practical circuits the problem is even more complex, and it is necessary to take extreme care to ensure that all the junction pairs in the circuitry around a thermocouple, except the measurement and reference junctions themselves, are at the same temperature.

Thermocouples generate a voltage, albeit a very small one, and do not require excitation. As shown in Figure 3.33D, however, two junctions (T1, the measurement junction and T2, the reference junction) are involved. If T2 = T1, then V2 = V1, and the output voltage V = 0. Thermocouple output voltages are often defined with a reference junction temperature of 0ºC (hence the term *cold* or *ice point* junction), so the thermocouple provides an output voltage of 0 V at 0ºC. To maintain system accuracy, the reference junction must therefore be at a well-defined temperature (but not necessarily 0ºC). A conceptually simple approach to this need is shown in Figure 3.34. Although an ice/water bath is relatively easy to define, it is quite inconvenient to maintain.

Today an ice-point reference, and its inconvenient ice/water bath, is generally replaced by electronics. A temperature sensor of another sort (often a semiconductor sensor, sometimes a thermistor) measures the temperature of the cold junction and is used to inject a voltage into the thermocouple circuit which compensates for the difference between the actual cold junction temperature and its ideal value (usually 0°C) as shown in Figure 3.35. Ideally, the compensation voltage should be an exact match for the difference voltage required, which is why the diagram gives the voltage as f(T2) (a *function* of T2) rather than KT2, where K is a simple constant. In practice, since the cold

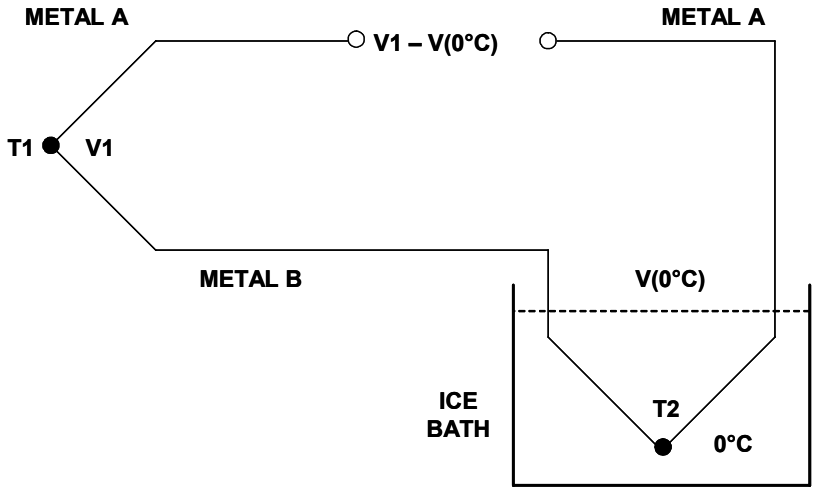

Figure 3.34: *Classic Cold-Junction Compensation Using an Ice-Point (0°C) Reference Junction*

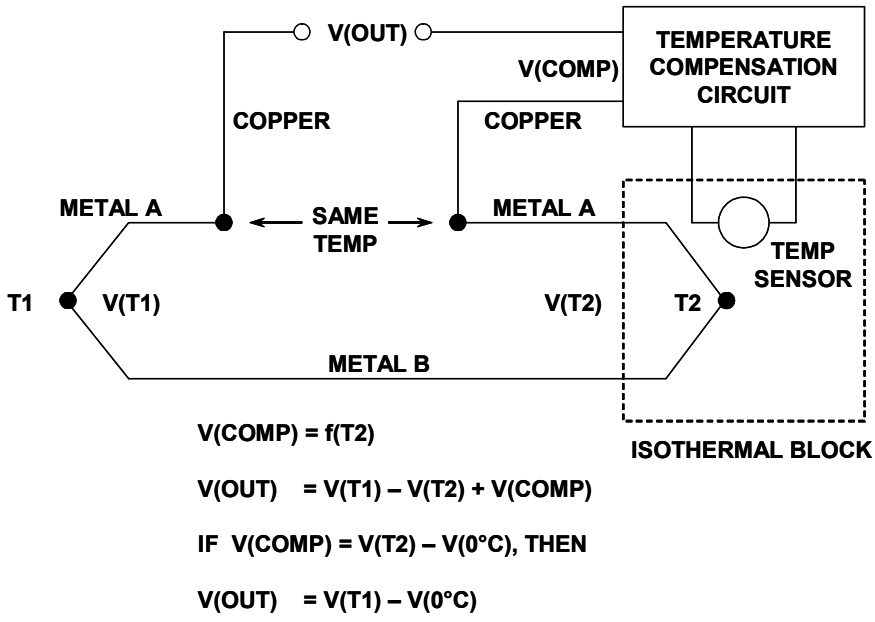

Figure 3.35: *Using a Temperature Sensor for Cold-Junction Compensations*

junction is rarely more than a few tens of degrees from 0°C, and generally varies by little more than ±10°C, a linear approximation (V = KT2) to the more complex reality is sufficiently accurate and is what is often used. (The expression for the output voltage of a thermocouple with its measuring junction at T°C and its reference at 0°C is a polynomial of the form $V = K_1T + K_2T^2 + K_3T^3 + ...$, but the values of the coefficients K_2, K_3, etc.

are very small for most common types of thermocouple. References 8 and 9 give the values of these coefficients for a wide range of thermocouples.)

When electronic cold-junction compensation is used, it is common practice to eliminate the additional thermocouple wire and terminate the thermocouple leads in the isothermal block in the arrangement shown in Figure 3.36. The Metal A-Copper and the Metal B-Copper junctions, if at the same temperature, are equivalent to the Metal A-Metal B thermocouple junction in Figure 3.35.

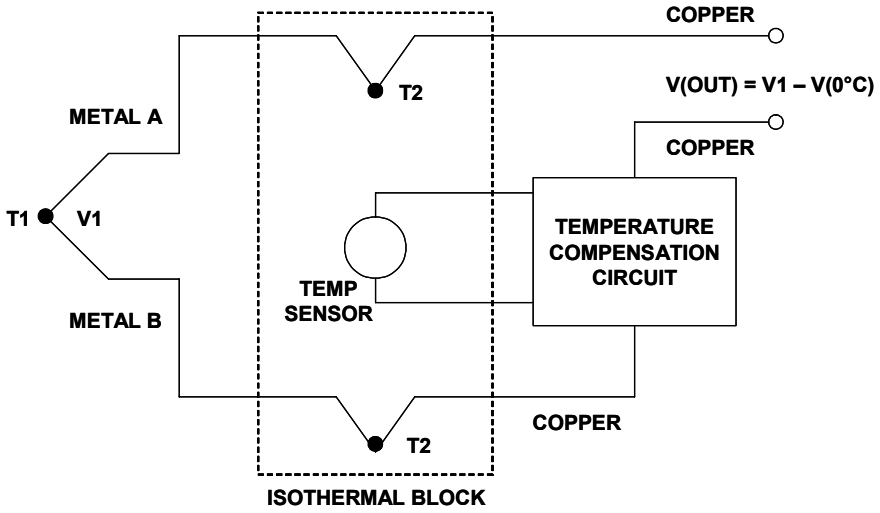

Figure 3.36: *Terminating Thermocouple Leads Directly to an Isothermal Block*

The circuit in Figure 3.37 conditions the output of a Type K thermocouple, while providing cold-junction compensation, for temperatures between 0ºC and 250ºC. The circuit operates from single +3.3 V to +12 V supplies and has been designed to produce an output voltage transfer characteristic of 10 mV/ºC.

A Type K thermocouple exhibits a Seebeck coefficient of approximately 41 µV/ºC; therefore, at the cold junction, the TMP35 voltage output sensor with a temperature coefficient of 10 mV/ºC is used with R1 and R2 to introduce an opposing cold-junction temperature coefficient of –41 µV/ºC. This prevents the isothermal, cold-junction connection between the circuit's printed circuit board traces and the thermocouple's wires from introducing an error in the measured temperature. This compensation works extremely well for circuit ambient temperatures in the range of 20ºC to 50ºC. Over a 250ºC measurement temperature range, the thermocouple produces an output voltage change of 10.151 mV. Since the required circuit's output full-scale voltage change is 2.5 V, the gain of the circuit is set to 246.3. Choosing R4 equal to 4.99 kΩ sets R5 equal to 1.22 MΩ. Since the closest 1% value for R5 is 1.21 MΩ, a 50 kΩ potentiometer is used with R5 for fine trim of the full-scale output voltage. Although the OP193 is a single-supply op amp, its output stage is not rail-to-rail, and will only go down to about 0.1 V above ground. For this reason, R3 is added to the circuit to supply an output offset voltage of about 0.1V for a nominal supply voltage of 5 V. This offset (10°C) must be

subtracted when making measurements referenced to the OP193 output. R3 also provides an open thermocouple detection, forcing the output voltage to greater than 3 V should the thermocouple open. Resistor R7 balances the DC input impedance of the OP193, and the 0.1 µF film capacitor reduces noise coupling into its non-inverting input.

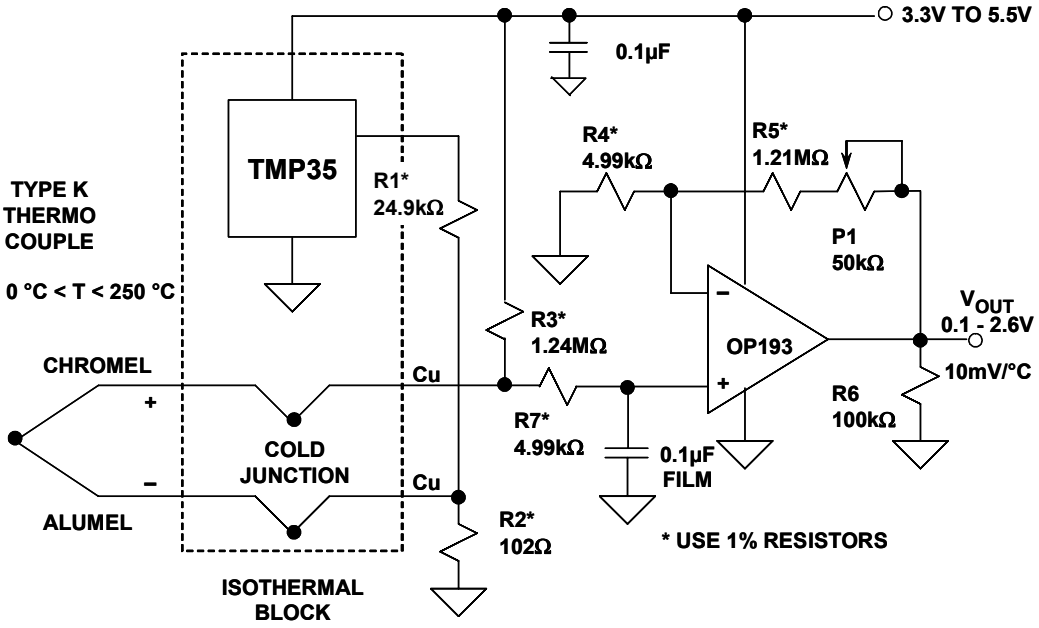

Figure 3.37: *Using a Temperature Sensor for Cold-Junction Compensation (TMP35)*

The AD594/AD595 is a complete instrumentation amplifier and thermocouple cold junction compensator on a monolithic chip (see Figure 3.38). It combines an ice point reference with a precalibrated amplifier to provide a high level (10 mV/°C) output directly from the thermocouple signal. Pin-strapping options allow it to be used as a linear amplifier-compensator or as a switched output set-point controller using either fixed or remote set-point control. It can be used to amplify its compensation voltage directly, thereby becoming a stand-alone Celsius transducer with 10 mV/°C output. In such applications it is very important that the IC chip is at the same temperature as the cold junction of the thermocouple, which is usually achieved by keeping the two in close proximity and isolated from any heat sources.

The AD594/AD595 includes a thermocouple failure alarm that indicates if one or both thermocouple leads open. The alarm output has a flexible format which includes TTL drive capability. The device can be powered from a single-ended supply (which may be as low as +5 V), but by including a negative supply, temperatures below 0°C can be measured. To minimize self-heating, an unloaded AD594/AD595 will operate with a supply current of 160 µA, but is also capable of delivering ±5 mA to a load.

The AD594 is precalibrated by laser wafer trimming to match the characteristics of type J (iron/constantan) thermocouples, and the AD595 is laser trimmed for type K

(chromel/alumel). The temperature transducer voltages and gain control resistors are available at the package pins so that the circuit can be recalibrated for other thermocouple types by the addition of resistors. These terminals also allow more precise calibration for both thermocouple and thermometer applications. The AD594/AD595 is available in two performance grades. The C and the A versions have calibration accuracies of ±1°C and ±3°C, respectively. Both are designed to be used with cold junctions between 0 to +50°C. The circuit shown in Figure 7.11 will provide a direct output from a type J thermocouple (AD594) or a type K thermocouple (AD595) capable of measuring 0 to +300°C.

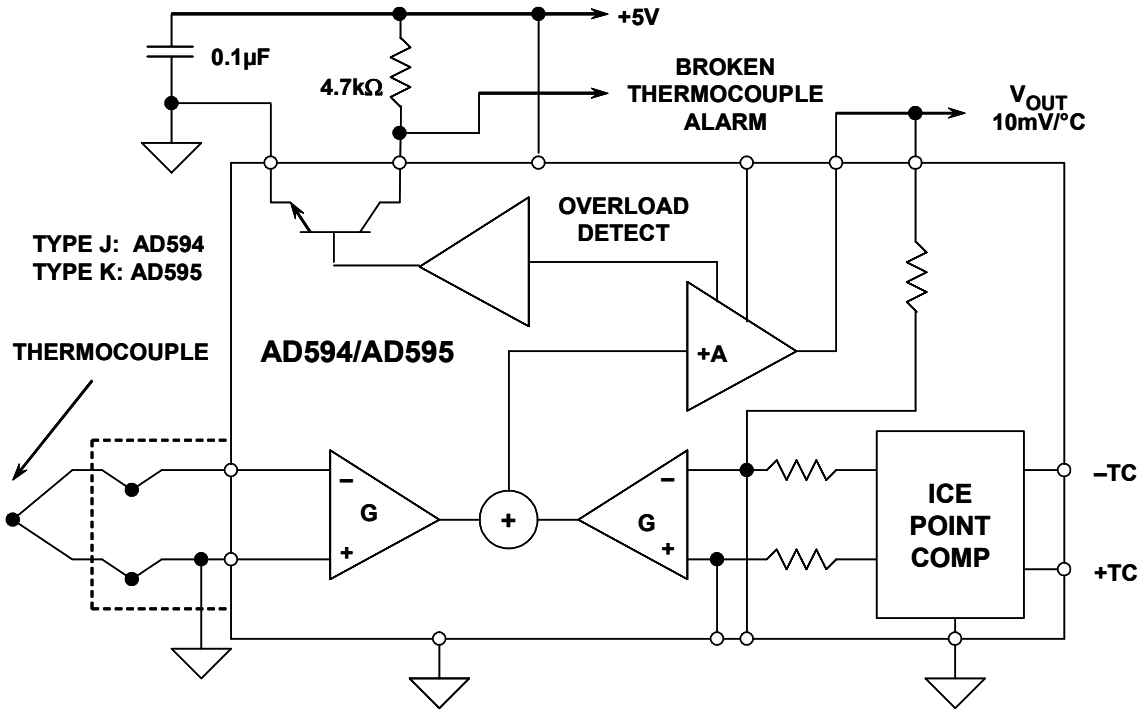

Figure 3.38: *AD594/AD595 Monolithic Thermocouple Amplifier with Cold-Junction Compensation*

The AD596/AD597 are monolithic set-point controllers which have been optimized for use at elevated temperatures as are found in oven control applications. The device cold-junction compensates and amplifies a type J/K thermocouple to derive an internal signal proportional to temperature. They can be configured to provide a voltage output (10mV/°C) directly from type J/K thermocouple signals. The device is packaged in a 10-pin metal can and is trimmed to operate over an ambient range from +25°C to +100°C. The AD596 will amplify thermocouple signals covering the entire –200°C to +760°C temperature range recommended for type J thermocouples while the AD597 can accommodate –200°C to +1250°C type K inputs. They have a calibration accuracy of ±4°C at an ambient temperature of 60°C and an ambient temperature stability specification of 0.05°C/°C from +25°C to +100°C.

None of the thermocouple amplifiers previously described compensate for thermocouple non-linearity, they only provide conditioning and voltage gain. High resolution ADCs

such as the AD77XX family can be used to digitize the thermocouple output directly, allowing a microcontroller to perform the transfer function linearization as shown in Figure 3.39. The two multiplexed inputs to the ADC are used to digitize the thermocouple voltage and the cold-junction temperature sensor outputs directly. The input PGA gain is programmable from 1 to 128, and the ADC resolution is between 16 and 22 bits (depending upon the particular ADC selected). The mIcrocontroller performs both the cold-junction compensation and the linearization arithmetic.

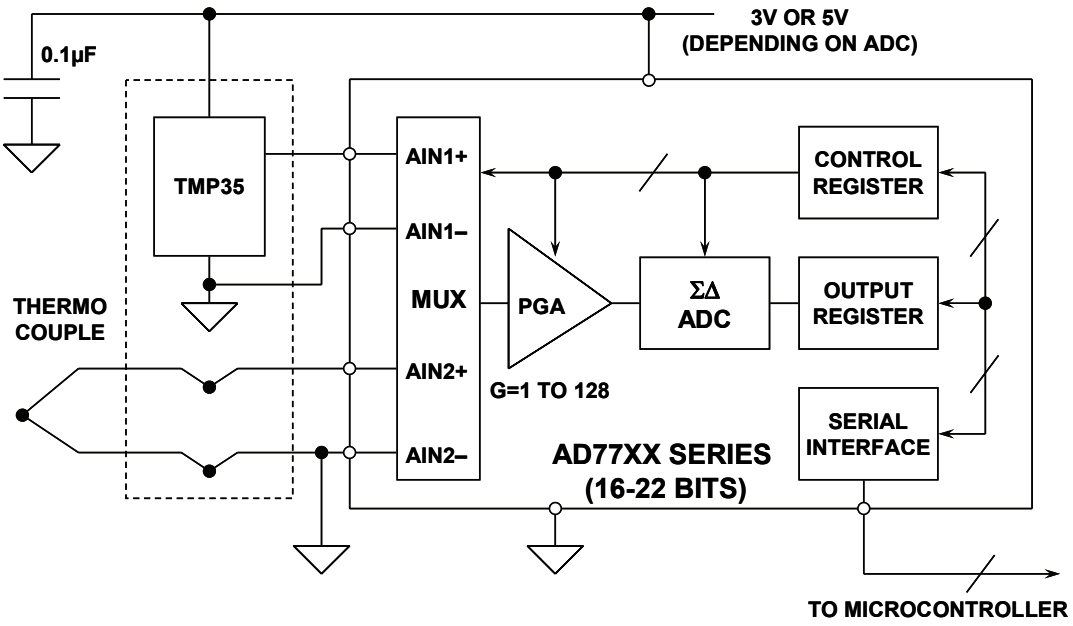

Figure 3.39: *AD77XX ΣΔ ADC Used with TMP35 Temperature Sensor for Cold-Junction Compensation*

Auto-zero Amplifier for Thermocouple Measurements

In addition to the devices mentioned above, ADI has released an auto-zero instrumentation amplifier, the AD8230, designed to amplify thermocouple and bridge outputs. Through the use of auto-zeroing, this product has an offset voltage drift of less than 50 nV/°C which is 1,000 times less than the signal produced by a typical thermocouple. This allows very accurate measurement of the thermocouple signal. In addition, the instrumentation amplifier architecture rejects common mode voltages that often appear when using thermocouples for temperature measurement. This product is typically used in applications involving a bank of thermocouples with one temperature reference point which is compensated for in the system micro-controller. Other applications include highly accurate bridge transducer measurements.

Auto-zeroing is a dynamic offset and drift cancellation technique that reduces input referred voltage offset to the μV level and voltage offset drift to the nV/°C level. A further advantage of dynamic offset cancellation is the reduction of low frequency noise, in particular the 1/f component.

The AD8230 is an instrumentation amplifier that uses an auto-zeroing topology and combines it with high common-mode signal rejection. The internal signal path consists of an active differential sample-and-hold stage (pre-amp) followed by a differential amplifier (gain amp). Both amplifiers implement auto-zeroing to minimize offset and drift. A fully differential topology increases the immunity of the signals to parasitic noise and temperature effects. Amplifier gain is set by two external resistors for convenient TC matching.

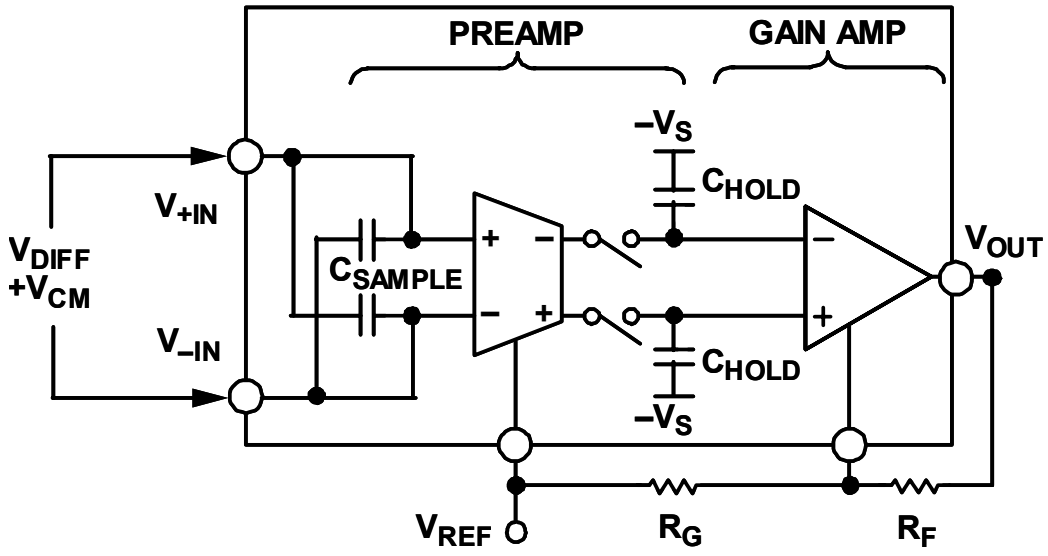

Figure 3.40: Phase A of the Sampling Phase

The signal sampling rate is controlled by an on-chip, 6 kHz oscillator and logic to derive the required nonoverlapping clock phases. For simplification of the functional description, two sequential clock phases, A and B, are used to distinguish the order of internal operation as depicted in the first figure, respectively.

During Phase A, the sampling capacitors are connected to the inputs. The input signal's difference voltage, V_{DIFF}, is stored across the sampling capacitors, C_{SAMPLE}. Since the sampling capacitors only retain the difference voltage, the common-mode voltage is rejected. During this period, the gain amplifier is not connected to the preamplifier so its output remains at the level set by the previously sampled input signal held on C_{HOLD}, as shown in the second figure.

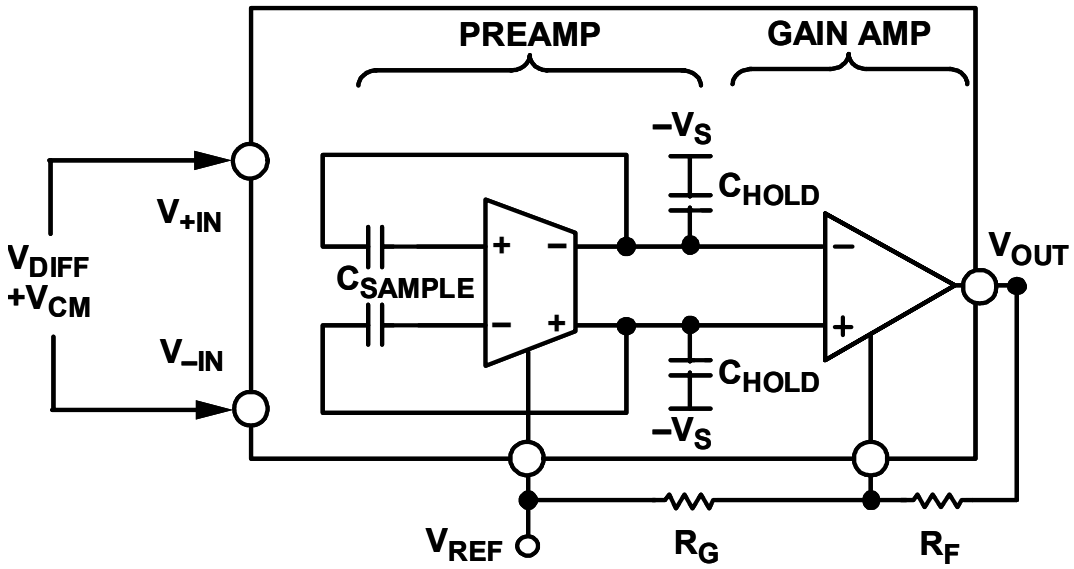

Figure 3.41: *Phase B of the Sampling Phase*

In Phase B, the differential signal is transferred to the hold capacitors refreshing the value stored on C_{HOLD}. The output of the preamplifier is held at a common-mode voltage determined by the reference potential, V_{REF}. In this manner, the AD8230 is able to condition the difference signal and set the output voltage level. The gain amplifier conditions the updated signal stored on the hold capacitors, C_{HOLD}.

The AD8230 may be used to condition thermocouples as shown in the figure. It has voltage overload protection and an RFI filter in front. Input overload protection is provided by the BAV199 diodes at each input.

Resistance Temperature Detectors (RTDs)

The Resistance Temperature Detector, or the RTD, is a sensor whose resistance changes with temperature. Typically built of a platinum (Pt) wire wrapped around a ceramic bobbin, the RTD exhibits behavior which is more accurate and more linear over wide temperature ranges than a thermocouple. Figure 3.42 illustrates the temperature coefficient of a 100Ω RTD and the Seebeck coefficient of a Type S thermocouple. Over the entire range (approximately –200°C to +850°C), the RTD is a more linear device. Hence, linearizing an RTD is less complex.

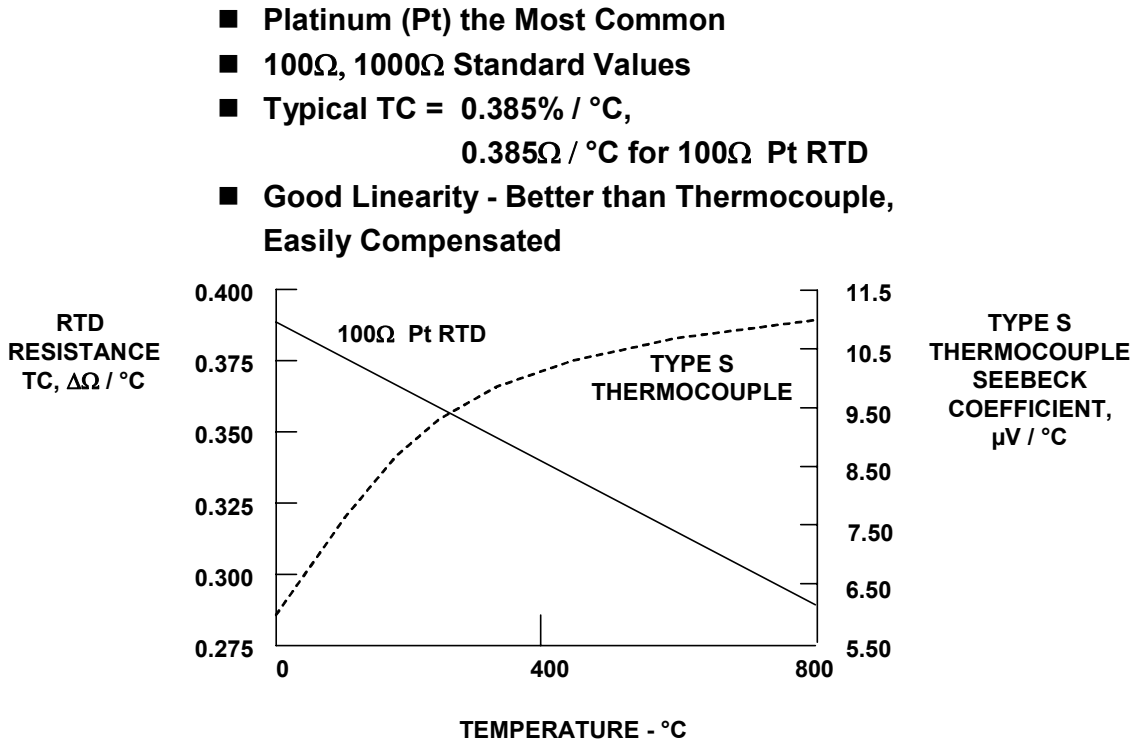

Figure 3.42: *Resistance Temperature Detectors (RTD)*

Unlike a thermocouple, however, an RTD is a passive sensor and requires current excitation to produce an output voltage. The RTD's low temperature coefficient of 0.385%/°C requires similar high-performance signal conditioning circuitry to that used by a thermocouple; however, the voltage drop across an RTD is much larger than a thermocouple output voltage. A system designer may opt for large value RTDs with higher output, but large-valued RTDs exhibit slow response times. Furthermore, although the cost of RTDs is higher than that of thermocouples, they use copper leads, and thermoelectric effects from terminating junctions do not affect their accuracy. And finally, because their resistance is a function of the absolute temperature, RTDs require no cold-junction compensation.

Caution must be exercised using current excitation because the current through the RTD causes heating. This self-heating changes the temperature of the RTD and appears as a measurement error. Hence, careful attention must be paid to the design of the signal conditioning circuitry so that self-heating is kept below 0.5°C. Manufacturers specify self-heating errors for various RTD values and sizes in still and in moving air. To reduce the error due to self-heating, the minimum current should be used for the required system resolution, and the largest RTD value chosen that results in acceptable response time.

Another effect that can produce measurement error is voltage drop in RTD lead wires. This is especially critical with low-value 2-wire RTDs because the temperature coefficient and the absolute value of the RTD resistance are both small. If the RTD is located a long distance from the signal conditioning circuitry, then the lead resistance can be ohms or tens of ohms, and a small amount of lead resistance can contribute a significant error to the temperature measurement. To illustrate this point, let us assume that a 100Ω platinum RTD with 30-gauge copper leads is located about 100 feet from a controller's display console. The resistance of 30-gauge copper wire is 0.105 Ω/ft, and the two leads of the RTD will contribute a total 21 Ω to the network which is shown in Figure 3.43. This additional resistance will produce a 55°C error in the measurement! The leads' temperature coefficient can contribute an additional, and possibly significant, error to the measurement. To eliminate the effect of the lead resistance, a 4-wire technique is used.

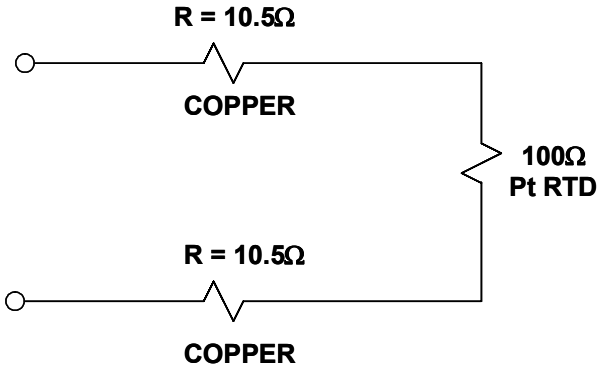

Figure 3.43: *A 100 Ω Pt RTD with 100 Feet of 30- Gauge Lead Wires*

In Figure 3.44, a 4-wire, or Kelvin, connection is made to the RTD. A constant current is applied though the FORCE leads of the RTD, and the voltage across the RTD itself is measured remotely via the SENSE leads. The measuring device can be a DVM or an instrumentation amplifier, and high accuracy can be achieved provided that the measuring device exhibits high input impedance and/or low input bias current. Since the SENSE leads do not carry appreciable current, this technique is insensitive to lead wire

length. Sources of errors are the stability of the constant current source and the input impedance and/or bias currents in the amplifier or DVM.

RTDs are generally configured in a four-resistor bridge circuit. The bridge output is amplified by an instrumentation amplifier for further processing. However, high resolution measurement ADCs such as the AD77XX series allow the RTD output to be digitized directly. In this manner, linearization can be performed digitally, thereby easing the analog circuit requirements.

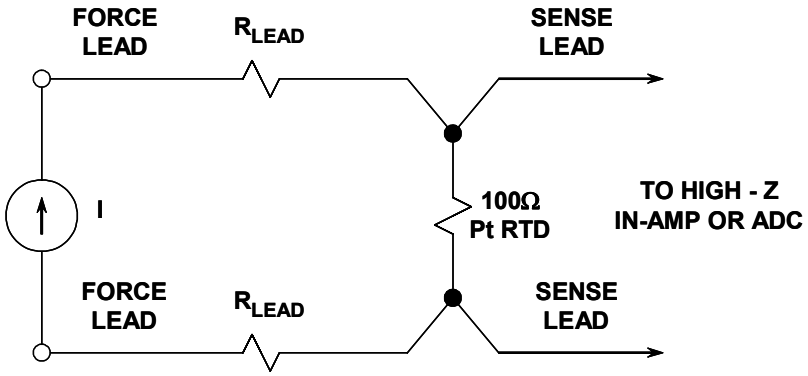

Figure 3.44: *Four-Wire or Kelvin Connection to Pt RTD For Accurate Measurements*

Figure 3.45 shows a 100 Ω Pt RTD driven with a 400 μA excitation current source. The output is digitized by one of the AD77XX series ADCs. Note that the RTD excitation current source also generates the 2.5 V reference voltage for the ADC via the 6.25 kΩ resistor. Variations in the excitation current do not affect the circuit accuracy, since both the input voltage and the reference voltage vary ratiometrically with the excitation current. However, the 6.25 kΩ resistor must have a low temperature coefficient to avoid errors in the measurement. The high resolution of the ADC and the input PGA (gain of 1 to 128) eliminates the need for additional conditioning circuits.

The ADT70 is a complete Pt RTD signal conditioner which provides an output voltage of 5 mV/°C when using a 1 kΩ RTD (see Figure 3.46). The Pt RTD and the 1 kΩ reference resistor are both excited with 1mA matched current sources. This allows temperature measurements to be made over a range of approximately –50°C to +800°C.

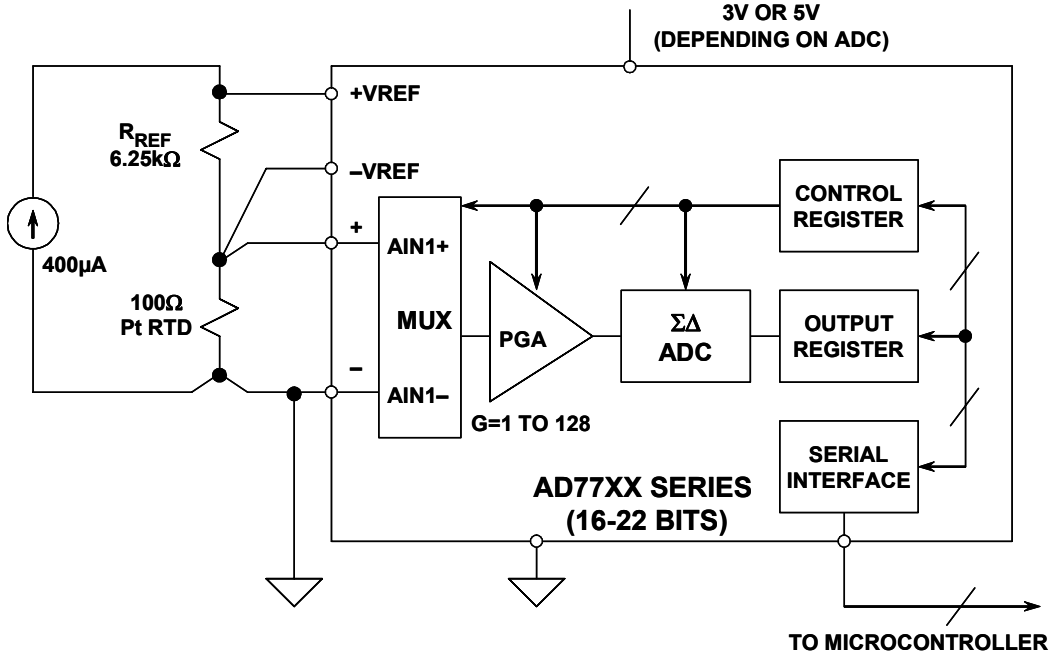

Figure 3.45: *Interfacing a Pt RTD to a High Resolution ΣΔ ADC*

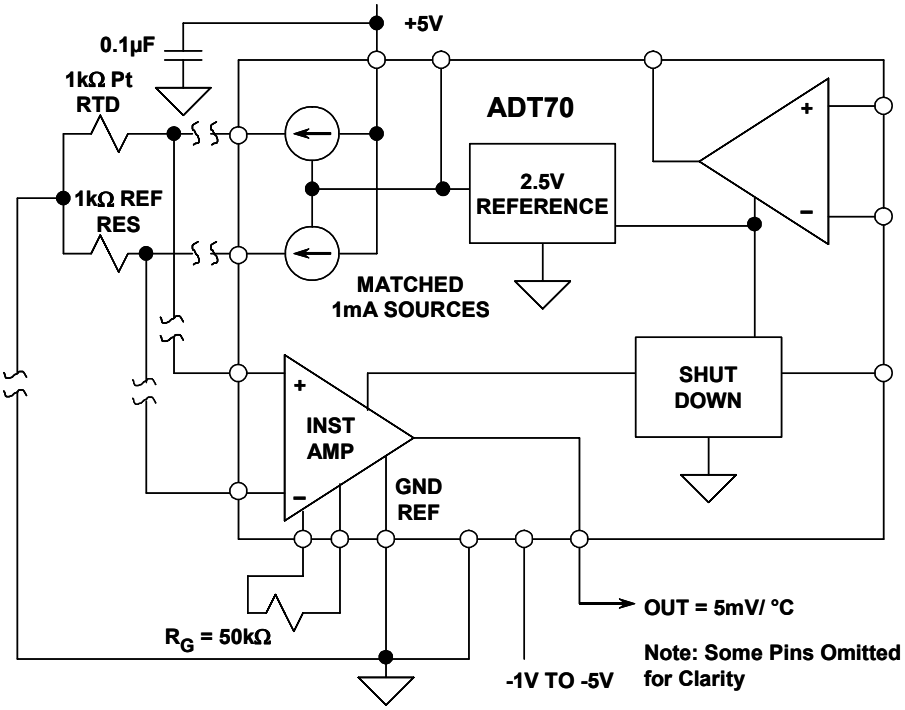

Figure 3.46: *Conditioning the Pt RTD Using the ADT70*

The ADT70 contains the two matched current sources, a precision rail-to-rail output instrumentation amplifier, a 2.5 V reference, and an uncommitted rail-to-rail output op amp. The ADT71 is the same as the ADT70 except the internal voltage reference is omitted. A shutdown function is included for battery powered equipment that reduces the quiescent current from 3 mA to 10 μA. The gain or full-scale range for the Pt RTD and ADT701 system is set by a precision external resistor connected to the instrumentation amplifier. The uncommitted op amp may be used for scaling the internal voltage reference, providing a "Pt RTD open" signal or "over temperature" warning, providing a heater switching signal, or other external conditioning determined by the user. The ADT70 is specified for operation from –40°C to +125°C and is available in 20-pin DIP and SOIC packages.

Thermistors

Similar in function to the RTD, thermistors are low-cost temperature-sensitive resistors and are constructed of solid semiconductor materials which exhibit a positive or negative temperature coefficient. Although positive temperature coefficient devices are available, the most commonly used thermistors are those with a negative temperature coefficient. Figure 3.47 shows the resistance-temperature characteristic of a commonly used NTC (Negative Temperature Coefficient) thermistor. The thermistor is highly non-linear and, of the three temperature sensors discussed, is the most sensitive.

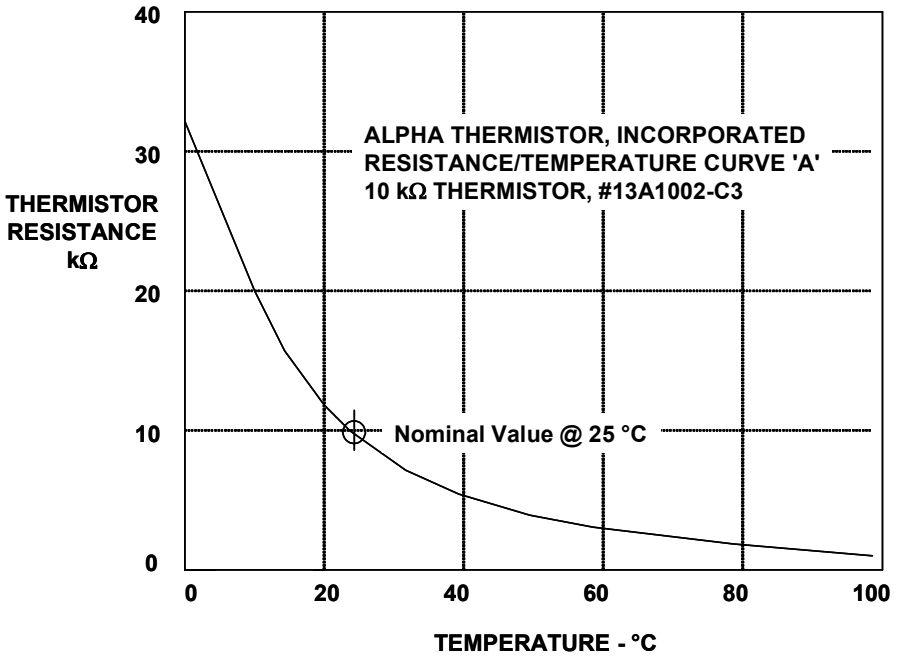

Figure 3.45: *Resistance Characteristics of a 10 kΩ NTC Thermistors*

The thermistor's high sensitivity (typically, –44,000 ppm/°C at 25°C, as shown in Figure 3.46), allows it to detect minute variations in temperature which could not be observed with an RTD or thermocouple. This high sensitivity is a distinct advantage over the RTD in that 4-wire Kelvin connections to the thermistor are not needed to compensate for lead wire errors. To illustrate this point, suppose a 10 kΩ NTC thermistor, with a typical 25°C temperature coefficient of –44,000 ppm/°C, were substituted for the 100 Ω Pt RTD in the example given earlier, then a total lead wire resistance of 21 Ω would generate less than 0.05°C error in the measurement. This is roughly a factor of 500 improvement in error over an RTD.

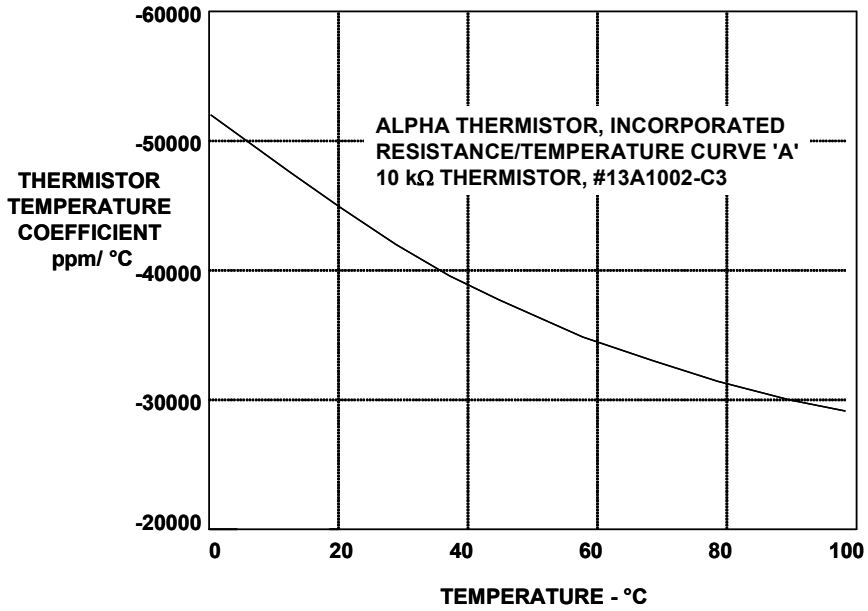

Figure 3.46: *Temperature Coefficient of a 10 kΩ NTC Thermistor*

However, the thermistor's high sensitivity to temperature does not come without a price. As was shown in Figure 3.46, the temperature coefficient of thermistors does not decrease linearly with increasing temperature as it does with RTDs; therefore, linearization is required for all but the narrowest of temperature ranges. Thermistor applications are limited to a few hundred degrees at best because they are more susceptible to damage at high temperatures. Compared to thermocouples and RTDs, thermistors are fragile in construction and require careful mounting procedures to prevent crushing or bond separation. Although a thermistor's response time is short due to its small size, its small thermal mass makes it very sensitive to self-heating errors.

Thermistors are very inexpensive, highly sensitive temperature sensors. However, we have shown that a thermistor's temperature coefficient varies from –44,000 ppm/°C at 25°C to –29,000 ppm/°C at 100°C. Not only is this non-linearity the largest source of error in a temperature measurement, it also limits useful applications to very narrow temperature ranges if linearization techniques are not used.

It is possible to use a thermistor over a wide temperature range only if the system designer can tolerate a lower sensitivity to achieve improved linearity. One approach to linearizing a thermistor is simply shunting it with a fixed resistor. Paralleling the thermistor with a fixed resistor increases the linearity significantly. As shown in Figure 3.47, the parallel combination exhibits a more linear variation with temperature compared to the thermistor itself. Also, the sensitivity of the combination still is high compared to a thermocouple or RTD. The primary disadvantage to this technique is that linearization can only be achieved within a narrow range.

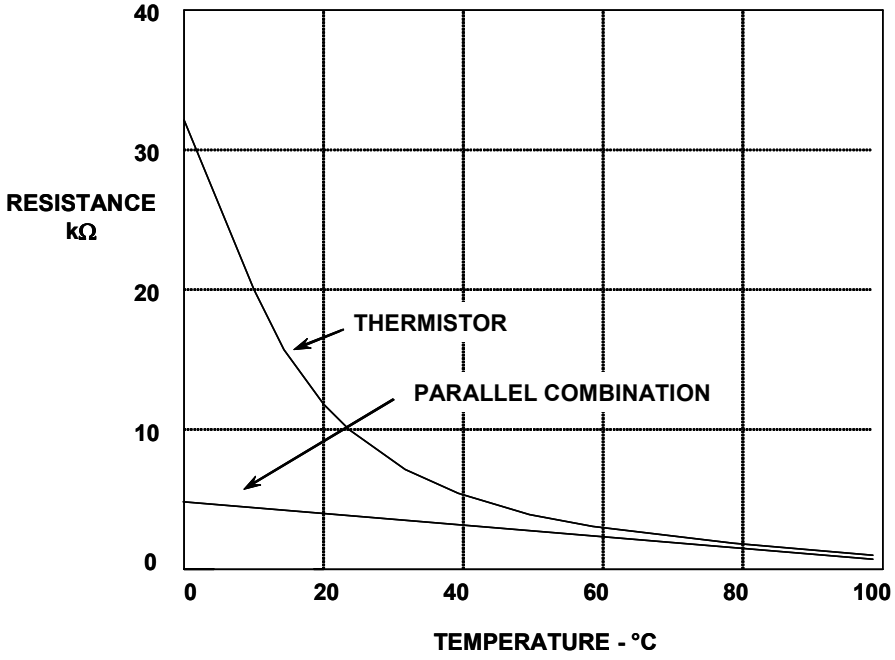

Figure 3.47: *Linearization of NTC Thermistor Using a 5.17 kΩ Shunt Resistor*

The value of the fixed resistor can be calculated from the following equation:

$$R = \frac{RT2 \cdot (RT1 + RT3) - 2 \cdot RT1 \cdot RT3}{RT1 + RT3 - 2 \cdot RT2}, \qquad \text{Eq. 3-31}$$

where RT1 is the thermistor resistance at T1, the lowest temperature in the measurement range, RT3 is the thermistor resistance at T3, the highest temperature in the range, and RT2 is the thermistor resistance at T2, the midpoint, T2 = (T1 + T3)/2.

For a typical 10 kΩ NTC thermistor, RT1 = 32,650 Ω at 0°C, RT2 = 6,532 Ω at 35°C, and RT3 = 1,752 Ω at 70°C. This results in a value of 5.17 kΩ for R. The accuracy needed in the signal conditioning circuitry depends on the linearity of the network. For the example given above, the network shows a non-linearity of – 2.3°C / + 2.0 °C.

The output of the network can be applied to an ADC to perform further linearization as shown in Figure 7.21. Note that the output of the thermistor network has a slope of approximately –10 mV/°C, which implies a 12-bit ADC has more than sufficient resolution.

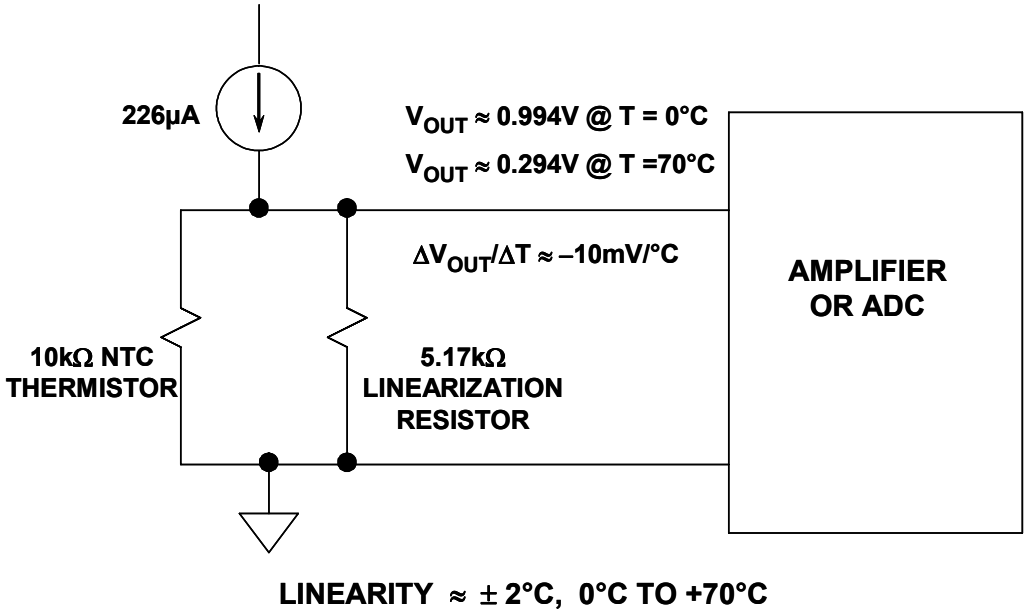

Figure 3.48: *Linearized Thermistor Amplifier*

Digital Output Temperature Sensors

Temperature sensors which have digital outputs have a number of advantages over those with analog outputs, especially in remote applications. Opto-isolators can also be used to provide galvanic isolation between the remote sensor and the measurement system. A voltage-to-frequency converter driven by a voltage output temperature sensor accomplishes this function, however, more sophisticated ICs are now available which are more efficient and offer several performance advantages.

The TMP03/TMP04 digital output sensor family includes a voltage reference, V_{PTAT} generator, sigma-delta ADC, and a clock source (see Figure 3.49). The sensor output is digitized by a first-order sigma-delta modulator, also known as the "charge balance" type analog-to-digital converter. This converter utilizes time-domain oversampling and a high accuracy comparator to deliver 12 bits of effective accuracy in an extremely compact circuit.

The output of the sigma-delta modulator is encoded using a proprietary technique which results in a serial digital output signal with a mark-space ratio format (see Figure 3.50) that is easily decoded by any microprocessor into either degrees centigrade or degrees Fahrenheit, and readily transmitted over a single wire. Most importantly, this encoding method avoids major error sources common to other modulation techniques, as it is clock-independent. The nominal output frequency is 35 Hz at +25ºC, and the device operates with a fixed high-level pulse width (T1) of 10ms.

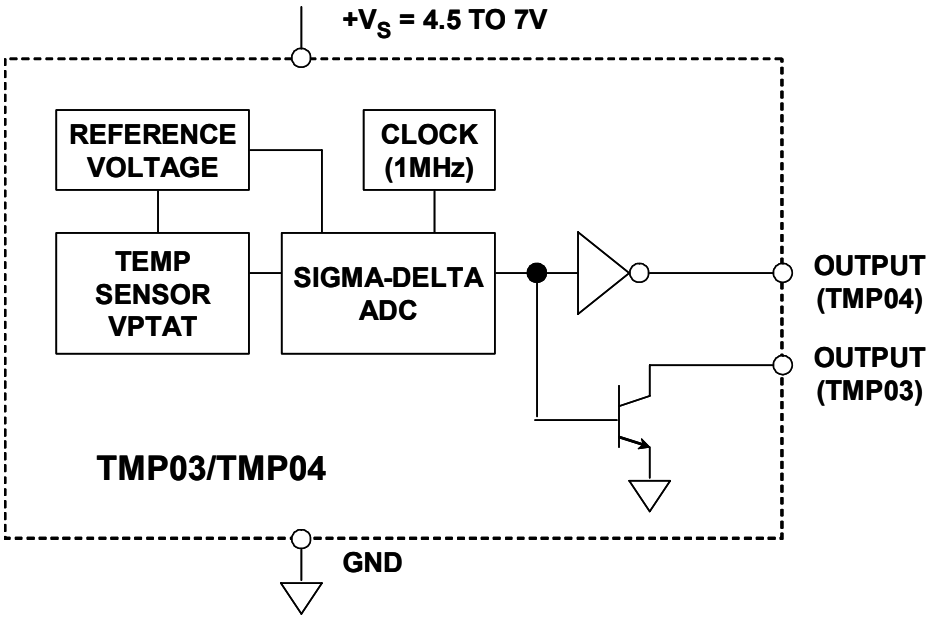

Figure 3.49: *Digital Out Temperature Sensor: TMP03/04*

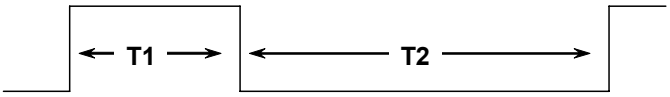

$$\text{TEMPERATURE (°C)} = 235 - \left(\frac{400 \times T1}{T2}\right)$$

$$\text{TEMPERATURE (°F)} = 455 - \left(\frac{720 \times T1}{T2}\right)$$

- **T1 Nominal Pulse Width = 10ms**
- **±1.5°C Error Over Temp, ±0.5°C Non-Linearity (Typical)**
- **Specified –40°C to +100°C**
- **Nominal T1/T2 @ 0°C = 60%**
- **Nominal Frequency @ +25°C = 35Hz**
- **6.5mW Power Consumption @ 5V**
- **TO-92, SO-8, or TSSOP Packages**

Figure 3.50: *TMP03/TMP04 Output Format*

The TMP03/TMP04 output is a stream of digital pulses, and the temperature information is contained in the mark-space ratio per the equations:

$$\text{Temperature}(°C) = 235 - \left(\frac{400 \times T1}{T2}\right) \qquad \text{Eq. 3-32}$$

$$\text{Temperature}(°F) = 455 - \left(\frac{720 \times T1}{T2}\right). \qquad \text{Eq. 3-33}$$

Popular microcontrollers, such as the 80C51 and 68HC11, have on-chip timers which can easily decode the mark-space ratio of the TMP03/TMP04. A typical interface to the 80C51 is shown in Figure 3.51. Two timers, labeled *Timer 0* and *Timer 1* are 16 bits in length. The 80C51's system clock, divided by twelve, provides the source for the timers. The system clock is normally derived from a crystal oscillator, so timing measurements are quite accurate. Since the sensor's output is ratiometric, the actual clock frequency is not important. This feature is important because the microcontroller's clock frequency is often defined by some external timing constraint, such as the serial baud rate.

Software for the sensor interface is straightforward. The microcontroller simply monitors I/O port P1.0, and starts *Timer 0* on the rising edge of the sensor output. The microcontroller continues to monitor P1.0, stopping *Timer 0* and starting *Timer 1* when the sensor output goes low. When the output returns high, the sensor's T1 and T2 times are contained in registers *Timer 0* and *Timer 1*, respectively. Further software routines can then apply the conversion factor shown in the equations above and calculate the temperature.

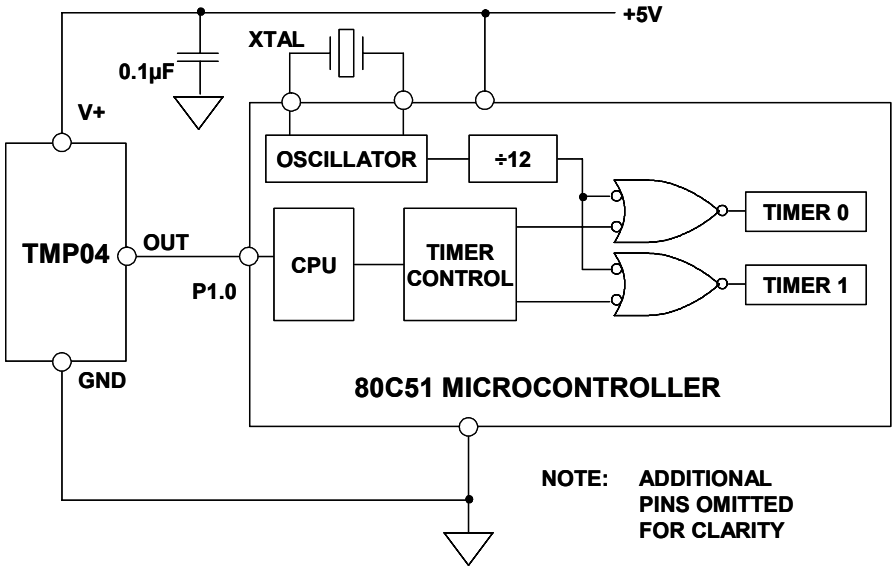

Figure 3.51: *Interfacing a TMP04 to a Microcontroller*

Thermostatic Switches and Setpoint Controllers

Temperature sensors used in conjunction with comparators can act as thermostatic switches. ICs such as the AD22105 accomplish this function at low cost and allow a single external resistor to program the setpoint to 2ºC accuracy over a range of –40ºC to +150ºC (see Figure 3.52). The device asserts an open collector output when the ambient temperature exceeds the user-programmed setpoint temperature. The ADT05 has approximately 4ºC of hysteresis which prevents rapid thermal on/off cycling. The ADT05 is designed to operate on a single supply voltage from +2.7 V to +7.0 V facilitating operation in battery powered applications as well as industrial control systems. Because of low power dissipation (200 µW @ 3.3 V), self-heating errors are minimized, and battery life is maximized. An optional internal 200 kΩ pull-up resistor is included to facilitate driving light loads such as CMOS inputs.

The setpoint resistor is determined by the equation:

$$R_{SET} = \frac{39\,M\Omega^{\circ}C}{T_{SET}(^{\circ}C) + 281.6^{\circ}C} - 90.3\,k\Omega. \qquad \text{Eq.3-34}$$

The setpoint resistor should be connected directly between the R_{SET} pin (Pin 4) and the GND pin (Pin 5). If a ground plane is used, the resistor may be connected directly to this plane at the closest available point.

The setpoint resistor can be of nearly any resistor type, but its initial tolerance and thermal drift will affect the accuracy of the programmed switching temperature. For most

applications, a 1% metal-film resistor will provide the best tradeoff between cost and accuracy. Once R_{SET} has been calculated, it may be found that the calculated value does not agree with readily available standard resistors of the chosen tolerance. In order to achieve a value as close as possible to the calculated value, a compound resistor can be constructed by connecting two resistors in series or parallel.

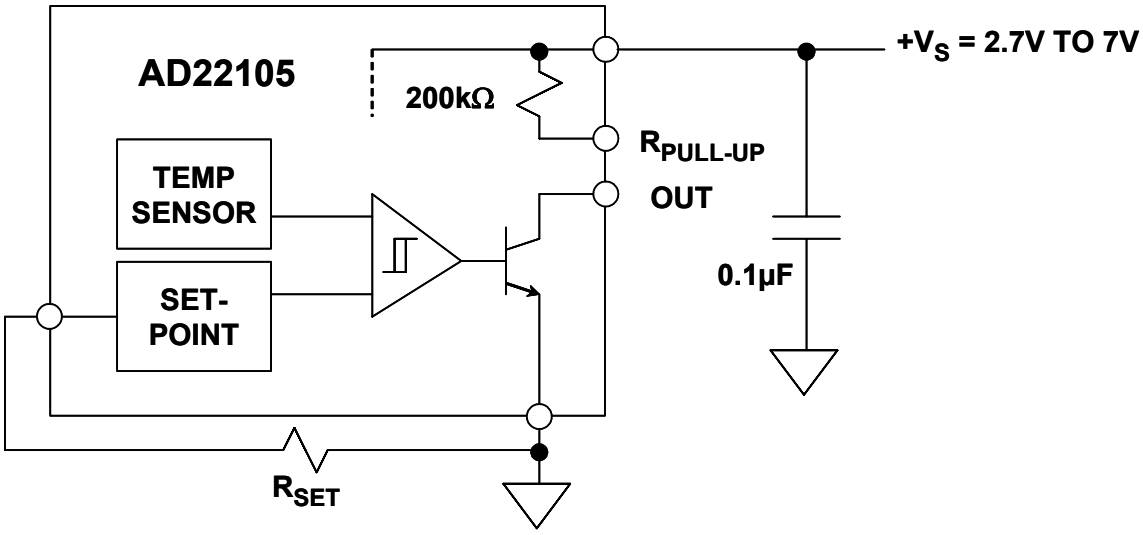

Figure 3.52: *AD22105 Thermostatic Switch*

The TMP01 is a dual setpoint temperature controller which also generates a PTAT output voltage (see Figure 3.53). It also generates a control signal from one of two outputs when the device is either above or below a specific temperature range. Both the high/low temperature trip points and hysteresis band are determined by user-selected external resistors.

The TMP01 consists of a bandgap voltage reference combined with a pair of matched comparators. The reference provides both a constant 2.5 V output and a PTAT output voltage which has a precise temperature coefficient of 5 mV/K and is 1.49 V (nominal) at +25ºC. The comparators compare VPTAT with the externally set temperature trip points and generate an open-collector output signal when one of their respective thresholds has been exceeded.

Hysteresis is also programmed by the external resistor chain and is determined by the total current drawn out of the 2.5 V reference. This current is mirrored and used to generate a hysteresis offset voltage of the appropriate polarity after a comparator has been tripped. The comparators are connected in parallel, which guarantees that there is no hysteresis overlap and eliminates erratic transitions between adjacent trip zones.

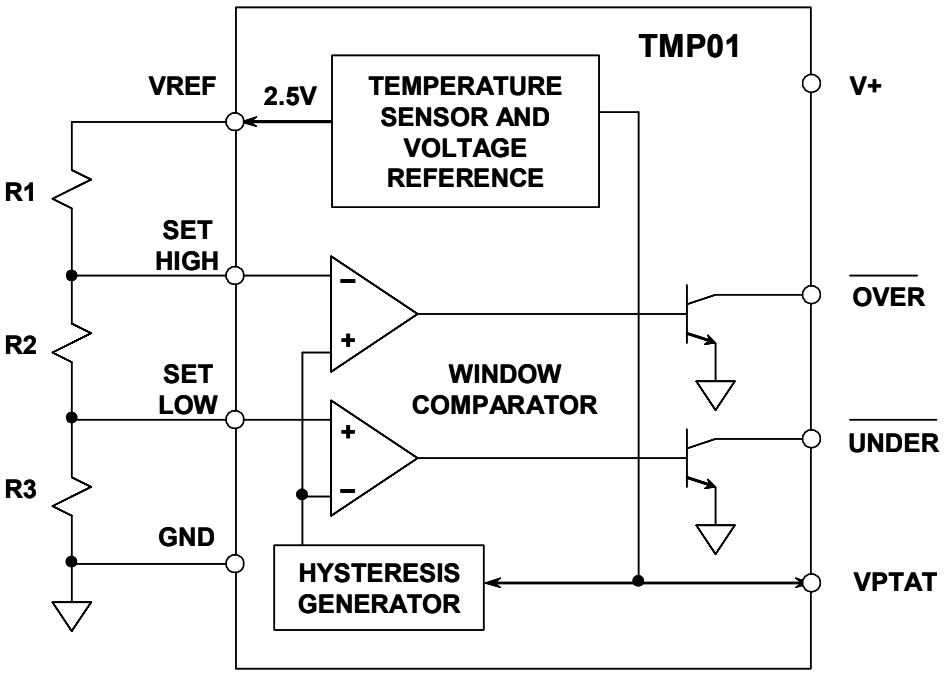

Figure 3.53: *TMP01 Programmable Setpoint Controller*

Microprocessor Temperature Monitoring

Today's computers require that hardware as well as software operate properly, in spite of the many things that can cause a system crash or lockup. The purpose of hardware monitoring is to monitor the critical items in a computing system and take corrective action should problems occur.

Microprocessor supply voltage and temperature are two critical parameters. If the supply voltage drops below a specified minimum level, further operations should be halted until the voltage returns to acceptable levels. In some cases, it is desirable to reset the microprocessor under "brownout" conditions. It is also common practice to reset the microprocessor on power-up or power-down. Switching to a battery backup may be required if the supply voltage is low.

Under low voltage conditions it is mandatory to inhibit the microprocessor from writing to external CMOS memory by inhibiting the Chip Enable signal to the external memory.

Many microprocessors can be programmed to periodically output a "watchdog" signal. Monitoring this signal gives an indication that the processor and its software are functioning properly and that the processor is not stuck in an endless loop.

The need for hardware monitoring has resulted in a number of ICs, traditionally called "microprocessor supervisory products," which perform some or all of the above functions. These devices range from simple manual reset generators (with debouncing) to complete microcontroller-based monitoring sub-systems with on-chip temperature sensors and ADCs. Analog Devices' ADM-family of products is specifically to perform the various microprocessor supervisory functions required in different systems.

CPU temperature is critically important in the Pentium microprocessors. For this reason, all new Pentium devices have an on-chip substrate PNP transistor which is designed to monitor the actual chip temperature. The collector of the substrate PNP is connected to the substrate, and the base and emitter are brought out on two separate pins of the Pentium II.

The ADM1021 Microprocessor Temperature Monitor is specifically designed to process these outputs and convert the voltage into a digital word representing the chip temperature. The simplified analog signal processing portion of the ADM1021 is shown in Figure 3.54.

The technique used to measure the temperature is identical to the "ΔV_{BE}" principle previously discussed. Two different currents (I and N·I)are applied to the sensing transistor, and the voltage measured for each. In the ADM1021, the nominal currents are I = 6 μA, (N = 17), N·I = 102 μA.

The change in the base-emitter voltage, ΔV_{BE}, is a PTAT voltage and given by the equation:

$$\Delta V_{BE} = \frac{kT}{q} \ln(N). \qquad \text{Eq. 3-35}$$

Figure 3.54 shows the external sensor as a substrate transistor, provided for temperature monitoring in the microprocessor, but it could equally well be a discrete transistor. If a discrete transistor is used, the collector should be connected to the base and not grounded. To prevent ground noise interfering with the measurement, the more negative terminal of the sensor is not referenced to ground, but is biased above ground by an internal diode. If the sensor is operating in a noisy environment, C may be optionally added as a noise filter. Its value is typically 2200 pF, but should be no more than 3000 pF.

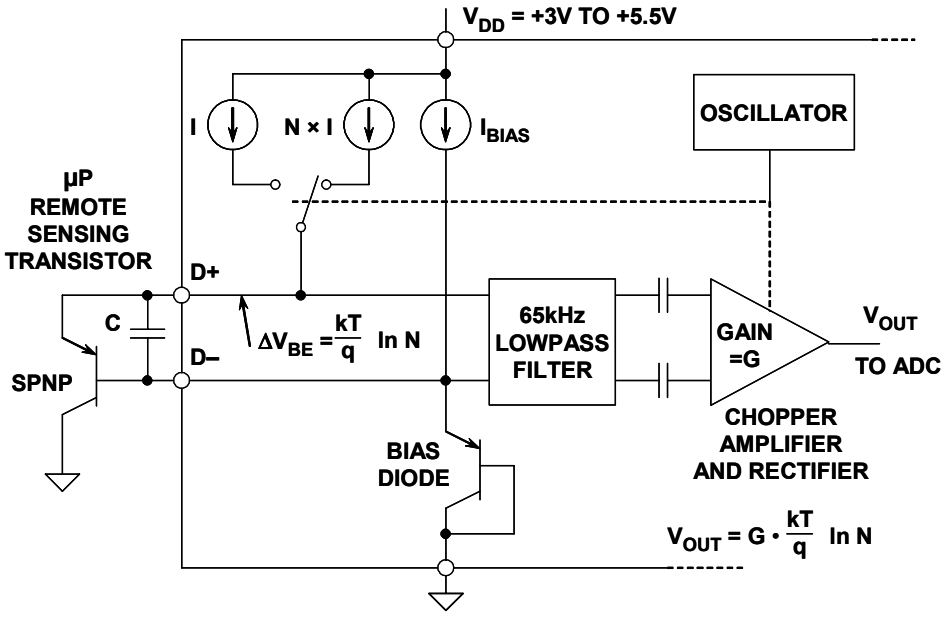

Figure 3.54: *ADM1021 Microprocessor Temperature Monitor Input Signal Conditioning Circuits*

To measure ΔV_{BE}, the sensing transistor is switched between operating currents of I and N·I. The resulting waveform is passed through a 65 kHz lowpass filter to remove noise, then to a chopper-stabilized amplifier which performs the function of amplification and synchronous rectification. The resulting DC voltage is proportional to ΔV_{BE} and is digitized by an 8-bit ADC. To further reduce the effects of noise, digital filtering is performed by averaging the results of 16 measurement cycles.

In addition, the ADM1021 contains an on-chip temperature sensor, and its signal conditioning and measurement is performed in the same manner.

One LSB of the ADC corresponds to 1ºC, so the ADC can theoretically measure from –128ºC to +127ºC, although the practical lowest value is limited to –65ºC due to device maximum ratings. The results of the local and remote temperature measurements are stored in the local and remote temperature value registers, and are compared with limits programmed into the local and remote high and low limit registers as shown in Figure 3.55. An $\overline{\text{ALERT}}$ output signals when the on-chip or remote temperature is out of range. This output can be used as an interrupt, or as an SMBus alert.

The limit registers can be programmed, and the device controlled and configured, via the serial System Management Bus (SMBus). The contents of any register can also be read back by the SMBus. Control and configuration functions consist of: switching the device between normal operation and standby mode, masking or enabling the $\overline{\text{ALERT}}$ output, and selecting the conversion rate which can be set from 0.0625 Hz to 8 Hz.

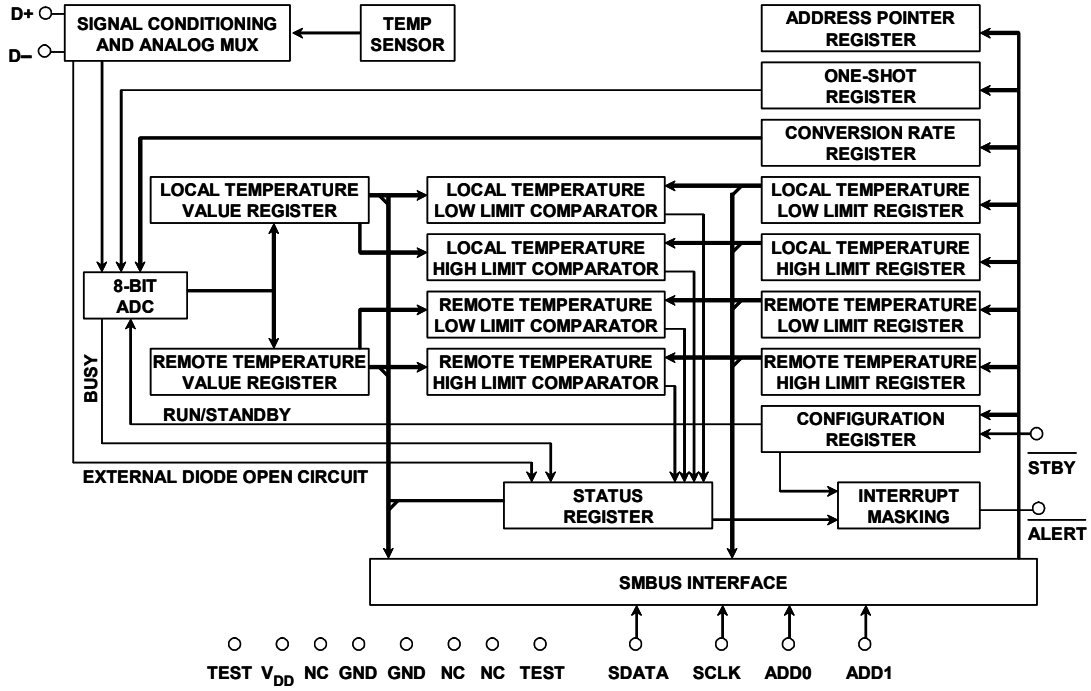

Figure 3.55: *ADM1021 Simplified Block Diagram*

REFERENCES

1. Ramon Pallas-Areny and John G. Webster, **Sensors and Signal Conditionin**g, John Wiley, New York, 1991.

2. Dan Sheingold, Editor, **Transducer Interfacing Handbook**, Analog Devices, Inc., 1980.

3. Walt Kester, Editor, **1992 Amplifier Applications Guide**, Section 2, 3, Analog Devices, Inc., 1992.

4. Walt Kester, Editor, **System Applications Guide**, Section 1, 6, Analog Devices, Inc., 1993.

5. Dan Sheingold, **Nonlinear Circuits Handbook**, Analog Devices, Inc.

6. James Wong, *Temperature Measurements Gain from Advances in High-precision Op Amps*, **Electronic Design**, 15 May 1986.

7. *OMEGA Temperature Measurement Handbook*, Omega Instruments, Inc.

8. **Handbook of Chemistry and Physics**, CRC.

9. Paul Brokaw, *A Simple Three-Terminal IC Bandgap Voltage Reference*, **IEEE Journal of Solid State Circuits**, Vol. SC-9, December, 1974.

SECTION 3.3: CHARGE COUPLED DEVICES (CCDs)

Charge coupled devices (CCDs) contain a large number of small photocells called photosites or pixels which are arranged either in a single row (linear arrays) or in a matrix (area arrays). CCD area arrays are commonly used in video applications, while linear arrays are used in facsimile machines, graphics scanners, and pattern recognition equipment.

The linear CCD array consists of a row of image sensor elements (photosites, or pixels) which are illuminated by light from the object or document. During one exposure period each photosite acquires an amount of charge which is proportional to its illumination. These photosite charge packets are subsequently switched simultaneously via transfer gates to an analog shift register. The charge packets on this shift register are clocked serially to a charge detector (storage capacitor) and buffer amplifier (source follower) which convert them into a string of photo-dependent output voltage levels (see Figure 3.56). While the charge packets from one exposure are being clocked out to the charge detector, another exposure is underway. The analog shift register typically operates at frequencies between 1 and 10 MHz.

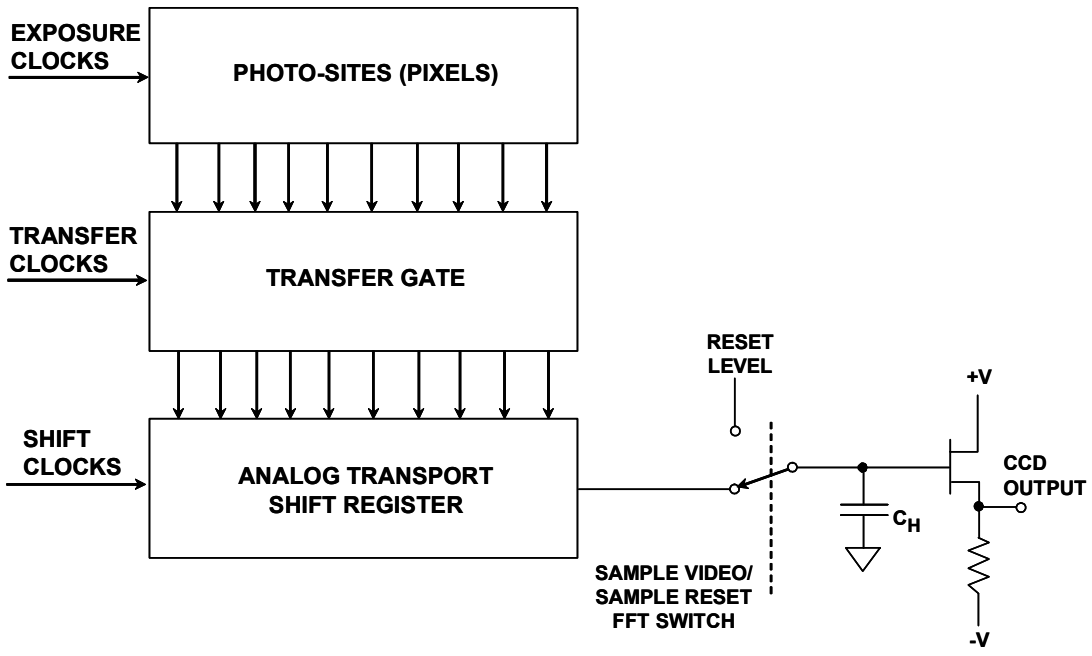

Figure 3.56: *Linear CCD Array*

The charge detector readout cycle begins with a reset pulse which causes a FET switch to set the output storage capacitor to a known voltage. The switching FETs capacitive feedthrough causes a reset glitch at the output as shown in Figure 3.57. The switch is then opened, isolating the capacitor, and the charge from the last pixel is dumped onto the capacitor causing a voltage change. The difference between the reset voltage and the final

voltage (video level) shown in Figure 9.87 represents the amount of charge in the pixel. CCD charges may be as low as 10 electrons, and a typical CCD output sensitivity is 0.6 μV/electron. Most CCDs have a saturation output voltage of about 1 V (see Reference 16).

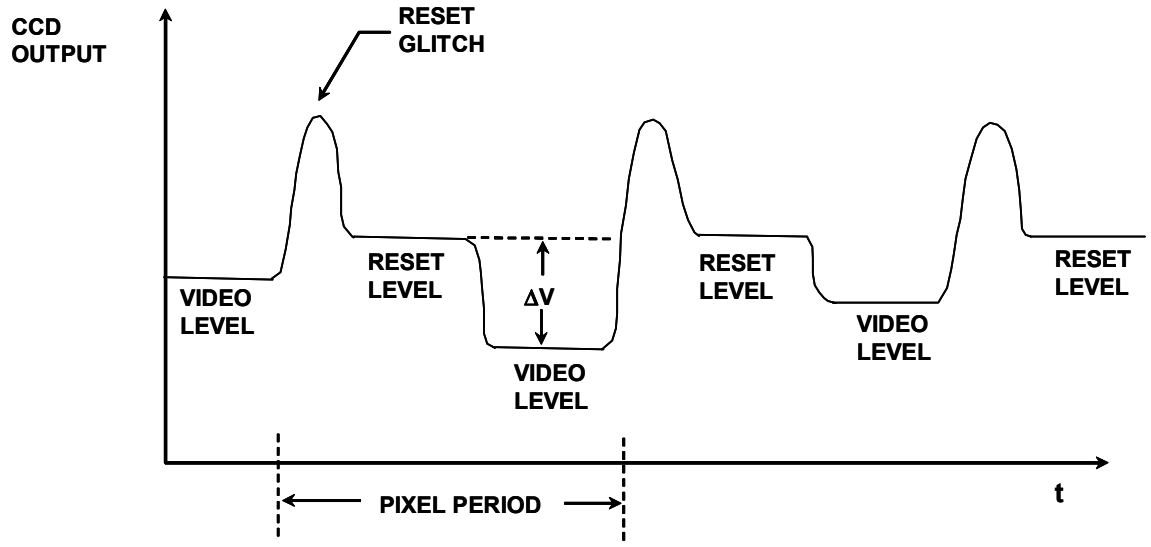

Figure 3.57: *CCD Output Waveform*

Since CCDs are generally fabricated on MOS processes, they have limited capability to perform on-chip signal conditioning. Therefore the CCD output is generally processed by external conditioning circuits.

CCD output voltages are small and quite often buried in noise. The largest source of noise is the thermal noise in the resistance of the FET reset switch. This noise may have a typical value of 100 to 300 electrons rms (approximately 60 to 180 mV_{rms}). This noise occurs as a *sample-to-sample* variation in the CCD output level and is common to both the reset level and the video level for a given pixel period. A technique called *correlated double sampling* (CDS)is often used to reduce the effect of this noise. Figure 9.88 shows two circuit implementations of the CDS scheme. In the top circuit, the CCD output drives both SHAs. At the end of the reset interval, SHA1 holds the reset voltage level. At the end of the video interval, SHA2 holds the video level. The SHA outputs are applied to a difference amplifier which subtracts one from the other. In this scheme, there is only a short interval during which both SHA outputs are stable, and their difference represents ΔV, so the difference amplifier must settle quickly.

Another arrangement is shown in the bottom half of Figure 3.58, which uses three SHAs and allows either for faster operation or more time for the difference amplifier to settle. In this circuit, SHA1 holds the reset level so that it occurs simultaneously with the video level at the input to SHA2 and SHA3. When the video clock is applied simultaneously to SHA2 and SHA3, the input to SHA2 is the reset level, and the input to SHA3 the video

level. This arrangement allows the entire pixel period (less the acquisition time of SHA2 and SHA3) for the difference amplifier to settle.

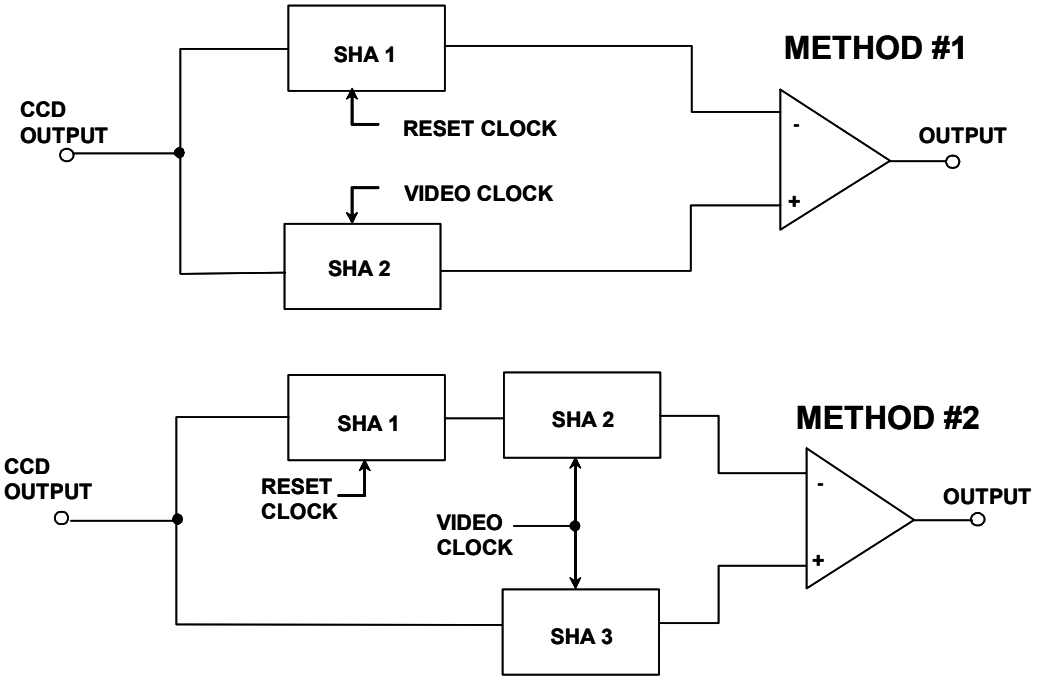

Figure 3.58: *Correlated Double Sampling (CDS)*

REFERENCES:

1. Walt Kester, Editor, **1992 Amplifier Applications Guide**, Section 2, 3, Analog Devices, Inc., 1992.

2. Walt Kester, Editor, **System Applications Guide**, Section 1, 6, Analog Devices, Inc., 1993.

3. **Optoelectronics Data Book**, EG&G Vactec, St. Louis, MO, 1990.

4. Silicon Detector Corporation, Camarillo, CA, Part Number SD-020-12-001 Data Sheet.

5. **Photodiode 1991 Catalog**, Hamamatsu Photonics, Bridgewater, NJ

6. Ralph Morrison, **Grounding and Shielding Techniques in Instrumentation, Third Edition**, John Wiley, Inc., 1986.

7. Henry W. Ott, **Noise Reduction Techniques in Electronic Systems, Second Edition**, John Wiley, Inc., 1988.

8. *An Introduction to the Imaging CCD Array*, Technical Note 82W-4022, Tektronix, Inc., Beaverton, OR., 1987.

9. **Handbook of Chemistry and Physics**, CRC.

SECTION 3-4: BRIDGE CIRCUITS

An Introduction to Bridges

This section discusses the fundamental bridge circuit concept. To gain greatest appreciation of these ideas, it should be studied along with those sections discussing precision op amp in Chapters 1. These sections can be read sequentially if the reader already understands the design issues related to precision op amp applications.

Resistive elements are some of the most common sensors. They are inexpensive, and relatively easy to interface with signal-conditioning circuits. Resistive elements can be made sensitive to temperature, strain (by pressure or by flex), and light. Using these basic elements, many complex physical phenomena can be measured, such as: fluid or mass flow (by sensing the temperature difference between two calibrated resistances), dew-point humidity (by measuring two different temperature points), etc.

◆ **Strain Gages**	**120Ω, 350Ω, 3500Ω**
◆ **Weigh-Scale Load Cells**	**350Ω - 3500Ω**
◆ **Pressure Sensors**	**350Ω - 3500Ω**
◆ **Relative Humidity**	**100kΩ - 10MΩ**
◆ **Resistance Temperature Devices (RTDs)**	**100Ω , 1000Ω**
◆ **Thermistors**	**100Ω - 10MΩ**

Figure 3.59: *Sensor resistances used in bridge circuits span a wide dynamic range*

Sensor element resistance can range from less than 100 Ω to several hundred kΩ, depending on the sensor design and the physical environment to be measured. Figure 3.59 indicates the wide range of sensor resistance encountered. For example, RTDs are typically 100 Ω or 1000 Ω. Thermistors are typically 3500 Ω or higher.

Resistive sensors such as RTDs and strain gages produce relatively small percentage changes in resistance, in response to a change in a physical variable such as temperature or force. For example, platinum RTDs have a temperature coefficient of about 0.385%/°C. Thus, in order to accurately resolve temperature to 1ºC, the overall measurement accuracy must be much better than 0.385 Ω when using a 100 Ω RTD.

Strain gages present a significant measurement challenge because the typical change in resistance over the entire operating range of a strain gage may be less than 1% of the

nominal resistance value. Accurately measuring small resistance changes is therefore critical when applying resistive sensors.

A simple method for measuring resistance is to force a constant current through the resistive sensor, and measure the voltage output. This requires both an accurate current source and an accurate means of measuring the voltage. Any change in the current will be interpreted as a resistance change. In addition, the power dissipation in the resistive sensor must be small and in accordance with the manufacturer's recommendations, so that self-heating does not produce errors. As a result, the drive current must be small, which tends to limit the resolution of this approach.

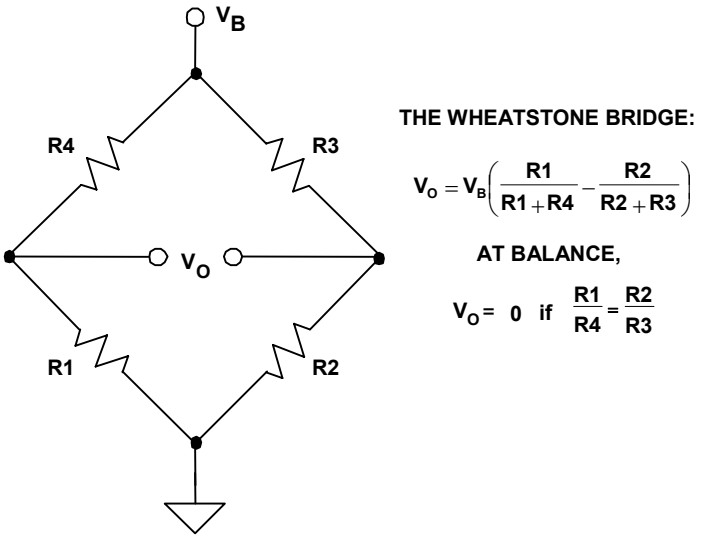

Figure 3.60: *The basic Wheatstone bridge produces an output null when the ratios of sidearm resistances match*

A *resistance bridge,* shown in Figure 3.60, offers an attractive alternative for measuring small resistance changes accurately. This is a basic Wheatstone bridge (actually developed by S. H. Christie in 1833), and is a prime example. It consists of four resistors connected to form a quadrilateral, a source of excitation voltage V_B (or, alternately, a current) connected across one of the diagonals, and a voltage detector connected across the other diagonal. The detector measures the difference between the outputs of the two voltage dividers connected across the excitation voltage, V_B. The general form of the bridge output V_O is noted in the figure.

There are two principal ways of operating a bridge such as this. One is by operating it as a null detector, where the bridge measures resistance indirectly by comparison with a similar standard resistance. On the other hand, it can be used as a device that reads a resistance difference directly, as a proportional voltage output.

When R1/R4 = R2/R3, the resistance bridge is said to be at a *null*, irrespective of the mode of excitation (current or voltage, AC or DC), the magnitude of excitation, the mode of readout (current or voltage), or the impedance of the detector. Therefore, if the ratio of

R2/R3 is fixed at K, a null is achieved when R1 = K·R4. If R1 is unknown and R4 is an accurately determined variable resistance, the magnitude of R1 can be found by adjusting R4 until an output null is achieved. Conversely, in sensor-type measurements, R4 may be a fixed reference, and a null occurs when the magnitude of the external variable (strain, temperature, etc.) is such that R1 = K·R4.

Null measurements are principally used in feedback systems involving electromechanical and/or human elements. Such systems seek to force the active element (strain gage, RTD, thermistor, etc.) to balance the bridge by influencing the parameter being measured.

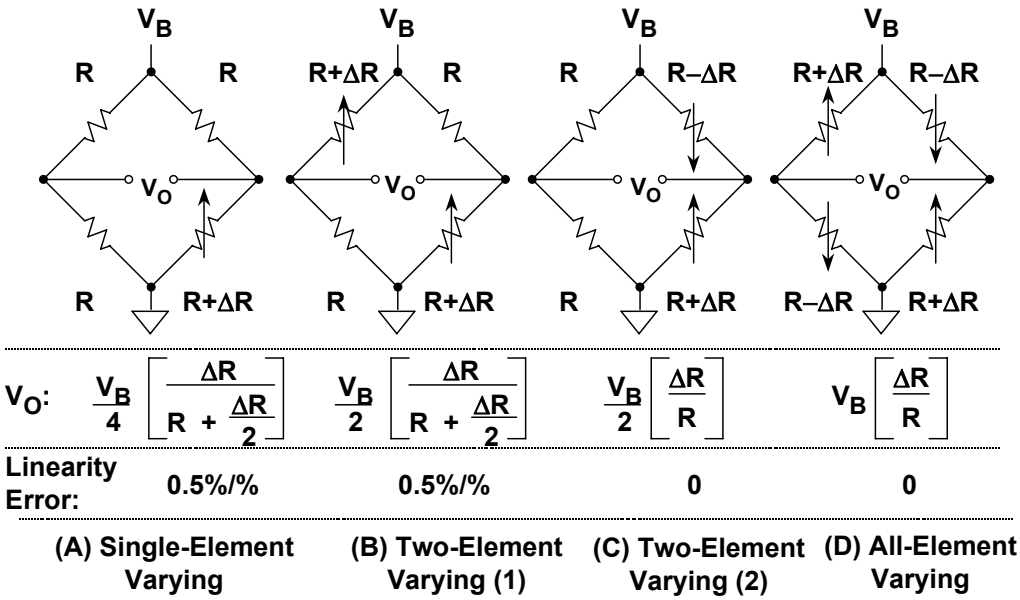

Figure 3.61: *The output voltage sensitivity and linearity of constant voltage drive bridge configurations differs according to the number of active elements*

For the majority of sensor applications employing bridges, however, the deviation of one or more resistors in a bridge from an initial value is measured as an indication of the magnitude (or a change) in the measured variable. In these cases, the output voltage change is an indication of the resistance change. Because very small resistance changes are common, the output voltage change may be as small as tens of millivolts, even with the excitation voltage V_B = 10 V (typical for a load cell application).

In many bridge applications, there may not just be a single variable element, but two, or even four elements, all of which may vary. Figure 3.61 above shows a family of four voltage-driven bridges, those most commonly suited for sensor applications. In the four cases the corresponding equations for V_O relate the bridge output voltage to the excitation voltage and the bridge resistance values. In all cases we assume a constant voltage drive, V_B. Note that since the bridge output is always directly proportional to V_B, the measurement accuracy can be no better than that of the accuracy of the excitation voltage.

In each case, the value of the fixed bridge resistor "R" is chosen to be equal to the nominal value of the variable resistor(s). The deviation of the variable resistor(s) about the nominal value is assumed to be proportional to the quantity being measured, such as strain (in the case of a strain gage), or temperature (in the case of an RTD).

The *sensitivity* of a bridge is the ratio of the maximum expected change in the output voltage to the excitation voltage. For instance, if V_B = 10 V, and the fullscale bridge output is 10 mV, then the sensitivity is 1 mV/V. For the four cases of Figure 3.61, sensitivity can be said to increase going left-right, or as more elements are made variable.

The *single-element varying* bridge of Figure 3.61A is most suited for temperature sensing using RTDs or thermistors. This configuration is also used with a single resistive strain gage. All the resistances are nominally equal, but one of them (the sensor) is variable by an amount ΔR. As the equation indicates, the relationship between the bridge output and ΔR is not linear. For example, if R = 100 Ω and ΔR = 0.1 Ω (0.1% change in resistance), the output of the bridge is 2.49875 mV for V_B = 10 V. The error is 2.50000 mV – 2.49875 mV, or 0.00125 mV. Converting this to a % of fullscale by dividing by 2.5 mV yields an end-point linearity error in percent of approximately 0.05%. (Bridge end-point linearity error is calculated as the worst error in % FS from a straight line which connects the origin and the end point at FS, i.e., the FS gain error is not included). If ΔR = 1 Ω, (1% change in resistance), the output of the bridge is 24.8756 mV, representing an end-point linearity error of approximately 0.5%. The end-point linearity error of the single-element bridge can be expressed in equation form:

Single-Element Varying Bridge End-Point Linearity Error ≈ % Change in Resistance ÷ 2

It should be noted that the above nonlinearity refers to the nonlinearity of the bridge itself and not *the sensor*. In practice, most sensors themselves will exhibit a certain specified amount of nonlinearity, which must also be accounted for in the final measurement.

In some applications, the bridge nonlinearity noted above may be acceptable. But, if not, there are various methods available to linearize bridges. Since there is a fixed relationship between the bridge resistance change and its output (shown in the equations), software can be used to remove the linearity error in digital systems. Circuit techniques can also be used to linearize the bridge output directly, and these will be discussed shortly.

There are two cases to consider in the instance of a *two-element varying* bridge. In Case 1 (Figure 3.61B), both of the diagonally opposite elements change in the same direction. An example would be two identical strain gages mounted adjacent to each other, with their axes in parallel.

The nonlinearity for this case, 0.5%/%, the same as that of the single-element varying bridge of Figure 3.61A. However, it is interesting to note the sensitivity is now improved by a factor of 2, vis-à-vis the single-element varying setup. The two-element varying bridge is commonly found in pressure sensors and flow meter systems.

A second case of the two-element varying bridge, Case 2, is shown in Figure 3.61C. This bridge requires two identical elements that vary in *opposite* directions. This could correspond to two identical strain gages: one mounted on top of a flexing surface, and one on the bottom. Note that this configuration is now linear, and like two-element varying Case 1, it has twice the sensitivity of the Figure 3.61A configuration. Another way to view this configuration is to consider the terms R+ΔR and R–ΔR as comprising two sections of a linear potentiometer.

The *all-element varying* bridge of Figure 3.61D produces the most signal for a given resistance change, and is inherently linear. It is also an industry-standard configuration for load cells constructed from four identical strain gages. Understandably, it is also one of the most popular bridge configurations.

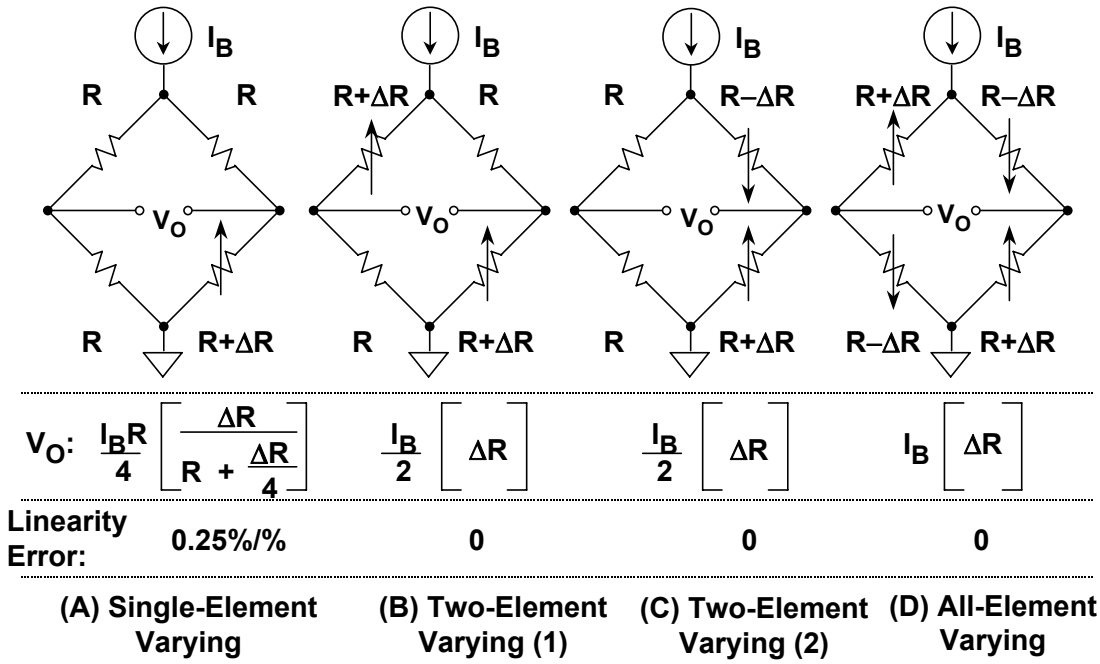

Figure 3.62: *The output voltage sensitivity and linearity of constant current drive bridge configurations also differs according to the number of active elements*

Bridges may also be driven from constant current sources, as shown in Figure 3.62, for the corresponding cases of single, dual, dual, and four active element(s). As with the voltage-driven bridges, the analogous output expressions are noted, along with the sensitivities.

Current drive, although not as popular as voltage drive, does have advantages when the bridge is located remotely from the source of excitation. One advantage is that the wiring resistance doesn't introduce errors in the measurement; another is simpler, less expensive cabling. Note also that with constant current excitation, all bridge configurations are linear except the single-element varying case of Figure 3.62A.

In summary, there are many design issues relating to bridge circuits, as denoted by Figure 3.63 below. After selecting the basic configuration, the excitation method must be

determined. The value of the excitation voltage or current must first be determined, as this directly influences sensitivity. Recall that the fullscale bridge output is directly proportional to the excitation voltage (or current). Typical bridge sensitivities are 1 mV/V to 10 mV/V.

Although large excitation voltages yield proportionally larger fullscale output voltages, they also result in higher bridge power dissipation, and thus raise the possibility of sensor resistor self-heating errors. On the other hand, low values of excitation voltage require more gain in the conditioning circuits, and also increase sensitivity to low level errors such as noise and offset voltages.

- **Selecting Configuration (1, 2, 4 - Element Varying)**
- **Selection of Voltage or Current Excitation**
- **Ratiometric Operation**
- **Stability of Excitation Voltage or Current**
- **Bridge Sensitivity: FS Output / Excitation Voltage**
  1mV / V to 10mV / V Typical
- **Fullscale Bridge Outputs: 10mV - 100mV Typical**
- **Precision, Low Noise Amplification / Conditioning**
  Techniques Required
- **Linearization Techniques May Be Required**
- **Remote Sensors Present Challenges**

Figure 3.63: *A number of bridge considerations impact design choices*

Regardless of the absolute level, the stability of the excitation voltage or current directly affects the overall accuracy of the bridge output, as is evident from the V_B and I_B terms in the output expressions. Therefore stable references and/or *ratiometric* drive techniques are required, to maintain highest accuracy.

Here, ratiometric simply refers to the use of the bridge drive voltage of a voltage-driven bridge (or a current-proportional voltage, for a current-driven bridge) as the reference input to the ADC that digitizes the amplified bridge output voltage. In this manner the absolute accuracy and stability of the excitation voltage becomes a second order error. Examples to follow illustrate this point further.

Amplifying and Linearizing Bridge Outputs

The output of a single-element varying bridge may be amplified by a single precision op-amp connected as shown in Figure 3.64. Unfortunately this circuit, although attractive because of relative simplicity, has poor overall performance. Its gain predictability and accuracy are poor, and it unbalances the bridge due to loading from R_F and the op amp bias current. The R_F resistors must be carefully chosen and matched to maximize common mode rejection (CMR). Also, it is difficult to maximize the CMR while at the same time allowing different gain options. Gain is dependent upon the bridge resistances and R_F. In addition, the output is nonlinear, as the configuration does nothing to address the intrinsic bridge non-linearity. In summary, the circuit isn't recommended for precision use.

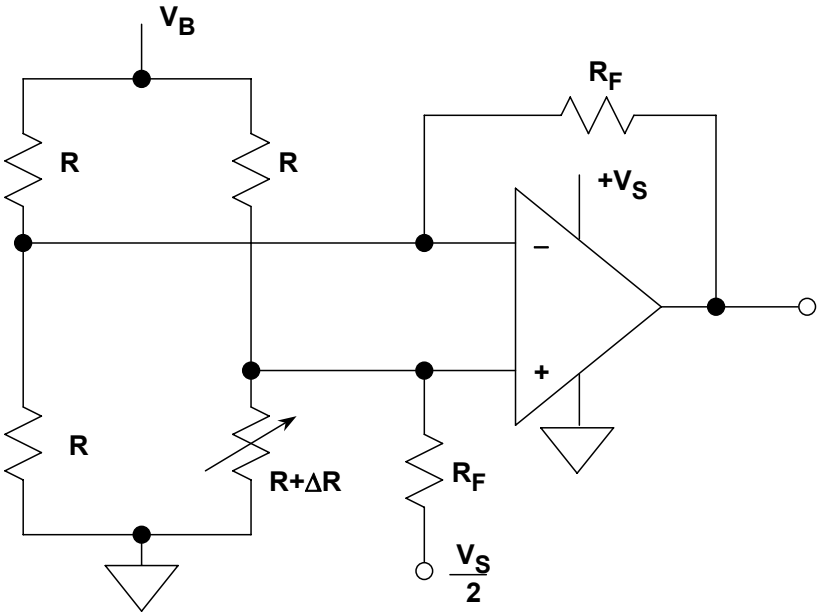

Figure 3.64: *Using a single op amp as a bridge amplifier*

However, a redeeming feature of this circuit is that it is capable of single supply operation, with a solitary op amp. Note that the R_F resistor connected to the non-inverting input is returned to $V_S/2$ (rather than ground) so that both positive and negative ΔR values can be accommodated, with the bipolar op amp output swing referenced to $V_S/2$.

A much better approach is to use an *instrumentation amplifier* (in-amp) for the required gain, as shown in Figure 3.65. This efficient circuit provides better gain accuracy, with the in-amp gain usually set with a single resistor, R_G. Since the amplifier provides dual, high-impedance loading to the bridge nodes, it does not unbalance or load the bridge. Using modern in-amp devices with gains ranging from 10-1000, excellent common mode rejection and gain accuracy can be achieved with this circuit.

However, due to the intrinsic characteristics of the bridge, the output is still nonlinear (see expression). As noted earlier, this can be corrected in software (assuming that the in-amp output is digitized using an analog-to-digital converter and followed by a microcontroller or microprocessor).

The in-amp can be operated on either dual supplies as shown, or alternately, on a single positive supply. In the figure, this corresponds to $-V_S = 0$. This is a key advantageous point, due the fact that all such bridge circuits bias the in-amp inputs at $V_B/2$, a voltage range typically compatible with amplifier bias requirements. In-amps such as the AD620 family, the AD623, and AD627 can be used in single (or dual) supply bridge applications, provided their restrictions on the gain and input and output voltage swings are observed.

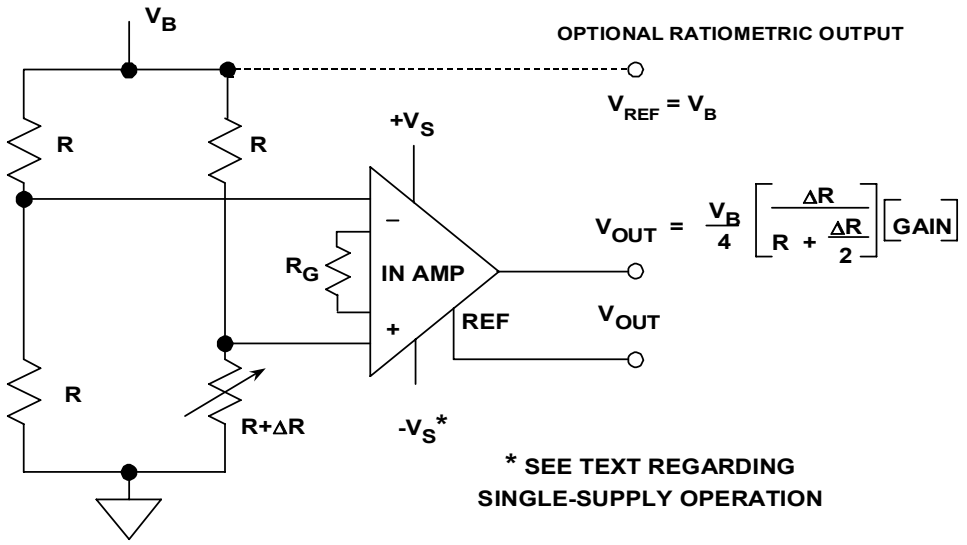

***Figure 3.65**: A generally preferred method of bridge amplification employs an instrumentation amplifier for stable gain and high CMR*

The bridge in this example is voltage driven, by the voltage V_B. This voltage can optionally be used for an ADC reference voltage, in which case it also is an additional output, V_{REF}.

Various techniques are available to linearize bridge outputs, but it is important to distinguish between the linearity of the bridge equation (discussed earlier), and the sensor response linearity to the phenomenon being sensed. For example, if the active sensor element is an RTD, the bridge used to implement the measurement might have perfectly adequate linearity; *yet the output could still be nonlinear,* due to the RTD device's intrinsic nonlinearity. Manufacturers of sensors employing bridges address the nonlinearity issue in a variety of ways, including keeping the resistive swings in the bridge small, shaping complementary nonlinear response into the active elements of the bridge, using resistive trims for first-order corrections, and others. In the examples which follow, what is being addressed is the linearity error of the bridge configuration itself (as opposed to a sensor element within the bridge).

Figure 3.66 shows a single-element varying active bridge circuit, in which an op amp produces a forced bridge null condition. For this single-element varying case, only the op amp feedback resistance varies, with the remaining three resistances fixed.

As used here, the op amp output provides a buffered, ground referenced, low impedance output for the bridge measurement, effectively suppressing the $V_B/2$ CM bridge component at the op amp inputs.

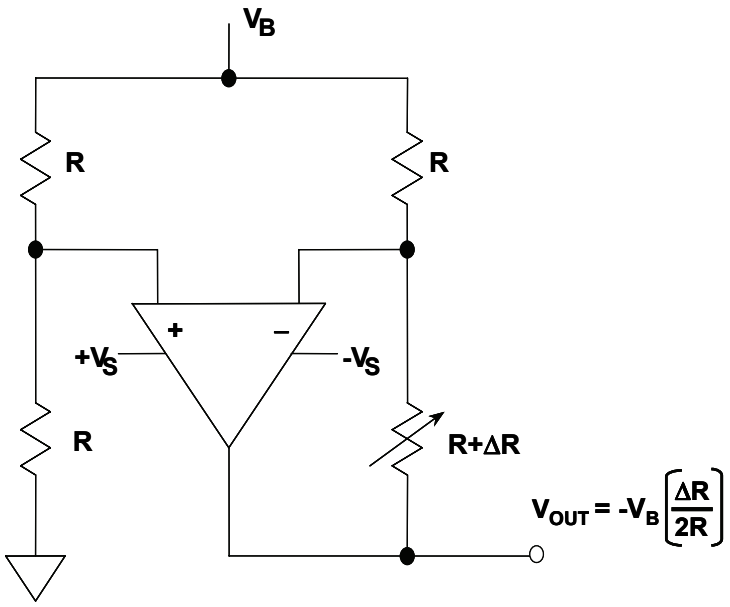

Figure 3.66: *Linearizing a single-element varying bridge (Method 1)*

The circuit works by adding a voltage in series with the variable resistance arm. This voltage is equal in magnitude and opposite in polarity to the incremental voltage across the varying element, and is linear with ΔR. As can be noted, the three constant "R" valued resistances and the op amp operate to drive a constant current in the variable resistance. This is the basic mechanism that produces the linearized output.

This active bridge has a sensitivity gain of two over the standard single-element varying bridge (Figure 3.62A, again). The key point is that the bridge's incremental resistance/ voltage output becomes linear, even for large values of ΔR. However, because of a still relatively small output signal, a second amplifier must usually follow this bridge. Note also that the op amp used in this circuit requires dual supplies, because its output must go negative for conditions where ΔR is positive.

Another circuit for linearizing a single-element varying bridge is shown in Figure 3.67. The top node of the bridge is excited by the voltage, V_B. The bottom of the bridge is driven in complementary fashion by the left op amp, which maintains a constant current of V_B/R in the varying resistance element, R + ΔR. Like the circuit of Figure 3.66, the constant current drive for the single-element variable resistance provides the mechanism for linearity improvement. Also, because of the fact that the bridge left-side center node is ground-referenced by the op amp, this configuration effectively suppresses CM voltages. This has the virtue of making the op amp selection somewhat less critical. Of course, performance parameters of high gain, low offset/noise, and high stability are all still needed.

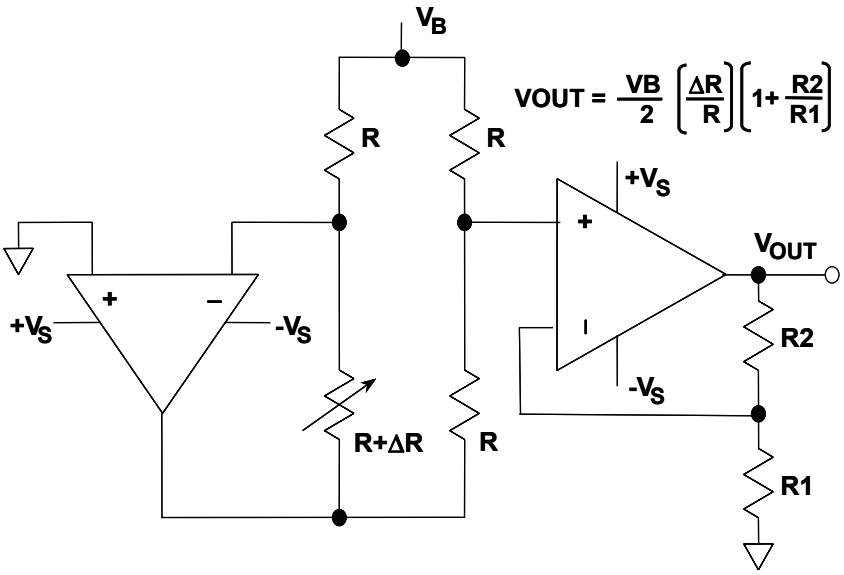

Figure 3.67: *Linearizing a single-element varying bridge (Method 2)*

The output signal is taken from the right-hand leg of the bridge, and is amplified by a second op amp, connected as a non-inverting gain stage. With the scaling freedom provided by the second op amp, the configuration is very flexible. The net output is linear, and has a bridge-output referred sensitivity comparable to the single-element varying circuit of Figure 3.66.

The circuit in Figure 3.67 requires two op amps operating on dual supplies. In addition, paired resistors R1-R2 must be ratio matched and stable types, for overall accurate and stable gain. The circuit can be a practical one using a dual precision op amp, such as an AD708, the OP2177 or the OP213.

A closely related circuit for linearizing a voltage-driven, *two-element* varying bridge can be adapted directly from the basic circuit of Figure 3.67. This form of the circuit, shown in Figure 3.68, is identical to the previous single-element varying case, with the exception that the resistance between V_B and the op amp (+) input is now also variable (i.e., both diagonal $R + \Delta R$ resistances vary, in a like manner).

For the same applied voltage V_B, this form of the circuit has twice the sensitivity, which is evident in the output expressions. A dual supply op amp is again required, and additional gain may also be necessary.

The two-element varying bridge circuit shown in Figure 3.69 uses an op amp, a sense resistor, and a voltage reference, set up in a feedback loop containing the sensing bridge. The net effect of the loop is to maintain a constant current through the bridge of $I_B = V_{REF}/R_{SENSE}$. The current through each leg of the bridge remains constant ($I_B/2$) as the resistances change, therefore the output is a linear function of ΔR. An in-amp provides the additional gain.

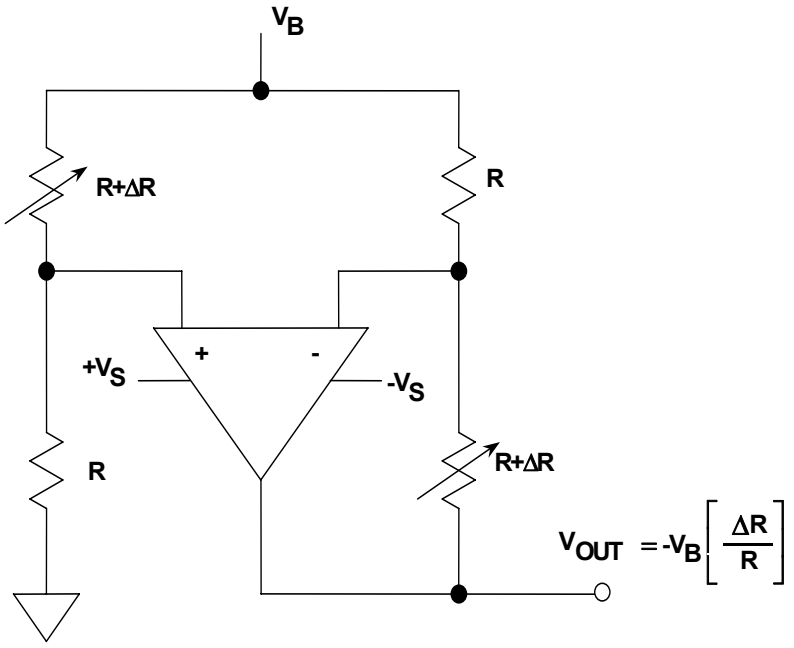

Figure 3.68: *Linearizing a two-element varying voltage-driven bridge (Method 1)*

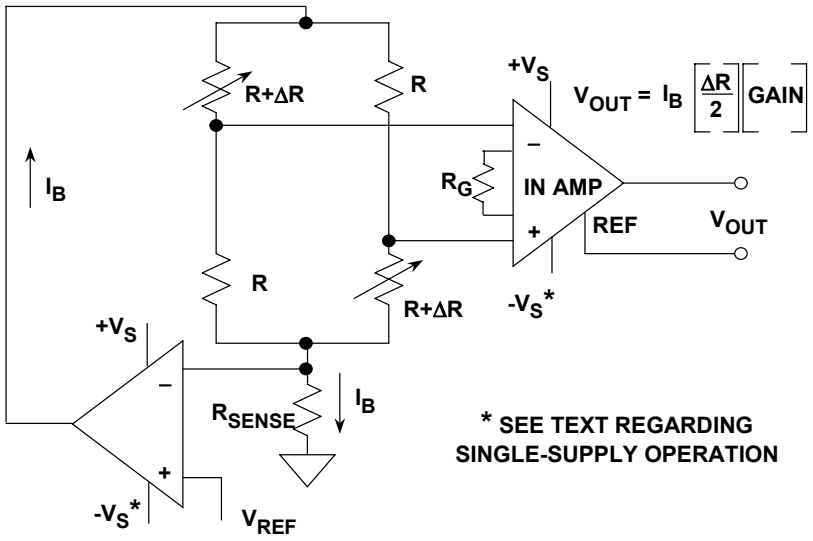

Figure 3.70: *Linearizing a two-element varying current-driven bridge (Method 2)*

This circuit can be operated on a single supply with the proper choice of amplifiers and signal levels. If ratiometric operation of an ADC is desired, the V_{REF} voltage can be used to drive the ADC.

Driving Remote Bridges

Wiring resistance and noise pickup are the biggest problems associated with remotely located bridges. Figure 3.71 shows a 350 Ω strain gage, which is connected to the rest of the bridge circuit by 100 feet of 30 gage twisted pair copper wire. The resistance of the wire at 25ºC is 0.105 Ω/ft, or 10.5 Ω for 100 ft. The total lead resistance in series with the 350 Ω strain gage is therefore 21 Ω. The temperature coefficient of the copper wire is 0.385%/ºC. Now we will calculate the gain and offset error in the bridge output due to a +10ºC temperature rise in the cable. These calculations are easy to make, because the bridge output voltage is simply the difference between the output of two voltage dividers, each driven from a +10 V source.

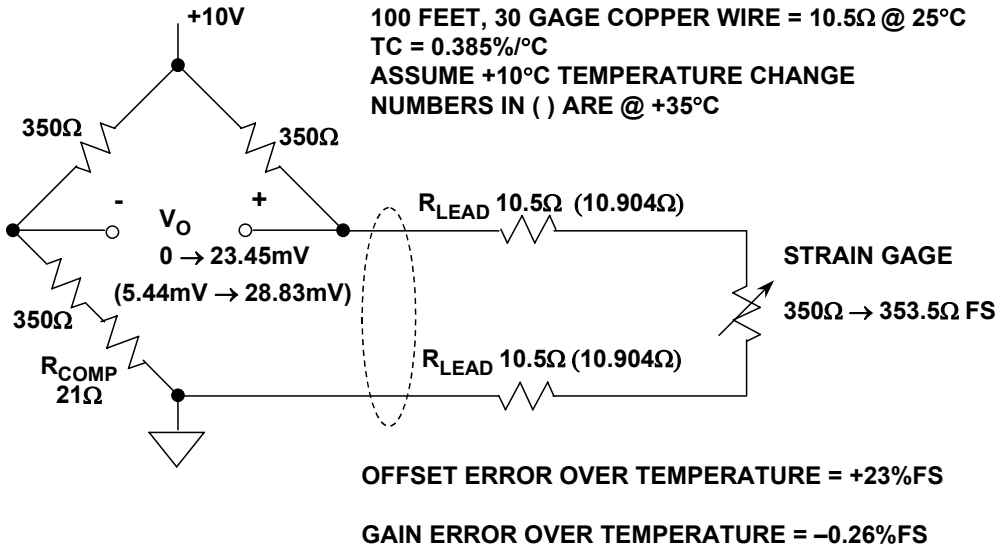

Figure 3.71: *Wiring resistance related errors with remote bridge sensor*

The fullscale variation of the strain gage resistance (with flex) above its nominal 350 Ω value is +1% (+3.5 Ω), corresponding to a fullscale strain gage resistance of 353.5 Ω which causes a bridge output voltage of +23.45 mV. Notice that the addition of the 21 Ω R_{COMP} resistor compensates for the wiring resistance and balances the bridge when the strain gage resistance is 350 Ω. Without R_{COMP}, the bridge would have an output offset voltage of 145.63 mV for a nominal strain gage resistance of 350 Ω. This offset could be compensated for in software just as easily, but for this example, we chose to do it with R_{COMP}.

Assume that the cable temperature increases +10ºC above nominal room temperature. This results in a total lead resistance increase of +0.404 Ω (10.5 Ω×0.00385/ºC×10ºC) in each lead. *Note: The values in parentheses in the diagram indicate the values at +35ºC.* The total additional lead resistance (of the two leads) is +0.808 Ω. With no strain, this additional lead resistance produces an offset of +5.44 mV in the bridge output. Fullscale strain produces a bridge output of +28.83 mV (a change of +23.39 mV from no strain).

Thus the increase in temperature produces an offset voltage error of +5.44 mV (+23% fullscale) and a gain error of –0.06 mV (23.39 mV – 23.45 mV), or –0.26% fullscale. Note that these errors are produced solely by the 30 gage wire, and do not include any temperature coefficient errors in the strain gage itself.

The effects of wiring resistance on the bridge output can be minimized by the 3-wire connection shown in Figure 3.72. We assume that the bridge output voltage is measured by a high impedance device, therefore there is no current in the sense lead. Note that the sense lead measures the voltage output of a divider: the top half is the bridge resistor plus the lead resistance, and the bottom half is strain gage resistance plus the lead resistance. The nominal sense voltage is therefore independent of the lead resistance. When the strain gage resistance increases to fullscale (353.5 Ω), the bridge output increases to +24.15 mV.

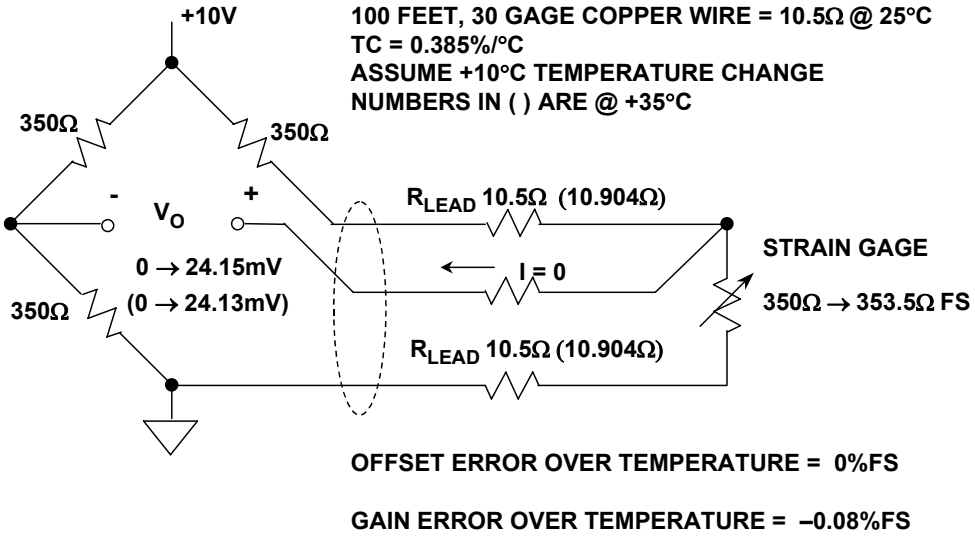

Figure 3.72: *Remote bridge wiring resistance errors are reduced with 3-wire sensor connection*

Increasing the temperature to +35ºC increases the lead resistance by +0.404 Ω in each half of the divider. The fullscale bridge output voltage decreases to +24.13 mV because of the small loss in sensitivity, but there is no offset error. The gain error due to the temperature increase of +10ºC is therefore only –0.02 mV, or –0.08% of fullscale. Compare this to the +23% fullscale offset error and the –0.26% gain error for the two-wire connection shown in Figure 3.72.

The three-wire method works well for remotely located resistive elements which make up one leg of a single-element varying bridge. However, all-element varying bridges generally are housed in a complete assembly, as in the case of a load cell. When these bridges are remotely located from the conditioning electronics, special techniques must be used to maintain accuracy.

Of particular concern is maintaining the accuracy and stability of the bridge excitation voltage. The bridge output is directly proportional to the excitation voltage, and any drift in the excitation voltage produces a corresponding drift in the output voltage.

For this reason, most all-element varying bridges (such as load cells) are six-lead ssemblies: two leads for the bridge output, two leads for the bridge excitation, and two *sense* leads. To take full advantage of the additional accuracy that these extra leads allow, a method called Kelvin or 4-wire sensing is employed, as shown in Figure 3.73 below.

In this setup the drive voltage V_B is not applied directly to the bridge, but goes instead to the input of the upper precision op amp, which is connected in a feedback loop around the bridge (+) terminal. Although there may be a substantial voltage drop in the +FORCE lead resistance of the remote cable, the op amp will automatically correct for it, since it has a feedback path through the +SENSE lead. The net effect is that the upper node of the remote bridge is maintained at a precise level of V_B (within the capability of the op amp used, of course). A similar situation occurs with the bottom precision op amp, which drives the bridge (-) terminal to a ground level, as established by the op amp input ground reference. Again, the voltage drop in the –FORCE lead is relatively immaterial, because of the sensing at the –SENSE terminal.

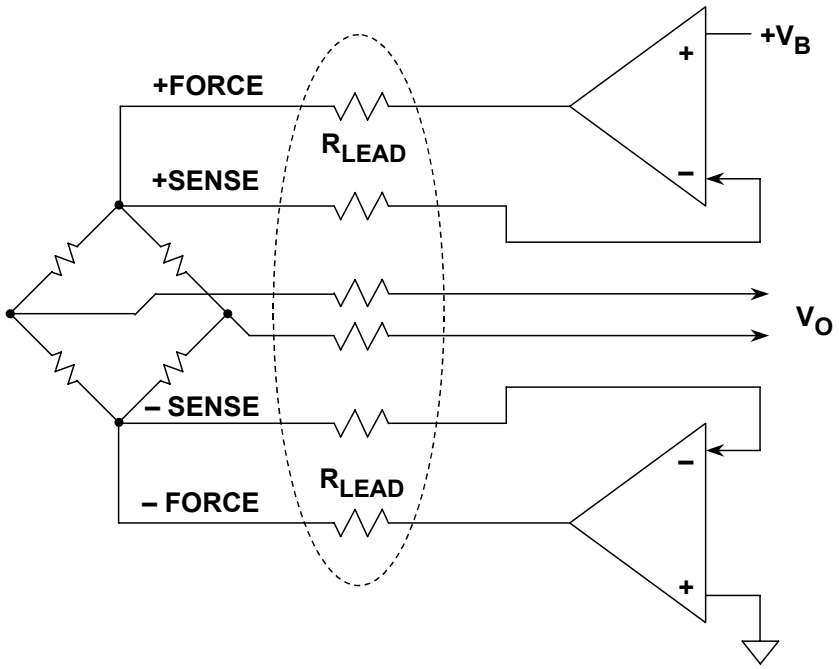

Figure 3.73: *A Kelvin sensing system with a 6-wire voltage-driven bridge connection and precision op amps minimizes errors due to wire lead resistances*

In both cases, the sense lines go to high impedance op amp inputs, thus there is minimal error due to the bias current induced voltage drop across their lead resistance. The op amps maintain the required excitation voltage at the remote bridge, to make the voltage measured between the (+) and (-) sense leads always equal to V_B.

Note— a subtle point is that the lower op amp will need to operate on dual supplies, since the drive to the -FORCE lead will cause the op amp output to go negative. Because of relatively high current in the bridge (~30 mA), current buffering stages at the op amp outputs are likely advisable for this circuit.

Although Kelvin sensing eliminates errors due to voltage drops in the bridge wiring resistance, the basic drive voltage V_B must still be highly stable since it directly affects the bridge output voltage. In addition, the op amps must have low offset, low drift, and low noise. Ratiometric operation can be optionally added, simply by using V_B to drive the ADC reference input.

The constant current excitation method shown in Figure 3.74 below is another method for minimizing the effects of wiring resistance on the measurement accuracy. This system drives a precise current I through the bridge, proportioned as per the expression in the figure. An advantage of the circuit in Figure 3.74 is that it only uses one amplifier.

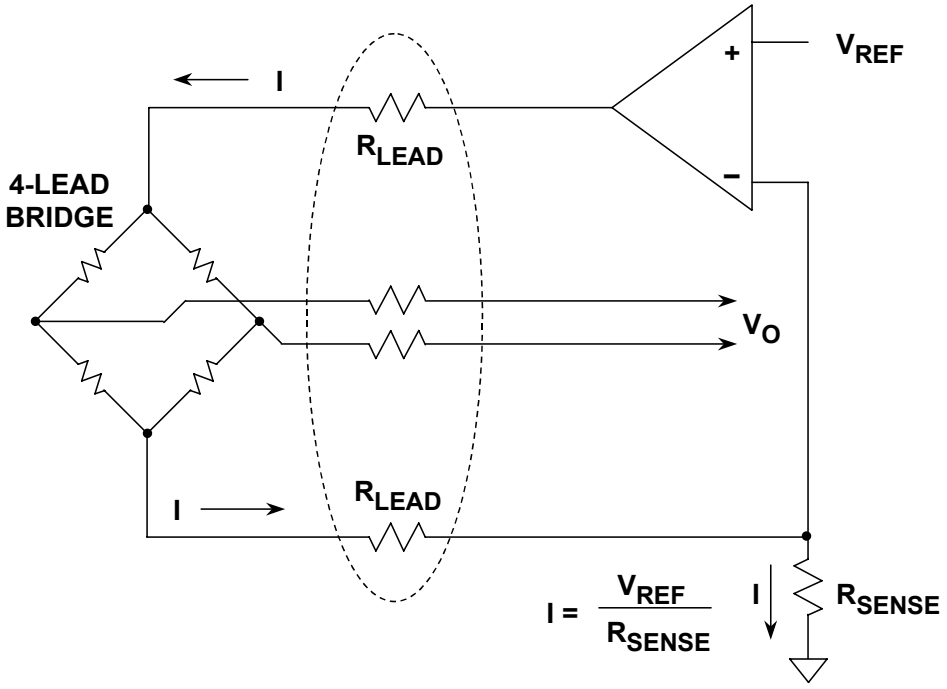

Figure 3.74: *A 4-wire current-driven bridge scheme also minimizes errors due to wire lead resistances, plus allows simpler cabling*

However, the accuracy of the reference, the sense resistor, and the op amp all influence the overall accuracy. While the precision required of the op amp should be obvious, one thing not necessarily obvious is that it may be required to deliver appreciable current, when I is more than a few mA (which it will be with standard 350 Ω bridges). In such cases, current buffering of the op amp is again in order.

Therefore for highest precision with this circuit, a buffer stage is recommended. This can be as simple as a small transistor, since the bridge drive is unidirectional.

System offset minimization

Maintaining an accuracy of 0.1% or better with a fullscale bridge output voltage of 20 mV requires that the sum of all offset errors be less than 20 μV. Parasitic thermocouples are cases in point, and if not given due attention, they can cause serious temperature drift errors. All dissimilar metal-metal connections generate voltages between a few and tens of microvolts for a 1ºC temperature differential, are basic thermocouple fact-of-life.

Fortunately however, within a bridge measurement system the signal connections are differential, therefore this factor can be used to minimize the impact of parasitic thermocouples.

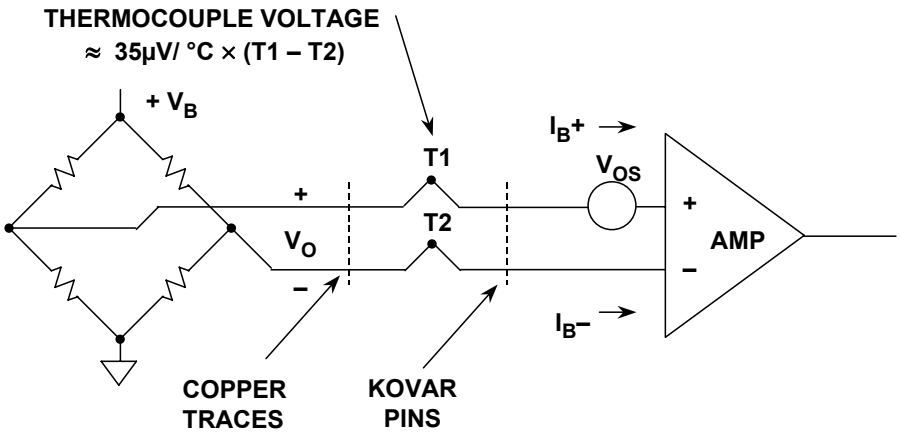

Figure 3.75: *Typical sources of offset voltage within bridge measurement systems*

Figure 3.75 shows some typical sources of offset error that are inevitable in a system. Within a differential signal path, only those thermocouple pairs whose junctions are actually at different temperatures will degrade the signal. The diagram shows a typical parasitic junction formed between the copper printed circuit board traces and the kovar pins of an IC amplifier.

This thermocouple voltage is about 35 μV/ºC temperature differential. Note that this package-PC trace thermocouple voltage is significantly less when using a plastic package with a copper lead frame (recommended). Regardless of what package is used, all metal-metal connections along the signal path should be designed so that minimal temperature differences occur between the sides.

The amplifier offset voltage and bias currents are further sources of offset error. The amplifier bias current must flow through the source impedance. Any unbalance in either the source resistances or the bias currents produce offset errors. In addition, the offset voltage and bias currents are a function of temperature.

High performance low offset, low offset drift, low bias current, and low noise precision amplifiers such as the AD707, the OP177 or OP1177 are required. In some cases, chopper-stabilized amplifiers such as the AD8551/AD8552/AD8554 may be a solution.

AC bridge excitation such as that shown in Figure 3.76 below can effectively remove offset voltage effects in series with a bridge output, V_O.

The concept is simple, and can be described as follows. The net bridge output voltage is measured under the two phased-sequence conditions, as shown. A first measurement (top) drives the bridge at the top node with excitation voltage V_B. This yields a first-phase measurement output V_A, where V_A is the sum of the desired bridge output voltage V_O and the net offset error voltage E_{OS}.

In the second measurement (bottom) the polarity of the bridge excitation is then reversed, and a second measurement, V_B, is made. Subtracting V_B from V_A yields $2V_O$, and the offset error term E_{OS} cancels as noted from the mathematical expression in the figure.

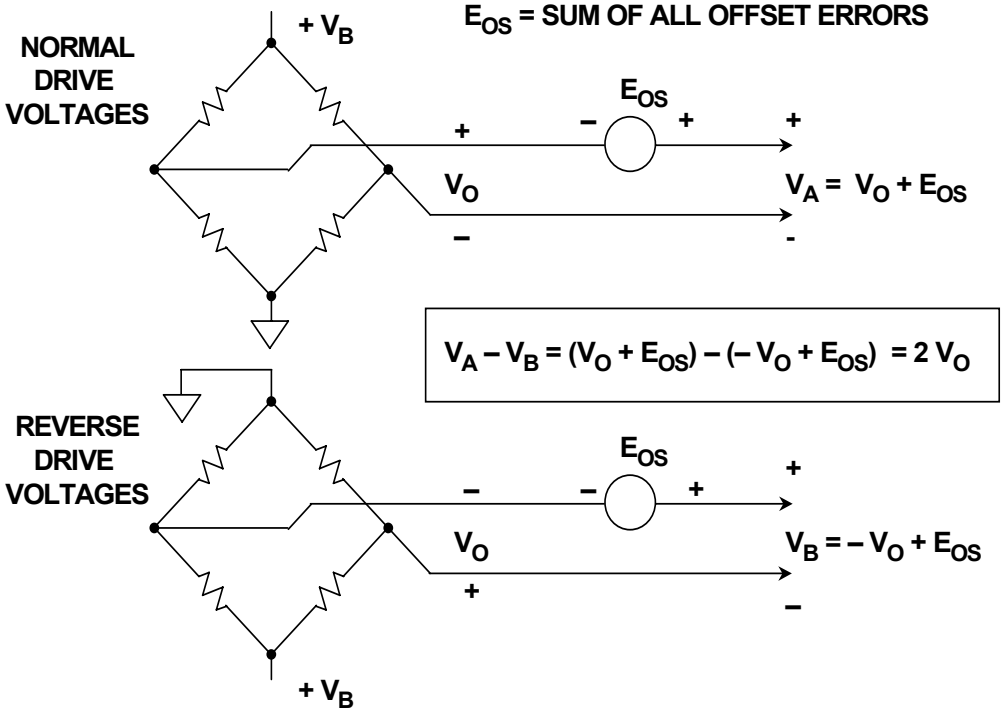

Figure 3.76: *AC bridge excitation minimizes system offset voltages*

Obviously, a full implementation of this technique requires a highly accurate measurement ADC such as the AD7730 (see Reference 5) as well as a microcontroller to perform the subtraction.

Note that if a ratiometric reference is desired, the ADC must also accommodate the changing polarity of the reference voltage, as well as sense the magnitude. Again, the AD7730 includes this capability.

A very powerful combination of bridge circuit techniques is shown in Figure 3.77, an example of a high performance ADC. In Figure 3.77A is shown a basic DC operated ratiometric technique, combined with Kelvin sensing to minimize errors due to wiring resistance, which eliminates the need for an accurate excitation voltage.

The AD7730 measurement ADC can be driven from a single supply voltage of 5 V, which in this case is also used to excite the remote bridge. Both the analog input and the reference input to the ADC are high impedance and fully differential. By using the + and – SENSE outputs from the bridge as the differential reference voltage to the ADC, there is no loss in measurement accuracy if the actual bridge excitation voltage varies.

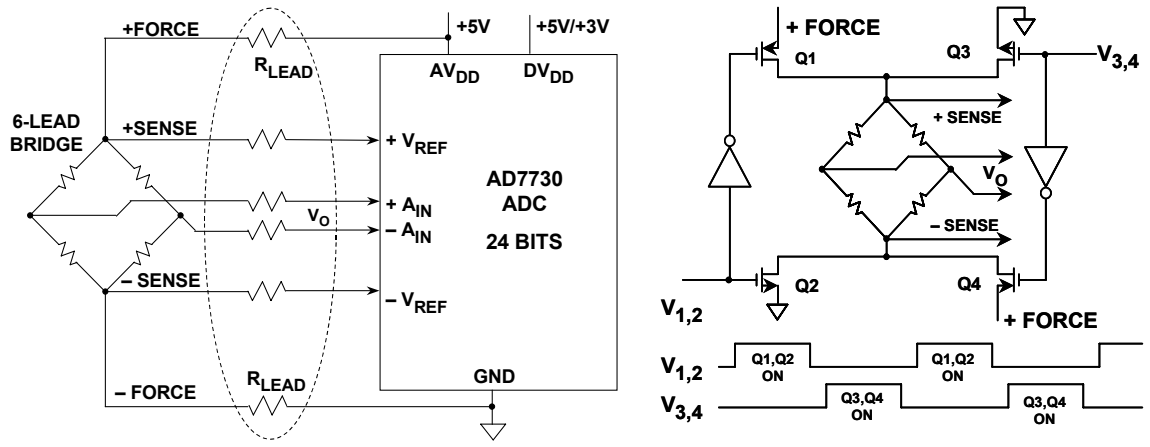

(A) DC excitation **(B) AC excitation (simplified)**

Figure 3.77: *Ratiometric DC or AC operation with Kelvin sensing can be implemented using the AD7730 ADC*

To implement AC bridge operation of the AD7730, an "H" bridge driver of P-Channel and N-Channel MOSFETs can be configured as shown in Figure 3.77B (note — dedicated bridge driver chips are available, such as the Micrel MIC4427). This scheme, added to the basic functionality of the AD7730 configuration of Figure 3.77A greatly increases the utility of the offset canceling circuit, as generally outlined in the preceding discussion of Figure 3.76.

Because of the on-resistance of the H-bridge MOSFETs, Kelvin sensing must also be used in these AC bridge applications. It is also important that the drive signals be non-overlapping, as noted, to prevent excessive MOSFET switching currents. The AD7730 ADC has on-chip circuitry which generates the required non-overlapping drive signals to implement this AC bridge excitation. All that needs adding is the switching bridge as noted in Figure 3.77B.

The AD7730 is one of a family of sigma-delta ADCs with high resolution (24 bits) and internal programmable gain amplifiers (PGAs) and is ideally suited for bridge applications. These ADCs have self- and system calibration features, which allow offset and gain errors due to the ADC to be minimized. For instance, the AD7730 has an offset drift of 5 nV/ºC and a gain drift of 2 ppm/ºC. Offset and gain errors can be reduced to a few microvolts using the system calibration feature.

REFERENCES: BRIDGE CIRCUITS

1. Ramon Pallas-Areny and John G. Webster, **Sensors and Signal Conditioning**, John Wiley, New York, 1991.

2. Dan Sheingold, Editor, **Transducer Interfacing Handbook**, Analog Devices, Inc., 1980, ISBN: 0-916550-05-2.

3. Sections 2, 3, Walt Kester, Editor, **1992 Amplifier Applications Guide**, Analog Devices, 1992, ISBN: 0-916550-10-9.

4. Sections 1, 6, Walt Kester, Editor, **System Applications Guide**, Analog Devices, 1993, ISBN: 0-916550-13-3.

5. Data sheet for **AD7730 Bridge Transducer ADC**, http://www.analog.com

SECTION 3-5: STRAIN, FORCE, PRESSURE AND FLOW MEASUREMENTS

Strain Gages

The most popular electrical elements used in force measurements include the resistance strain gage, the semiconductor strain gage, and piezoelectric transducers. The strain gage measures force indirectly by measuring the deflection it produces in a calibrated carrier. Pressure can be converted into a force using an appropriate transducer, and strain gage techniques can then be used to measure pressure. Flow rates can be measured using differential pressure measurements, which also make use of strain gage technology. These principles are summarized in Figure 3.78 below.

- **Strain:** **Strain Gage, PiezoElectric Transducers**
- **Force:** **Load Cell**
- **Pressure:** **Diaphragm to Force to Strain Gage**
- **Flow:** **Differential Pressure Techniques**

Figure 3.78: *Strain gages are directly or indirectly the basis for a variety of physical measurements*

The resistance-based strain gage uses a resistive element which changes in length, hence resistance, as the force applied to the base on which it is mounted causes stretching or compression. It is perhaps the most well known transducer for converting force into an electrical variable.

An *unbonded* strain gage consists of a wire stretched between two points. Force acting upon the wire (area = A, length = L, resistivity = ρ) will cause the wire to elongate or shorten, which will cause the resistance to increase or decrease proportionally according to:

$$R = \rho L/A \qquad \text{Eq. 3-36}$$

and,

$$\Delta R/R = GF \cdot \Delta L/L \qquad \text{Eq. 3-37}$$

where GF = Gage factor (2.0 to 4.5 for metals, and more than 150 for semiconductors).

In this expression, the dimensionless quantity $\Delta L/L$ is a measure of the force applied to the wire and is expressed in *microstrains* ($1\ \mu\varepsilon = 10^{-6}$ cm/cm) which is the same as parts-per-million (ppm).

From equation 3-37, note that larger gage factors result in proportionally larger resistance changes, hence this implies greater strain gage sensitivity. These concepts are summarized in the drawing of Figure 3.79 below.

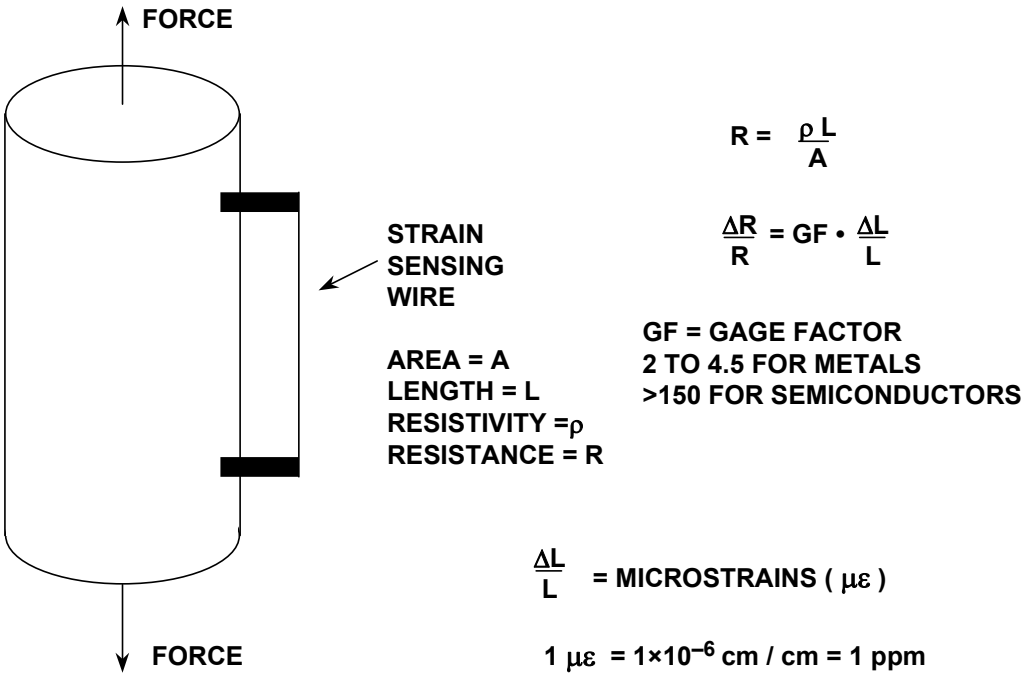

Figure 3.79: *Operating principles of a basic unbonded strain gage*

A *bonded* strain gage consists of a thin wire or conducting film arranged in a coplanar pattern and cemented to a base or carrier. The basic form of this type of gage is shown in Figure 3.80.

This strain gage is normally mounted so that as much as possible of the length of the conductor is aligned in the direction of the stress that is being measured, i.e., longitudinally. Lead wires are attached to the base and brought out for interconnection. Bonded devices are considerably more practical and are in much wider use than are the aforementioned unbonded devices.

Perhaps the most popular version is the *foil-type gage*, produced by photo-etching techniques, and using similar metals to the wire types. Typical alloys are of copper-nickel (Constantan), nickel-chromium (Nichrome), nickel-iron, platinum-tungsten, etc. This strain gage type is shown in Figure 3.81.

Gages having *wire sensing elements* present a small surface area to the specimen; this reduces leakage currents at high temperatures and permits higher isolation potentials between the sensing element and the specimen. Foil sensing elements, on the other hand, have a large ratio of surface area to cross-sectional area and are more stable under extremes of temperature and prolonged loading. The large surface area and thin cross section also permit the device to follow the specimen temperature and facilitate the dissipation of self-induced heat.

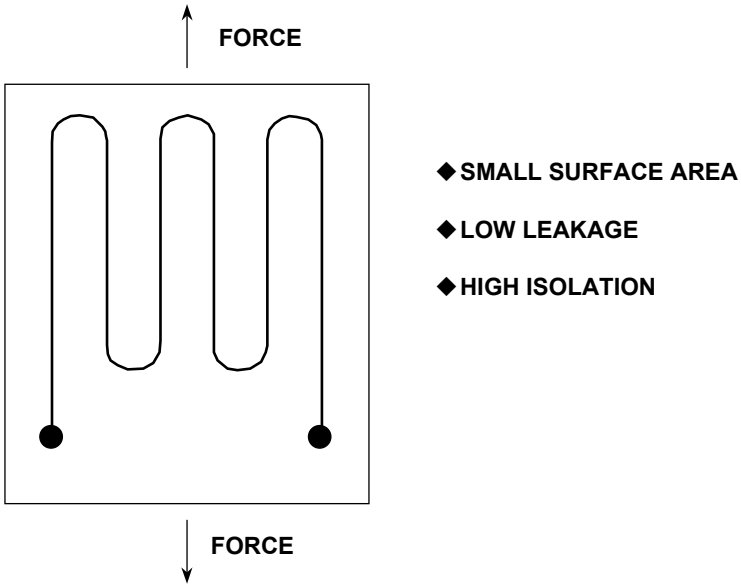

Figure 3.80: *A bonded wire strain gage*

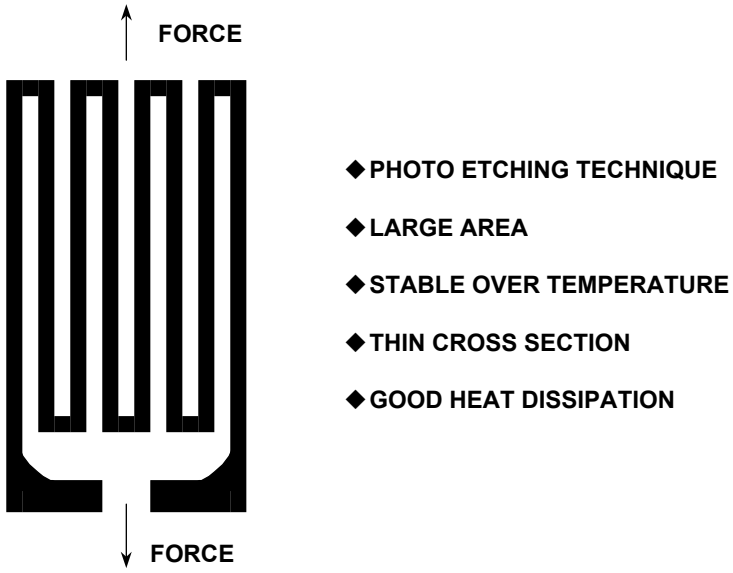

Figure 3.81: *A metal foil strain gage*

Semiconductor strain gages

Semiconductor strain gages make use of the piezoresistive effect in certain semiconductor materials such as silicon and germanium in order to obtain greater sensitivity and higher-level output.

Semiconductor gages can be produced to have either positive or negative changes when strained. They can be made physically small while still maintaining a high nominal resistance.

Semiconductor strain gage bridges may have 30 times the sensitivity of bridges employing metal films, but are temperature sensitive and difficult to compensate. Their change in resistance with strain is also nonlinear. They are not in as widespread use as the more stable metal-film devices for precision work; however, where sensitivity is important and temperature variations are small, they may have some advantage.

Instrumentation is similar to that for metal-film bridges but is less critical because of the higher signal levels and decreased transducer accuracy. Figure 3.82 summarizes the relative performance of metal and semiconductor strain gages.

PARAMETER	METAL STRAIN GAGE	SEMICONDUCTOR STRAIN GAGE
Measurement Range	0.1 to 40,000 με	0.001 to 3000 με
Gage Factor	2.0 to 4.5	50 to 200
Resistance, Ω	120, 350, 600, …, 5000	1000 to 5000
Resistance Tolerance	0.1% to 0.2%	1% to 2%
Size, mm	0.4 to 150 Standard: 3 to 6	1 to 5

Figure 3.82: *A comparison of metal and semiconductor type strain gages*

Strain gages can be used to measure force, as shown in Figure 3.82, where a cantilever beam is slightly deflected by the applied force. Four strain gages are used to measure the flex of the beam, two on the top, and two on the bottom. The gages are connected in a four-element bridge configuration. Recall from the last section that this configuration gives maximum sensitivity and is inherently linear. This configuration also offers first-order correction for temperature drift in the individual strain gages.

Strain gages are low-impedance devices, consequently they require significant excitation power to obtain reasonable levels of output voltage. A typical strain-gage based load cell bridge will have a 350 Ω impedance and is specified as having a sensitivity in a range 3-10 millivolts full scale, per volt of excitation.

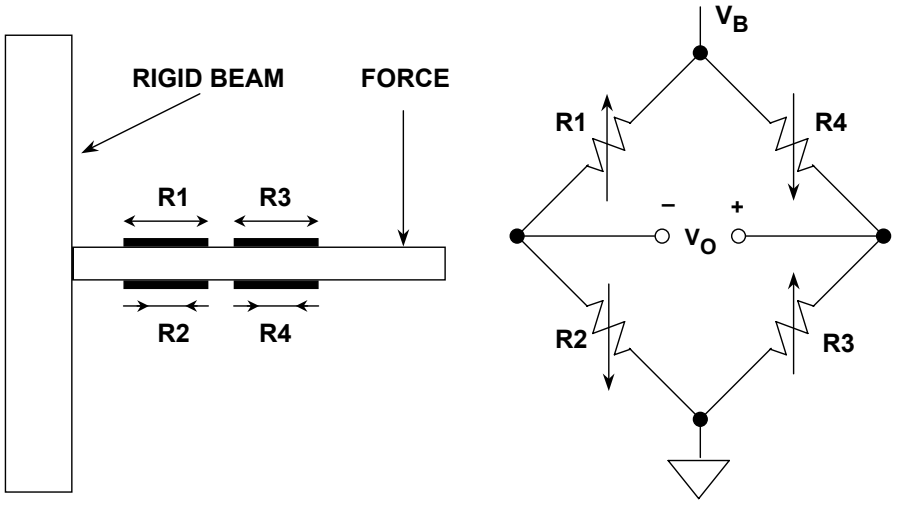

Figure 3.83: *A beam force sensor using a strain gage bridge*

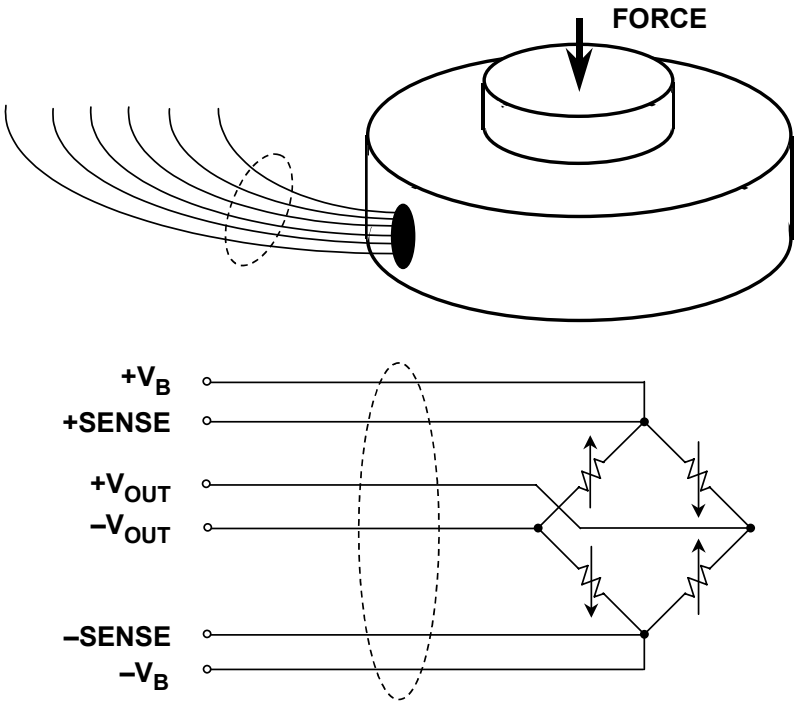

Figure 3.84: *A load cell comprised of 4 strain gages is shown in physical (top) and electrical (bottom) representations*

The load cell is composed of four individual strain gages arranged as a bridge, as shown in Figure 3.84. For a 10 V bridge excitation voltage with a rating of 3 mV/V, 30 millivolts of signal will be available at full scale loading.

While increasing the drive to the bridge can increase the output, self-heating effects are a significant limitation to this approach— they can cause erroneous readings, or even device destruction. One technique for evading this limitation is to use a low duty cycle pulsed drive signal for the excitation.

Many load cells have the ±"SENSE" connections as shown, to allow the signal-conditioning electronics to compensate for DC drops in the wires (Kelvin sensing as discussed in the last section). This brings the wires to a total of 6 for the fully instrumented bridge. Some load cells may also have additional internal resistors, for temperature compensation purposes.

Pressures in liquids and gases are measured electrically by a variety of pressure transducers. A number of mechanical converters (including diaphragms, capsules, bellows, manometer tubes, and Bourdon tubes) are used to measure pressure by measuring an associated length, distance, or displacement, and to measure pressure changes by the motion produced, as shown by Figure 3.85.

The output of this mechanical interface is then applied to an electrical converter such as a strain gage, or piezoelectric transducer. Unlike strain gages, piezoelectric pressure transducers are typically used for high-frequency pressure measurements (such as sonar applications, or crystal microphones).

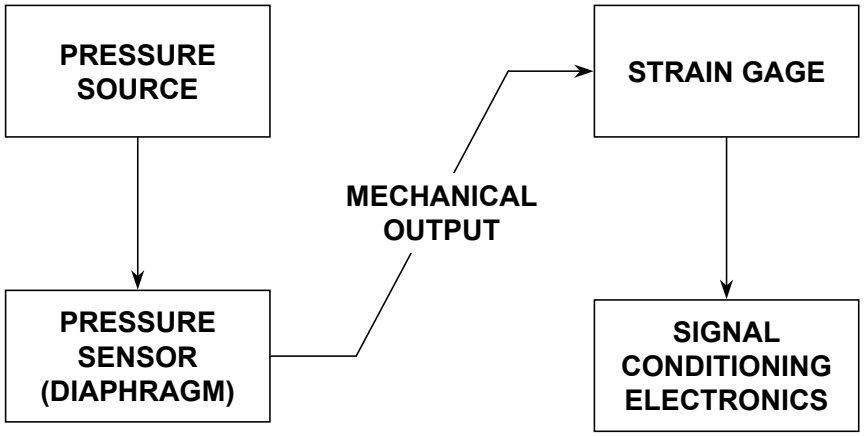

Figure 3.85: *Pressure sensors use strain gages for indirect pressure measurement*

There are many ways of defining flow (mass flow, volume flow, laminar flow, turbulent flow). Usually the *amount* of a substance flowing (mass flow) is the most important, and if the fluid's density is constant, a volume flow measurement is a useful substitute that is generally easier to perform. One commonly used class of transducers, which measures flow rate indirectly, involves the measurement of pressure.

Flow can be derived by taking the differential pressure across two points in a flowing medium - one at a static point and one in the flow stream. *Pitot tubes* are one form of

device used to perform this function, where flow rate is obtained by measuring the differential pressure with standard pressure transducers.

Differential pressure can also be used to measure flow rate using the *venturi* effect by placing a restriction in the flow. Although there are a wide variety of physical parameters being sensed, the electronics interface is very often strain gage based.

Bridge Signal Conditioning Circuits

The remaining discussions of this section deal with applications that apply the bridge and strain gage concepts discussed thus far in general terms.

An example of an all-element varying bridge circuit is a fatigue monitoring strain sensing circuit, as shown in Figure 3.86. The full bridge is an integrated unit, which can be attached to the surface on which the strain or flex is to be measured. In order to facilitate remote sensing, current mode bridge drive is used. The remotely located bridge is connected to the conditioning electronics through a 4-wire shielded cable. The OP177 precision op amp servos the bridge current to 10mA, being driven from an AD589 reference voltage of 1.235V. Current buffering of the op amp is employed in the form of the PNP transistor, for lowest op amp self-heating, and highest gain linearity.

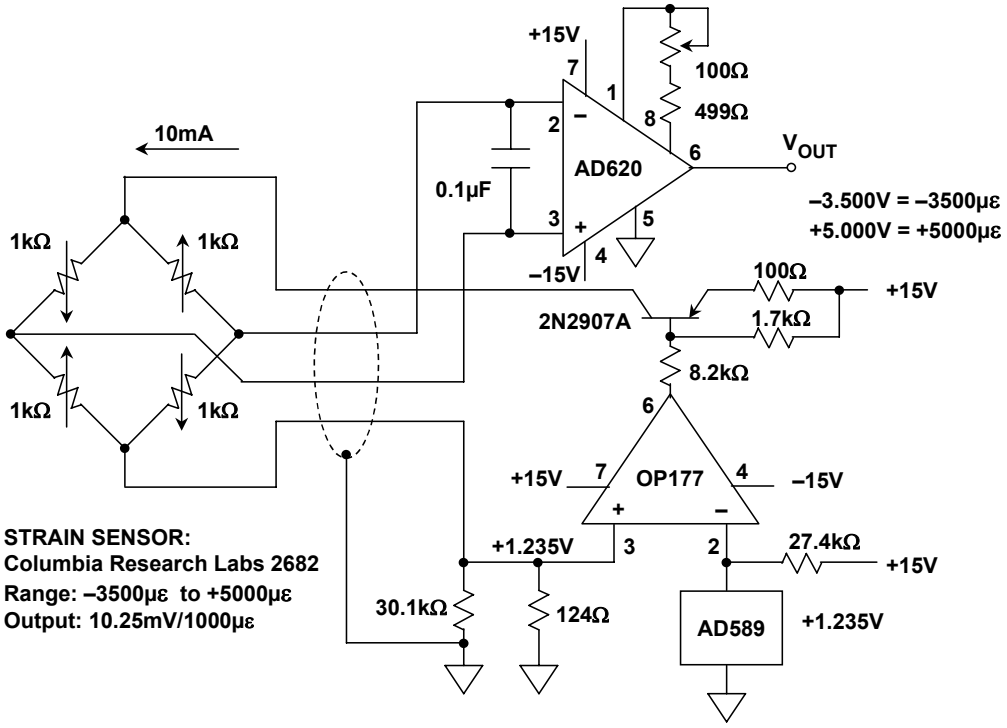

Figure 3.86: *A precision strain gage sensor amplifier using a remote current-driven 1kΩ bridge, a buffered precision op amp driver, and a precision in-amp 100X gain stage*

The strain gauge produces an output of 10.25 mV/1000 με. The signal is amplified by the AD620 in-amp, which is configured for a gain of 100 times, via an effective R_G of 500 Ω. Full-scale voltage calibration is set by adjusting the 100 Ω gain potentiometer such that, for a sensor strain of –3500 με, the output reads –3.500 V; and for a strain of +5000 με, the output registers +5.000 V. The measurement may then be digitized with an ADC which has a 10 V fullscale input range.

The 0.1μF capacitor across the AD620 input pins serves as an EMI/RFI filter in conjunction with the bridge resistance of 1 kΩ. The corner frequency of this filter is approximately 1.6 kHz.

Another example is a load cell amplifier circuit, shown in Figure 3.87. This circuit is more typical of a bridge workhorse application. It interfaces with a typical 350 Ω load cell, and can be configured to accommodate typical bridge sensitivities over a range of 3-10 mV/V.

A 10.000 V bridge excitation excitation is derived from an AD588 10 V reference, with an OP177 and 2N2219A used as a buffer. The 2N2219A is within the OP177 feedback loop and supplies the necessary bridge drive current (28.57 mA). This insures that the op amp performance will not be compromised. The Kelvin sensing scheme used at the bridge provides for low errors due to wiring resistances, and a precision zener diode reference, the AD588, provides lowest excitation drift and scaling with temperature changes.

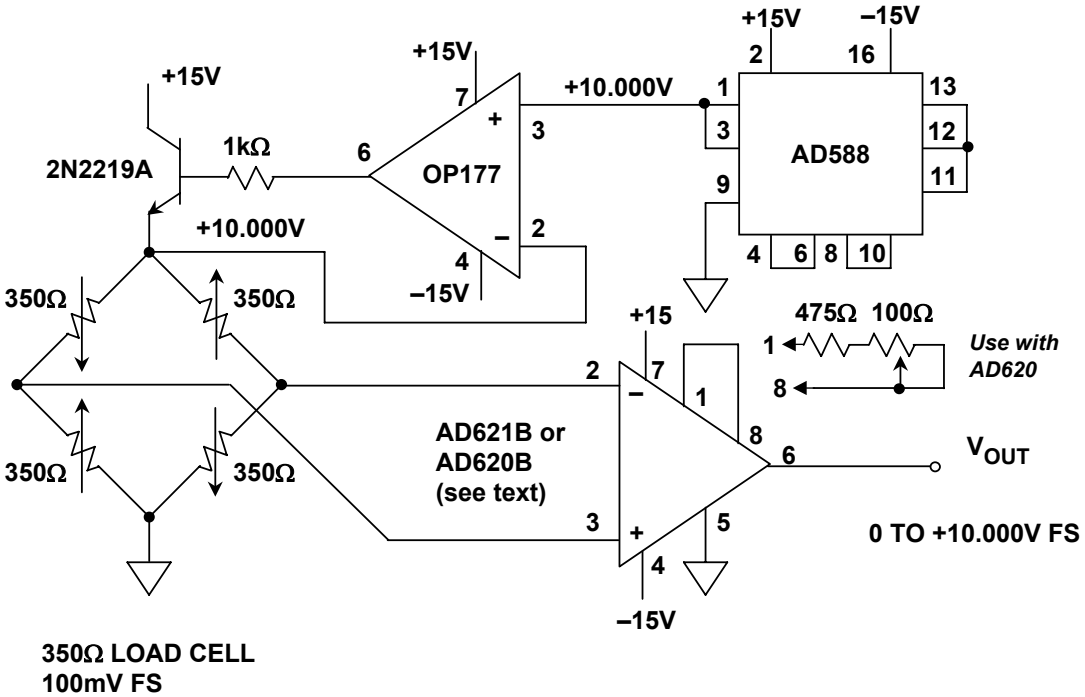

Figure 3.87: *A precision 350Ω load cell amplifier, using a buffered voltage-driven configuration with Kelvin sensing and a precision in-amp*

To ensure highest linearity is preserved, a low drift instrumentation amplifier is used as the gain stage. This design has a minimum number of critical resistors and amplifiers, making the entire implementation accurate, stable, and cost effective. In addition to low excitation voltage TC, another stability requirement is minimum in-amp gain TC. Both factors are critical towards insuring stable circuit scaling over temperature.

With the use of the AD621B in-amp as shown, the scaling is for a precise gain of 100 (as set by the pin 1-8 jumper), for lowest in-amp gain TC. The AD621B is specified for a very low gain TC, only 5 ppm/°C. The gain of 100 translates a 100 mV fullscale bridge output to a nominal 10 V output. Alternately, an AD620B could also be used, with the optional gain network consisting of the fixed 475 Ω resistor, and 100 Ω potentiometer for gain adjustment. This will provide a 50 ppm/°C gain TC for the in-amp, plus the TC of the external parts (which should have low temperature coefficients).

While the lowest TC is provided by the fixed gain AD621 setup, it doesn't allow direct control of overall scaling. To retain the very lowest TC, scaling could be accomplished via a software auto-calibration routine. Alternately, the AD588 and OP177 reference/op amp stage could be configured for a variable excitation voltage (as opposed to a fixed 10.000 V as shown). Variable gain in the reference voltage driver will effectively alter the excitation voltage as seen by the bridge, and thus provide flexible overall system scaling. Of course, it is imperative that such a scheme be implemented with low TC resistances.

As shown previously, a precision load cell is usually configured as a 350 Ω bridge. Figure 3.88 shows a precision load cell amplifier, within a circuit possessing the advantage of being powered from just a single power supply.

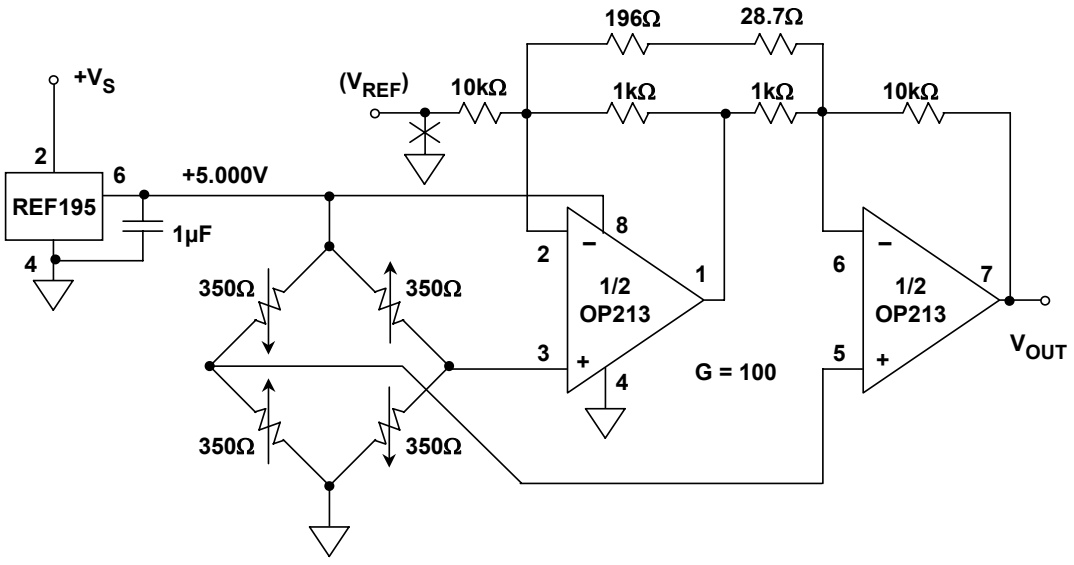

Figure 3.88: *A single-supply load cell amplifier*

As noted previously, the bridge excitation voltage must be both precise and stable, otherwise it can introduce measurement errors. In this circuit, a precision REF195 5 V reference is used as the bridge drive, allowing a TC as low as 5 ppm/°C. The REF195

reference can also supply more than 30 mA to a load, so it can drive a 350 Ω bridge (~14 mA) without need of a buffer. The dual OP213 is configured as a gain-of-100, two op amp in-amp. The resistor network sets the gain according to the formula:

$$G = 1 + \frac{10\,k\Omega}{1\,k\Omega} + \frac{20\,k\Omega}{196\Omega + 28.7\Omega} = 100 \qquad \text{Eq. 3-38}$$

For optimum CMR, the 10 kΩ/1 kΩ resistor ratio matching should be precise. Close tolerance resistors (±0.5% or better) should be used, and all resistors should be of the same type.

For a zero volt bridge output signal, the amplifier will swing to within 2.5 mV of 0 V. This is the minimum output limit of the OP213. Therefore, if an offset adjustment is required, the adjustment should start from a positive voltage at V_{REF} and adjust V_{REF} downward until the output (V_{OUT}) stops changing. This is the point where the amplifier limits the swing. Because of the single supply design, the amplifier cannot sense input signals which have negative polarity.

If linearity around or at zero volts input is required, or if negative polarity signals must be processed, the V_{REF} connection can be connected to a stable voltage which is mid-supply (i.e., 2.5 V) rather than ground. Note that when V_{REF} is not at ground, the output must be referenced to V_{REF}. An advantage of this type of referencing is that the output is now bipolar, with respect to V_{REF}.

The AD7730 24-bit sigma-delta ADC is ideal for direct conditioning of bridge outputs, and requires no interface circuitry (see Reference 10). A simplified connection diagram was shown in Figure 3.77A (again). The entire circuit operates on a single +5 V supply, which also serves as the bridge excitation voltage. Note that the measurement is ratiometric, because the sensed bridge excitation voltage is also used as the ADC reference. Variations in the +5 V supply do not affect the accuracy of the measurement.

The AD7730 has an internal programmable gain amplifier which allows a fullscale bridge output of ±10 mV to be digitized to 16-bit accuracy. The AD7730 has self and system calibration features which allow offset and gain errors to be minimized with periodic recalibrations.

A "chop" or AC mode option minimizes the offset voltage and drift and operates similarly to a chopper-stabilized amplifier. The effective input voltage noise RTI will be approximately 40 nV rms, or 264 nV peak-to-peak. This corresponds to a resolution of 13 ppm, or approximately 16.5-bits . Gain linearity is also approximately 16-bits.

REFERENCES: STRAIN, FORCE, PRESSURE AND FLOW MEASUREMENTS

1. Ramon Pallas-Areny and John G. Webster, **Sensors and Signal Conditioning**, John Wiley, New York, 1991.

2. Dan Sheingold, Editor, **Transducer Interfacing Handbook**, Analog Devices, Inc., 1980, ISBN: 0-916550-05-2.

3. Sections 2, 3, Walt Kester, Editor, **1992 Amplifier Applications Guide**, Analog Devices, 1992, ISBN: 0-916550-10-9.

4. Sections 1, 6, Walt Kester, Editor, **System Applications Guide**, Analog Devices, 1993, ISBN: 0-916550-13-3.

5. Harry L. Trietley, **Transducers in Mechanical and Electronic Design**, Marcel Dekker, Inc., 1986.

6. Jacob Fraden, **Handbook of Modern Sensors, 2nd Ed.**, Springer-Verlag, New York, NY, 1996.

7. **The Pressure, Strain, and Force Handbook, Vol. 29**, Omega Engineering, One Omega Drive, P.O. Box 4047, Stamford CT, 06907-0047, 1995. **http://www.omega.com**

8. **The Flow and Level Handbook, Vol. 29**, Omega Engineering, One Omega Drive, P.O. Box 4047, Stamford CT, 06907-0047, 1995. (http://www.omega.com)

9. Ernest O. Doebelin, **Measurement Systems Applications and Design, 4th Ed.**, McGraw-Hill, 1990.

10. Data sheet for **AD7730 Bridge Transducer ADC**, http://www.analog.com

NOTES: